UNIVERSITÉ DE SHERBROOKE
Faculté de génie
Département de génie mécanique

# Conception et Validation d'un Contrôleur Optimisant la Durée de Vie et la Consommation Énergétique d'un Actionneur Magnétorhéologique

Mémoire de maîtrise
Spécialité : génie mécanique

Marc-André Bégin

Jury : Alain BERRY (codirecteur)
Jean-Sébastien PLANTE (codirecteur)
Patrice MASSON
Alexandre GIRARD

Sherbrooke (Québec) Canada Juin 2018

# RÉSUMÉ

Les actionneurs magnétorhéologiques (MR) à glissement continu utilisent une combinaison d'une ou plusieurs sources de couple (p. ex. un moteur électrique rotatif) et d'un certain nombre d'embrayages magnétorhéologiques configurés en parallèle. Ces embrayages, dont le couple transmis est proportionnel au courant qui leur est fourni, agissent en quelque sorte à titre de filtres mécaniques en permettant un contrôle fin de l'effort transmis et ce, peu importe l'impédance de la source d'effort.

Alors que la plupart des travaux dans la littérature explorent l'impact des choix de conception sur certains indices de performance des actionneurs MR (tel que sa performance dynamique, sa consommation énergétique et la longévité du fluide MR), le présent document vise à explorer l'impact du choix de la stratégie de contrôle. Les travaux présentés dans ce mémoire sont basés sur une étude de cas pour une suspension active de siège de camion. Dans un premier temps, la caractérisation de l'actionneur permet de démontrer ses qualités intrinsèques pour une application de suspension active de siège dont une grande compacité, une grande transparence, une bande passante en force élevée (15 Hz) ainsi qu'une force maximale atteignant 1000 N sur tout le débattement du siège. Dans un deuxième temps, des expériences réalisées en laboratoire et sur route démontrent que cette suspension active peut, pour un profil de route raboteuse, réduire les vibrations transmises au conducteur de 66% par rapport à une suspension passive pour ainsi respecter les limites d'exposition définies par la norme ISO 2631-1. Enfin, la dernière partie des travaux présentés ici détaille une stratégie de contrôle qui permet de réduire d'environ 20% la consommation énergétique et d'allonger de 40% la durée de vie du fluide de l'actionneur pour une utilisation dans un camion roulant sur une route de carrière de pierre.

**Mots-clés :** Actionneur à glissement continu, embrayage magnétorhéologique, efficacité énergétique, durabilité des fluides magnétorhéologiques, contrôle actif de vibrations

# TABLE DES MATIÈRES

# LISTE DES FIGURES

# LISTE DES TABLEAUX

# CHAPITRE 1

# Introduction

## 1.1 Mise en Contexte et Problématique

Contrairement à un fluide newtonien conventionnel, les fluides magnétorhéologiques (MR) ont une viscosité apparente environ proportionnelle à l'intensité du flux magnétique auquel ils sont soumis [14]. À ce jour, freins, amortisseurs et embrayages exploitent déjà les fluides MR dans une panoplie d'applications allant de l'amortissement d'ondes sismiques au contrôle de vibrations d'un support moteur. Au sein du spectre des technologies MR existantes, certains actionneurs MR permettent le contrôle actif d'un système.

Les dispositifs MR développés au laboratoire CREATEK de l'Université de Sherbrooke (UdeS) [73] combinent un moteur électrique à engrenages et deux embrayages MR contra-rotatifs pour moduler activement le couple transmis à un système. Ces actionneurs MR sont abordables et combinent la densité de couple d'un moteur à engrenages avec la performance dynamique d'un moteur à entraînement direct. Les performances ont été démontrées dans nombreuses applications : suspension active de siège de camion, bras robotisés [97, 99], actionneur de volet d'avion [21, 24], actionneurs primaires de vol d'hélicoptères [23]. Toutes ces démonstrations ont cependant été réalisées avec des lois de contrôle cherchant uniquement à démontrer les performances dynamiques des prototypes. Les prototypes, tel qu'utilisés actuellement, ne considèrent pas la durée de vie ou l'efficacité énergétique comme critère de performance.

## 1.2 Définition du Projet de Recherche

Il s'avère donc utile d'explorer l'impact potentiel des lois de contrôle sur des indices de performance que sont la durée de vie prédite du fluide MR ainsi que la consommation énergétique de l'actionneur. Cependant, une des difficultés de cette entreprise est que ces indices de performance sont intrinsèquement reliés aux caractéristiques d'un actionneur MR particulier et à son type d'utilisation. Pour contourner cet obstacle, le projet de recherche s'articule autour d'un actionneur MR utilisé comme suspension active de véhicule lourd.

## 1.3 Objectifs du Projet de Recherche

Pour explorer l'impact des stratégies de contrôle sur la performance d'un actionneur MR, les objectifs secondaires suivants devaient d'abord être atteints :

1. Caractériser un actionneur MR utilisé pour une application concrète de suspension active de siège de véhicule lourd ;
2. Vérifier que la performance dynamique de l'actionneur MR justifie son emploi pour une application de suspension active de siège ;
3. Développer un contrôleur optimisant la durée de vie du fluide MR ainsi que sa consommation énergétique.

## 1.4 Contributions Originales

Ces travaux de maîtrise ont contribué à l'avancement de la science en proposant une des premières démonstrations de l'utilisation d'un actionneur MR à glissement continu pour une application concrète alors que la plupart des dispositifs présentés jusqu'à maintenant dans la littérature scientifique ne visaient pas d'application particulière. Qui plus est, une comparaison des performances de la suspension active avec différentes alternatives commerciales permet de soutenir avec chiffres à l'appui un des points forts des actionneurs MR à glissement continu : à volume et coût réduits, ils peuvent égaler la performance d'un actionneur électrique à couplage direct.

Un modèle d'actionneur MR à glissement continu a également été développé étant assez réaliste pour permettre d'apprécier le compromis existant entre les différents indices de performance de l'actionneur : sa performance dynamique, sa consommation énergétique, et la durée de vie attendue du fluide MR. Bien que ce modèle ait été validé pour une application de suspension active, la méthodologie employée pourrait facilement être transposée à d'autres applications.

Enfin, il a été démontré que l'utilisation d'une méthode de contrôle simple visant à minimiser l'énergie dissipée dans les embrayages d'un actionneur MR peut contribuer de manière significative à réduire sa consommation énergétique et allonger la durée de vie du fluide pour une application de suspension active.

## 1.5 Plan du Document

Le présent document introduit d'abord le lecteur aux enjeux reliés aux dispositifs MR actuels ainsi qu'aux limitations de la littérature concernant l'impact des lois de contrôle sur l'énergie dissipée dans les embrayages d'un actionneur MR. Les chapitres subséquents contiennent les trois articles auxquels j'ai contribué dans le cadre de ma maîtrise. Le premier aborde la conception et la caractérisation d'un actionneur MR utilisé comme suspension active de siège de véhicule lourd. Le deuxième détaille le développement d'un contrôleur LQG pour cette suspension active, offre une validation expérimentale de cette suspension et compare la performance de celle-ci vis-à-vis d'autres suspensions actives. Le troisième et dernier article offre enfin un aperçu d'un modèle plus raffiné d'un actionneur MR et du système qu'il contrôle afin de prédire la performance dynamique de l'actionneur, sa consommation énergétique et la durée de vie attendue du fluide. Il présente aussi une validation expérimentale d'une stratégie de contrôle visant à minimiser les pertes par glissement dans les embrayages MR.

# CHAPITRE 2
# État de l'Art

## 2.1 Catégorisation des Dispositifs MR

Les premiers travaux pionniers qui démontrent l'utilisation de fluides MR à l'intérieur de dispositifs mécaniques remontent aux années 50 avec la première conception d'un embrayage MR [75]. Depuis, bon nombre de dispositifs exploitant les fluides MR ont été développés dont certains se retrouvent aujourd'hui sur le marché. Les dispositifs MR existants peuvent être catégorisés en se basant sur leur rôle principal dans un système mécanique, c'est-à-dire s'ils sont utilisés pour :

- dissiper de l'énergie (p. ex. un frein ou un amortisseur) ;
- transmettre un effort (p. ex. un embrayage).

La famille des dispositifs MR ne se limite pas à ceux qui utilisent les fluides MR : il existe par exemple les élastomères MR qui sont souvent utilisés comme éléments à raideur variable [60]. Ce type de dispositif ne sera cependant pas abordé dans ce travail.

### 2.1.1 Dispositifs Dissipatifs

Les amortisseurs MR et les freins MR sont les applications les plus communes de dispositifs à fluide MR [14]. À titre d'exemple, la compagnie Lord manufacture depuis plusieurs années des amortisseurs MR pour des applications telles que des suspensions semi-actives pour sièges de véhicules lourds, le contrôle de vibrations sismiques dans les structures, et les supports de moteurs [53]. Les applications des freins MR abondent également. Ils sont notamment utilisés pour imposer une résistance dans des machines d'entrainement [13] ou des machines de réhabilitation [3], pour une orthèse d'articulation humaine [38, 45] ou simplement comme frein automobile [71].

Tout comme un amortisseur conventionnel, un amortisseur MR est composé d'une chambre remplie d'un fluide séparée en deux par un piston mobile (Fig. 2.1). Des passages à travers la tête du piston permettent au fluide de circuler d'une chambre à l'autre, mais la résistance du fluide à ce transfert entraîne une force proportionnelle et opposée à la vitesse relative entre les deux points d'attache de l'amortisseur. Dans le cas d'un amortisseur MR, les propriétés du fluide peuvent être modulées par l'imposition d'un champ magnétique généré par la circulation d'un courant à l'intérieur de bobines comprises dans le piston. L'ajustement en temps réel du taux d'amortissement confère à l'amortisseur MR des per-

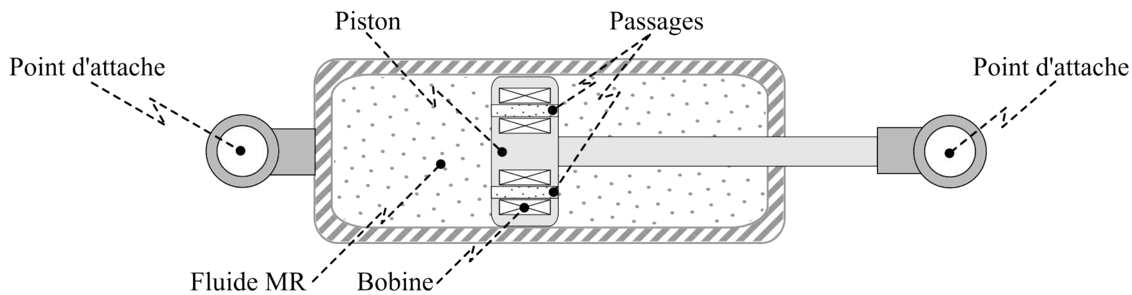


Figure 2.1 Schéma de fonctionnement d'un amortisseur MR

formances dynamiques nettement supérieures aux amortisseurs conventionnels passifs à air ou à fluide comme il l'a été démontré dans la littérature [66].

Dans leur forme la plus simple, les freins MR sont composés de deux pièces dont une fixe et une autre mobile avec une interface entre les deux remplie de fluide MR [15]. Le couple de freinage est modulé en imposant un champ magnétique au fluide généré par la circulation d'un courant dans la bobine interne du frein (Fig. 2.2-a). Contrairement aux freins à disque conventionnels, le fait qu'il n'y ait pas de contact direct entre les pièces du frein MR limite l'abrasion de surface [80].

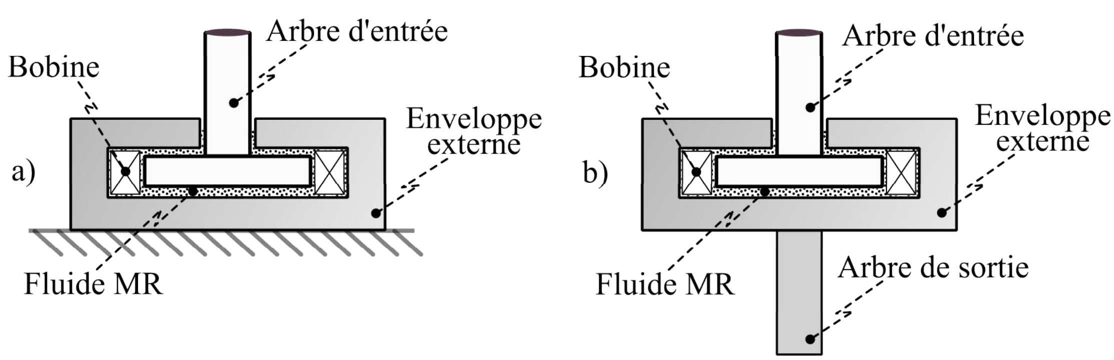


Figure 2.2 Schéma de fonctionnement d'un frein et d'un embrayage MR

## 2.1.2 Dispositifs de Transmission

Le principe de fonctionnement d'un embrayage MR est similaire à celui d'un frein MR, sauf que l'embrayage transmet un couple entre deux pièces mobiles reliées à une source d'effort mécanique à l'entrée et à une charge à la sortie (Fig. 2.2-b). Les embrayages MR peuvent être utilisés pour des applications classiques dites «à glissement limité» comme dans une transmission automobile [57]. L'embrayage permet alors d'éviter des dépassements de couple lors d'une transition entre deux vitesses ce qui améliore le confort des passagers [42]. Une autre approche consiste à combiner une source d'effort mécanique avec un embrayage MR dit "à glissement continu". L'assemblage est alors appelé «actionneur MR». Par exemple, un actionneur MR développé à l'UdeS combine un moteur électrique relié à deux embrayages MR utilisés en parallèles à travers 2 étages de courroies de réduction (Fig. 2.3). Chaque embrayage contrôle ainsi le couple transmis à 2 poulies tel que le câble de la poulie gauche tire le siège vers le haut alors que la poulie de droite tire le siège vers le bas.

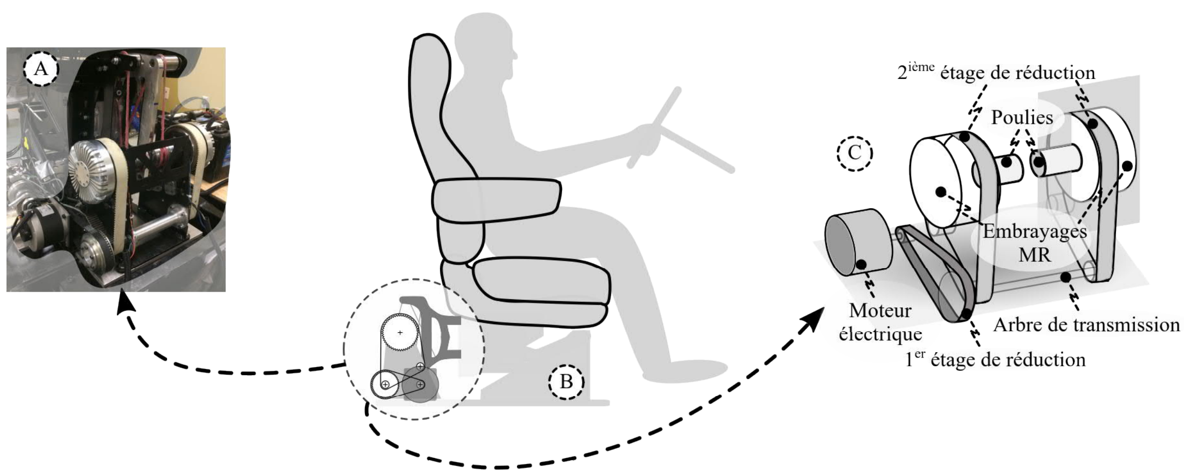


Figure 2.3 Exemple d'actionneur MR (A) utilisé comme suspension active de siège (B) et sa forme schématisée montrant les composantes principales (C).

Les actionneurs MR possèdent des caractéristiques avantageuses [35] par rapport à plusieurs actionneurs traditionnels tels que les actionneurs électromécaniques à haut ratio de réduction, les actionneurs pneumatiques et les actionneurs hydrauliques :

- une plus grande bande passante en raison du court temps de réponse de l'embrayage ;
- une meilleure transparence étant donné le découplage de la charge et de la source d'effort mécanique.

La transparence de l'actionneur qualifie sa capacité à agir comme une source d'effort pure sans que sa dynamique ait d'impact sur la charge à contrôler. Ainsi, le contrôleur d'un actionneur transparent n'a pas à incorporer de compensation pour des effets tels que le frottement sec et il n'est pas non plus constamment perturbé par des contrecoups de l'actionneur. Cette transparence permet également à l'actionneur d'être plus compact, puisque des mécanismes de réduction à grand ratio peuvent être utilisés sans introduire d'effets dynamiques non linéaires indésirables. Les actionneurs MR sont donc particulièrement intéressants pour les applications haptiques où l'interaction avec l'humain demande un retour d'information en force précis à l'utilisateur [61, 83, 97, 106]. D'autres exemples d'applications incluent des actionneurs aéronautiques [21, 55] ou encore un actionneur de suspension active de siège [22].

## 2.2 Limitations des Actionneurs MR

### 2.2.1 Durabilité

Dans la plupart des articles traitant de nouveaux dispositifs MR, la question de la durabilité du fluide MR n'est souvent que brièvement abordée ou complètement ignorée. Pourtant, plusieurs mécanismes de dégradation des fluides MR sont proposés dans la littérature. D'abord, certaines études suggèrent que l'oxydation graduelle des particules de fer en suspension dans le fluide réduirait la magnétisabilité du fluide [27]. D'autres études suggèrent plutôt que les efforts de cisaillement appliqués au fluide MR amèneraient la dégradation des polymères composant l'huile de base du fluide [95]. Cependant, les auteurs ne relient pas la dégradation de l'huile de base du fluide avec une baisse de l'effort transmis. Malgré la compréhension déficiente du mécanisme exact de dégradation des fluides MR, il est généralement admis que la durée de vie d'un fluide MR est directement reliée aux vitesses et aux efforts de cisaillement auxquels il est soumis. Ainsi, la durée de vie utile d'un volume donné de fluide MR serait atteinte lorsque l'énergie totale dissipée à l'intérieur du fluide atteindrait entre $6 \times 10^6$ [12] et $10^7$ J/mL [103]. Pour un embrayage MR, la durée de vie $t_v$ du fluide pour un volume de fluide $V$ ainsi qu'un couple $T$ et une vitesse de glissement $\Delta\omega$, tous deux fonctions du temps $t$, correspond à la solution implicite de l'équation :

$$\frac{1}{V}\int_0^{t_v} T\Delta\omega \; dt = 6 \text{ à } 10 \text{ MJ/mL}. \tag{2.1}$$

**Exemple appliqué de durée de vie** Dans le cas de l'actionneur présenté à la figure 2.3, une consigne de vitesse typique envoyée à l'actionneur est de 1520 RPM ce qui correspond à une vitesse de 190 RPM à l'entrée de l'embrayage (rotor externe). Étant donné le lien souple (c.-à-d. les câbles) qui unit l'actionneur et le siège, cette vitesse est nécessaire pour empêcher le relâchement de la tension des câbles pour un profil de route donné. Selon l'équation 2.1, pour un volume de 60 mL, un couple RMS de 2.5 N·m et considérant que la vitesse de glissement moyenne correspond à la vitesse du rotor externe de l'embrayage, la durée de vie du fluide MR serait d'environ 2000 h d'utilisation continue. Le couple RMS utilisé est nécessaire pour atténuer les vibrations transmises par le siège au conducteur lorsque le camion roule sur une route de gravier. À titre de comparaison, un changement d'huile d'un camion semi-remorque est recommandé à environ toutes les 500 h d'utilisation cumulées pour un total d'environ 4 changements d'huile par an. À 750 USD/L, les coûts d'entretien de l'actionneur seraient d'au moins 60 CAD par an alors que le siège actif commercial *Air Ride* fabriqué par la compagnie Bose pourrait, selon le manufacturier, fonctionner plus de 2 ans (c.-à-d. 1 million de miles) sans nécessiter de maintenance.

Enfin, la température de fonctionnement du fluide MR aurait également un impact direct sur sa durée de vie [28]. Il est donc important de concevoir un embrayage MR afin qu'il évacue bien la chaleur et, si c'est le cas, on néglige l'effet de la température lors du calcul de prédiction de durée de vie du fluide MR.

### 2.2.2 Efficacité

Même si les embrayages MR sont aussi touchés par les problèmes de durée de vie du fluide MR, ils se distinguent des dispositifs dissipatifs puisqu'ils sont utilisés comme élément de transmission. L'énergie dissipée par friction dans l'embrayage devient alors directement une perte énergétique. Ainsi, des résultats préliminaires indiquent qu'environ 30 % de l'énergie consommée par un actionneur MR à glissement continu utilisé dans une suspension active de siège de camion serait dissipée en friction dans l'embrayage lorsque la suspension est sollicitée pour répondre à un profil de route agité.

Encore une fois, malgré la multitude d'articles détaillant l'utilisation d'actionneurs MR en robotique, aucun n'aborde sérieusement l'efficacité énergétique de l'actionneur ou la durée de vie du fluide MR. Pourtant, ce sont justement sur ces deux points que les détracteurs de la technologie s'appuient pour critiquer les actionneurs MR [89].

## 2.3 Réponses aux Limitations des Actionneurs MR

Pour répondre aux problèmes d'efficacité des actionneurs MR et de durabilité des fluides MR, les trois grandes approches préconisées dans la littérature sont :

1. Améliorer la durabilité des fluides MR eux-mêmes ;
2. Modifier la conception des embrayages MR ;
3. Adapter l'approche de contrôle de l'embrayage.

**Solution 1 : Améliorer les Fluides MR** Pour améliorer la durabilité des fluides MR, différents types d'additifs sont ajoutés au fluide MR [54]. Ces additifs peuvent par exemple absorber l'oxygène du fluide pour empêcher l'oxydation des particules de fer ou limiter leur agglomération. Plus récemment, une étude a proposé d'utiliser un mélange de particules microscopiques et nanoscopiques pour diminuer la vitesse d'agglomération des particules par un ordre de grandeur [102]. La science des fluides MR reste cependant complexe et mal comprise et il arrive souvent que les changements proposés dans la formule des fluides MR s'avèrent en fait avoir un effet nuisible sur la durée de vie [32]. Il n'est donc pas certain que les nouvelles générations de fluides MR pourront apporter des améliorations plus qu'incrémentales.

**Solution 2 : Améliorer les Embrayages** Une stratégie envisagée dans plusieurs études pour améliorer la durée de vie du fluide MR consiste à mieux partager l'énergie de glissement à l'ensemble du volume de fluide. Dans ses travaux pionniers dans les années 50, Rabinow envisageait déjà d'inclure une pompe de recirculation du fluide dans son concept d'embrayage MR [76]. La recirculation du fluide pourrait aussi avoir des effets bénéfiques sur la dissipation de chaleur dans l'embrayage et pourrait limiter l'agglomération des particules. En pratique cependant, l'incorporation de mécanismes de recirculation actifs s'avèrerait peu pratique, coûteuse et énergivore.

**Solution 3 : Améliorer l'Asservissement de l'Actionneur** Typiquement, le moteur d'un actionneur MR est asservi à vitesse constante. Le contrôle du système mécanique est alors assuré par le couple transmis par l'embrayage [20]. Une stratégie de contrôle plus évoluée pour les actionneurs MR permettrait des gains substantiels autant en termes de durée de vie du fluide que d'efficacité globale de l'actionneur.

Smith et al. ont utilisé cette approche afin de limiter la dégradation du fluide dans un embrayage MR transmettant l'effort entre le moteur d'un camion et le ventilateur contrôlant la température du radiateur [86]. La stratégie de contrôle consiste à limiter uniquement le couple de sortie de l'embrayage (et donc la vitesse de sortie de l'embrayage) puisque le régime du moteur ne peut pas être modulé en fonction de la demande de l'embrayage. Pour certains régimes du moteur, on accepte donc de faire des compromis directement sur l'échauffement du radiateur afin de limiter la puissance dissipée dans l'embrayage.

Pourtant, pour certaines applications, il semblerait possible de limiter la puissance dissipée dans l'embrayage si la vitesse du moteur d'un actionneur MR était modulée sur demande. C'est du moins ce que semblent indiquer différents travaux réalisés pour certains systèmes hydrauliques qui utilisent une pompe à déplacement fixe couplée à un moteur entraîné à fréquence variable ainsi qu'une servovalve pour fournir la pression nécessaire à un cylindre [18, 19, 93]. Par analogie avec les actionneurs MR à glissement continu, on cherche ici à minimiser les pertes d'énergies causées par le passage du fluide dans la valve de contrôle.

Pour y parvenir, la vitesse du moteur électrique couplé à la pompe générant la pression en amont de la valve de contrôle est asservie selon une stratégie qui vise d'abord à réduire les pertes dans la valve (Fig. 2.4). La valve de contrôle sert quant à elle à fournir rapidement et précisément la pression requise au cylindre. Par exemple, dans le cas où une position est désirée, la commande à la valve sera dictée par un retour sur la position du cylindre.

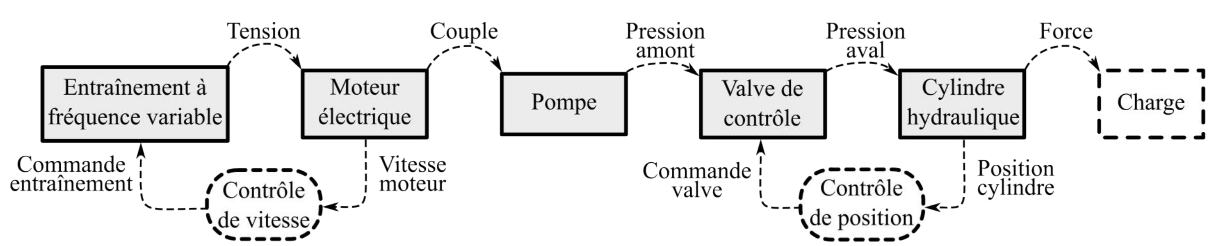


Figure 2.4 Diagramme de fonctionnement d'un actionneur hydraulique avec valve et pompe asservies

Une première stratégie pour générer la consigne variable de vitesse du moteur consiste à essayer de maintenir un différentiel constant entre la pression en amont et celle en aval de la valve de contrôle. Sous certaines conditions, la stratégie permet de réduire de 50 à 75 % la puissance consommée par l'actionneur [18, 19]. Cependant, comme le souligne Cho, bien que la consommation énergétique est réduite lorsque le différentiel de pression est réduit, l'erreur de positionnement s'accroit. Les auteurs ne soulignent cependant pas la sensibilité ni le seuil de cette dépendance entre la consommation énergétique et l'erreur de positionnement.

Alors que Cho et Chiang considèrent les boucles d'asservissement du moteur de la pompe et de la valve de contrôle comme indépendantes, Tivay propose plutôt une structure de contrôle coopérative [93]. Cette structure de contrôle manipule la variable auxiliaire (dans ce cas, la pression en amont du moteur) pour empêcher la variable primaire de saturer (dans ce cas, la pression en aval de la valve de contrôle) [41]. Tel que schématisé à la figure 2.5, les contrôleurs $C_1$ et $C_2$ imposent une commande $u_1$ à la valve de contrôle et $u_2$ au moteur respectivement et leur action est coordonnée par une fonction non linéaire $f(u_1)$ définie telle que :

$$f(u_1) = -|u_1| + \delta$$

où $\delta$ est une marge définie sur la commande $u_1$ du contrôleur. Ainsi, pour une consigne en position $r$, le contrôleur impose au système les commandes $u_1$ et $u_2$ dont les effets sur la position réelle du cylindre hydraulique sont prédits par les fonctions de transfert $G_{P1}$ et $G_{P2}$. En pratique, l'approche de Tivay se distingue uniquement de celles de Cho et Chiang du fait que la commande $u_2$ au moteur est générée à partir de la consigne $u_1$ à la valve de contrôle plutôt qu'à partir d'un retour d'état sur les pressions amont et aval de la valve de contrôle.

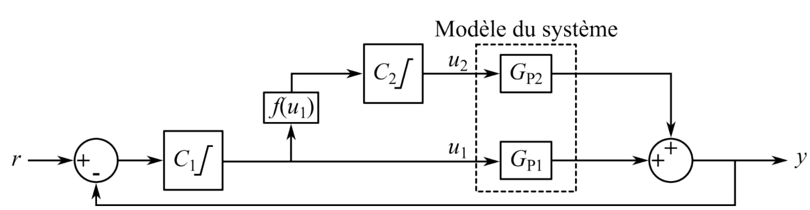


Figure 2.5 Schéma d'une structure de contrôle coopérative

Il serait intéressant de migrer les stratégies de contrôle appliquées aux actionneurs hydrauliques vers les actionneurs MR. L'analogie entre un actionneur hydraulique et un actionneur MR n'est cependant pas parfaite. D'abord, on note que la pompe d'un actionneur hydraulique est une source d'effort (pression) alors que la valve pilotée assure un contrôle local du débit. À l'inverse, le moteur électrique d'un actionneur MR est une source de débit (vitesse) et l'embrayage MR assure un contrôle local d'effort (couple). Ainsi, l'approche de contrôle devra tenir compte du fait que la force de l'actionneur MR relié par un lien souple à l'application est nulle si la vitesse du moteur est insuffisante alors que la force d'un actionneur hydraulique ne fait que saturer.

Par ailleurs, les études réalisées pour les actionneurs hydrauliques ne considèrent que des cas où la consigne du différentiel entre les pressions amont et aval de la valve est constante. Dans le cas où l'actionneur subit des niveaux de perturbation variables, il n'est pas garanti que cette consigne est toujours un bon compromis entre performance dynamique et consommation énergétique.

Une autre faiblesse des études réalisées sur les systèmes hydrauliques est que les auteurs ne considèrent pas l'impact de leur stratégie de contrôle sur la consommation énergétique de la source d'effort elle-même. En effet, lorsque le moteur est exploité pour maintenir une vitesse de glissement constante, ce dernier subit constamment des accélérations et des décélérations qui augmentent le courant moyen RMS qui passe dans les bobines du moteur.

# CHAPITRE 3

# Conception et Caractérisation d'un Actionneur MR utilisé comme Suspension Active de Siège de Véhicule Lourd

## 3.1 Avant-Propos

La partie expérimentale des travaux présentés dans ce document s'appuie principalement sur un prototype d'actionneur MR utilisé à l'intérieur d'une suspension active de siège de camion. Bien que ce prototype ait été conçu par Patrick Chouinard, postdoctorant à l'UdeS, j'ai contribué à la caractérisation de l'actionneur en effectuant une étude électromagnétique en éléments finis bidimensionnels des embrayages MR, en traitant certaines données de tests expérimentaux effectués par Patrick et en complétant un test expérimental pour qualifier la transparence de l'actionneur.

L'article suivant a été soumis à une conférence de l'ASME qui aura lieu en août 2018. Celui-ci résume les requis de conception de cet actionneur et présente les résultats des tests expérimentaux qui ont été complétés afin de valider ces requis.

**Titre :** Preventing Lower Back Pain Among Truck Drivers : Design and Performance of a Controlled Slippage Magnetorheological Actuator for an Active Seat Suspension

**Traduction française du titre :** Prévention des douleurs lombaires chez les conducteurs de camions : conception et performance d'un actionneur magnétorhéologique à glissement contrôlé pour une suspension de siège active

**Revue dans laquelle l'article a été soumis :** ASME 42nd Mechanisms and Robotics Conference (MR)

**Auteurs :**

- Patrick Chouinard, étudiant au postdoctorat
- Marc-André Bégin, étudiant à la maîtrise
- Jérémy Marchetta Fortin, ingénieur
- Alain Berry, Professeur
- Patrice Masson, Professeur
- Jean-Sébastien Plante, Professeur

**Date de soumission :** 12 mars 2018

**État de l'acceptation :** En révision

**Résumé de l'article :** Les suspensions pneumatiques passives sont couramment utilisées dans les suspensions de sièges de véhicules lourds modernes, car elles offrent une isolation suffisante des vibrations de la route tout en restant relativement bon marché. Cependant, seules les suspensions actives coûteuses peuvent complètement épargner les conducteurs de risques sérieux pour la santé dus aux vibrations de la route comme prescrit par la norme ISO-2631-1. Cet article présente la conception et la validation expérimentale d'une suspension de siège active simple et abordable qui utilise un actionneur magnétorhéologique (MR) à glissement contrôlé. La performance dynamique en boucle ouverte de l'actionneur est évaluée expérimentalement en fonction des exigences d'un actionneur de suspension de siège actif. Les résultats montrent que l'actionneur peut développer une force verticale maximale de 1000 N, a une fréquence de coupure en force de 15 Hz et affiche un haut niveau de transparence qui peut répondre aux exigences dynamiques d'une suspension active de siège. Cette fréquence de coupure en force est environ trois fois plus élevée que celle des suspensions actives de siège hydrauliques disponibles sur le marché. Les résultats expérimentaux des essais sur route effectués dans un camion semi-remorque à l'aide d'un contrôleur LQG confirment également que la performance de la suspension active de siège proposée dans cet article peut égaler celle de solutions commerciales.

## 3.2 Abstract

Passive air-spring suspensions are widely used in modern heavy vehicle seat suspensions because they provide a fair isolation from road vibrations while remaining relatively cheap. However, only expensive active suspensions can completely relieve drivers from serious health risks due to whole body vibrations as prescribed by the ISO-2631-1 standard. This article sets out the design and experimental validation of a simple and affordable active seat suspension that uses a controlled slippage MagnetoRheological (MR) actuator. The open-loop dynamic performance of the actuator is assessed experimentally in accordance with the requirements of an active seat suspension actuator. Results show that the actuator can develop a maximum vertical force of 1000 N, has a force cutoff frequency of 15 Hz and displays a high level of transparency that can match the dynamic requirements of an active seat suspension. This force cutoff frequency is about three times higher than that of commercially available hydraulic active seat suspensions. Experimental results of on-road tests performed in a long-haul truck using a LQG controller also confirm that the performance of the active seat suspension can match that of commercial alternatives, thus reducing to safe levels truck drivers' exposure to vibrations.

## 3.3 Introduction

Health issues related to prolonged exposure to whole body vibrations is a well-documented issue in the literature [82], [92]. In many vehicles, workers are systematically exposed to frequency-weighted Root Mean Squared (RMS) accelerations higher than recommended by the norm ISO-2631-1 even if air springs have proven their superiority over steel spring mechanisms in mainstream seat suspensions [5]. The performance of passive suspension systems, such as air springs, is fundamentally limited by a design tradeoff between the level of transmitted vibration at high frequencies and the ability to limit suspension travel at low frequencies [25].

Semi-active suspensions offer better overall performance than a passive suspension, but their performance is limited as they can only dissipate or store energy from the system using a variable stiffness or a variable damping element [94]. In comparison, active suspensions can dissipate and inject energy to the system, leading to a better performance as they have full control authority over the seat dynamics. An active seat suspension is typically composed of an actuator coupled in parallel with an air spring. Commercial products such as the John Deere active seat [31] and the Bose Ride [70] respectively use a hydraulic actuator and a direct-drive linear electric motor.

Hydraulic actuators have a high force-to-weight ratio. However, they have a limited bandwidth in the order of 0 to 4 Hz [31] and a high intrinsic impedance which prevents them from being used in road going vehicles as road disturbances relevant to vibration discomfort occur in the 0–15 Hz frequency band. Active hydraulic suspension systems can be scaled for a higher dynamic response, but this upgrade results in high power consumption [48] and high cost. Furthermore, vehicles must accommodate for the hydraulic circuitry in the cabin which complicates the retrofitting of hydraulic active suspensions.

When used in direct-drive fashion, electric actuators offer a wide bandwidth, low intrinsic impedance and can be used in regenerating braking mode ; all key characteristics for high performance active suspensions [91]. However, resulting systems tend to be bulky and costly, especially in high-force applications, since electric motors have a poor force density (force to weight ratio). When coupled to high reduction ratio mechanisms, electric motors have better costs and weights [78], but at the expense of a drastic reduction of dynamic performance because such geared systems are greatly hindered by the added impedance and non-linear effects (e.g. friction, backlashes) of the reduction ratio mechanism [81].

The requirements for active seat suspension actuators can be deduced from the ones of haptic actuators [33] since both applications have close interaction with humans. Ideal active seat suspension actuators would thus require :

1. compactness (low weight/high torque density) ;
2. high force bandwidth ;
3. high structural stiffness ;
4. low apparent inertia ;
5. low friction.

A "transparency" criterion shall later be introduced in the Requirements section of this article to comprise items 3 to 6. Cable-driven manipulators powered by MagnetoRheological (MR) fluid-based actuators have demonstrated to be a lightweight alternative to direct-drive electric motors in haptic applications [35, 55, 98]. In such systems, force exerted by the end effector is modulated by controlling the torque transmitted by MR clutches held in slippage by a highly geared electric motor. Cable-driven MR actuators offer ideal performance for active suspensions as they have :

- low overall weight since the system is composed of high power density (W/kg) electric motors and high torque density (N·m/kg) MR clutches [42] ;
- wide (0–15 to 0–50 Hz) open-loop bandwidth [23, 98] ;
- low impedance hindering the free motion of the suspended mass since the MR clutches, maintained in slippage, decouple the parasitic dynamics of the geared motor from the actuator's output [35].

This work studies the feasibility and potential of using MR actuators for a truck active seat suspension. Requirements are first established for system size ; weight ; maximum travel, relative velocity and acceleration ; open-loop force bandwidth, and overall dynamic transparency. The design of the proof-of-concept active suspension is then presented along with experimental results assessing the performance of the active suspension with respect to design requirements. Finally, results of on-road tests are included and the performance of the active seat suspension is compared to that of commercially available products.

## 3.4 Requirements

### 3.4.1 Size and Weight

For the specific application targeted in this work, the actuator should be contained in a maximum enclosing volume of 544 mm wide by 300 mm high by 528 mm deep in order to fit underneath a typical seat such as a Corsair seat (National Seating). For this particular seat, the suspension frame would need minor modifications in order to use all the space available underneath the driver seat cushion.

Weight target is defined from the Bose Ride system which includes an active suspension. The complete system including the seat itself has a mass of 73 kg [8]. Given that an entirely passive Corsair seat altogether weights 45 kg (base frame included), the mass of the cable actuator should therefore be under 28 kg.

## 3.4.2 Maximum Travel, Speed and Acceleration

There are no universally accepted requirements for the loads and speeds needed for an active seat suspension actuator. Hence, sizing of the proof-of-concept MR actuator is done by measuring the acceleration profile of a dump truck's (International Trucks) cabin floor during a normal workday on a quarry road and estimating, using basic assumptions, the force and speed requirements of the actuator. Although these measurements were made on a seat equipped with a passive air suspension, the authors believe that they are representative of the worst conditions under which the active seat suspension will have to operate. During these tests, the cabin experienced a maximal vertical acceleration of 7.7 m/s$^2$. The maximum relative speed of the seat with respect to the cabin floor and the maximum suspension travel were of 0.54 m/s and 14 cm respectively. A RMS acceleration of 0.65 m/s$^2$ was evaluated for the entire workday, notwithstanding time segments when the truck was at rest.

## 3.4.3 Open-Loop Force Bandwidth

The actuator bandwidth requirement is fixed based on the same data set as the one used to determine the maximum travel, speed and acceleration requirements. Fig. 3.1 shows the power spectral density of a six-minute long acceleration signal that corresponds to the worst (i.e. largest RMS acceleration) working conditions recorded during the day. The power spectrum shows two dominant frequency components around 2 and 7 Hz which suggests that the required cutoff frequency of the actuator should be above 7 Hz.

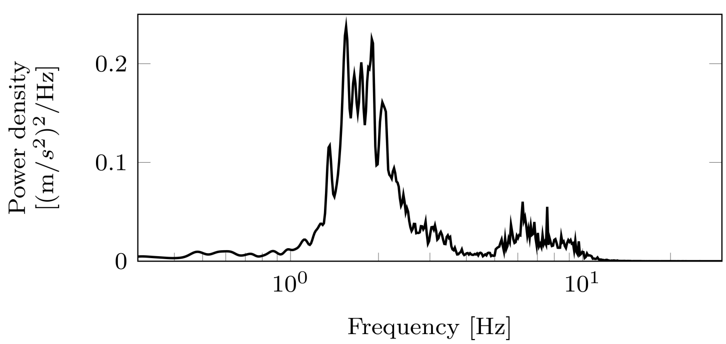


Figure 3.1 Power spectral density of the dump truck cabin floor while it is performing a normal work day on a quarry road. Data is acquired at 200 Hz and is post-processed with a 0.3 to 15 Hz, 4th order Butterworth band-pass filter. Power spectral density is evaluated with 30 s Hanning windows with 22.5 s overlap using Welch's method.

### 3.4.4 Overall Dynamic Transparency

In theory, a perfectly transparent actuator would have no inertia and would not dissipate or store any energy [35, 107] such that a transparent actuator approaches a pure source of effort without the need for any inertia, friction or backlash compensation inside the actuator's controller [67].

To assess the transparency of a robotic device, an impact mitigation factor has been proposed in the literature for a walking robot which roughly reflects how much inertia is felt at each impact with the floor compared to the case where all of the device joints would be locked [101]. Such a metric is, however, not directly applicable to an active seat suspension. Instead, a comparison between the open-loop response of the seat acceleration expressed in the frequency domain with and without the disabled actuator is used.

## 3.5 Design

### 3.5.1 Actuator

The working principle of the actuator and its embodiment into an active suspension system are shown in Fig. 3.2. The actuator (Fig. 3.2-a) is fixed on the back of a passive seat suspension used in a commercially available Corsair seat (National Seating) that had its fluid damper removed (Fig. 3.2-b).

The actuator is composed of an electric motor (RP34-112V) which provides mechanical power to the two custom-made MR clutches via two belt drives having a combined reduction ratio of 8 (Fig. 3.2-c). A cable and pulley reducer converts the torque transmitted by each clutch into a net vertical force applied to the seat. The clutches are placed antagonistically where a single clutch controls the amount of force being delivered in one direction, and the other in the opposite direction.

The motor control of an active seat actuated by a geared electric motor alone is unlike one actuated with a MR actuator. In the former case, the speed of the electric motor is directly coupled to the linear speed of the seat. The motor alone is responsible for providing the desired force to the seat while it is subject to the parasitic torque of the gearbox (friction,

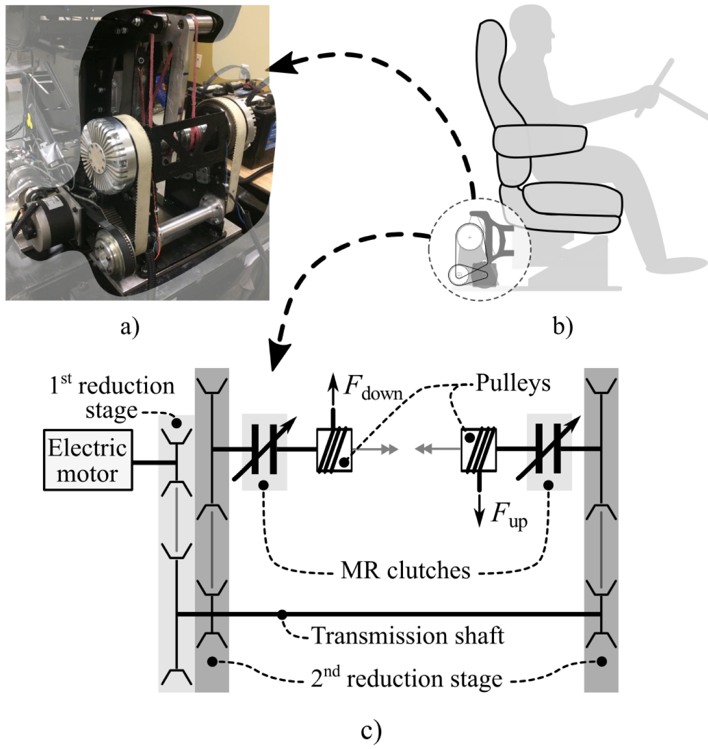


Figure 3.2 Location of the proposed MR actuator (a) with respect to the truck seat (b) and its simplified mechanical diagram (c).

backlash). In the latter case, the motor can rotate freely with respect to the seat, therefore the force control of the actuator is accomplished by the MR clutches as long as the clutches are in slippage (the clutches input speed is larger than their output speed). Hence, a typical control strategy for electrical motors in MR actuators is to use an outer velocity loop to impose a constant reference velocity in cascade with an inner fast current loop.

The net force $F$ applied by the MR actuator on the seat corresponds to the difference between cable tensions $F_{\text{up}}$ and $F_{\text{down}}$ as :

$$F = F_{\text{up}} - F_{\text{down}}, \tag{3.1}$$

$$F_{\text{up}} = \frac{1}{r}\left[T_{\text{mag-up}} + \tau_{\text{visc}}\left(\omega_{\text{mot}} - \frac{v_{\text{seat}}}{r}\right)\right] + F_{\text{spring-up}} \tag{3.2}$$

and

$$F_{\text{down}} = \frac{1}{r}\left[T_{\text{mag-down}} + \tau_{\text{visc}}\left(\omega_{\text{mot}} + \frac{v_{\text{seat}}}{r}\right)\right] + F_{\text{spring-down}} \tag{3.3}$$

where $r$ is the pulley radius (25 mm) ; $T_{\text{mag-up}}$ and $T_{\text{mag-down}}$, the torques due to magnetic effects transmitted by the right and left pulleys respectively ; $\tau_{\text{visc}}$, the viscous coefficient of a clutch ; $\omega_{\text{mot}}$, the angular speed of the clutches outer shells ; $v_{\text{seat}}$, the vertical velocity of the seat ; $F_{\text{spring-up}}$ and $F_{\text{spring-down}}$, forces exerted by tensioning springs on the cables. The tensioning springs are used to avoid the cables unreeling from the pulley when the actuator is inactive (before truck engine ignition for instance). Given the low stiffness of the tensioning springs, they can be approximated as

$$F_{\text{spring-up}} = F_{\text{spring-down}} = F_{\text{spring}} \tag{3.4}$$

where $F_{\text{spring}}$ is the constant pretension in the cable. To avoid backlashes ($F_{\text{up}} < 0$ or $F_{\text{down}} < 0$) when the actuator is inactive ($T_{\text{mag-up}} = T_{\text{mag-down}} = 0$ and $\omega_{\text{mot}} = 0$), then from (3.2) to (3.4) :

$$F_{\text{spring}} > \frac{\tau_{\text{visc}}}{r^2} v_{\text{seat}} \tag{3.5}$$

The viscous coefficient $\tau_{\text{visc}}$ was experimentally measured as $55 \times 10^{-3}$ N·m·s. Let the driver experience an initial drop of 4 cm above the seat as he is seating down, then the seat reaches a maximum velocity of about 0.7 m/s such that, according to (3.5), the pretension in each cable has to be greater than 60 N. Finally, combining (3.1) to (3.4), the net force applied on the seat is :

$$F = \frac{1}{r}\left[T_{\text{mag-up}} - T_{\text{mag-down}} - 2\tau_{\text{visc}}\frac{v_{\text{seat}}}{r}\right]. \tag{3.6}$$

It is worth noting that the antagonist clutches cancel each other's viscous torque due to the motor rotation ($\tau_{\text{visc}}\omega_{\text{mot}}$) such that the overall system sees a damping force opposing only the vertical velocity $v_{\text{seat}}$ of the seat.

### 3.5.2 Cable-Actuator Interface

Unlike many rotary-to-linear motion converters, cable-pulley systems are linear and have high efficiency as well as high reduction ratios [11]. The cable drive uses a 3.125 mm (1/8 in.) diameter, 12-strand construction, synthetic Lightning cables (Samson Rope Technologies) made from a mix of Dyneema® and Vectran®. Dyneema® is known for its natural lubricant properties whereas Vectran® procures high stiffness and low creep. According to the manufacturer, these cables offer a stiffness varying between 300 and 500 kN/m. Synthetic cables are selected over steel cables as they allow, for a given cable diameter and durability, 1.3 to 1.6 times smaller pulley diameters, and thus, more gearing [79].

A potential drawback of a cable-driven system is a low natural frequency of the actuating system due to the combination of a low cable stiffness and high actuator output inertia which acts as a mass-spring system [90]. The proposed actuator has a theoretical natural frequency estimated in the range of 108–141 Hz depending on cable stiffness. The estimated time constant of the actuator itself is thus at least 1 order of magnitude smaller than the system to be controlled (Fig. 3.1) and can therefore be neglected.

### 3.5.3 Clutches

The clutches used in the proposed actuator can be simplified to three main components : the input rotor, the static stator and the output rotor (Fig. 3.3-a). In normal operation, torque is applied on the input rotor through an integrated belt sprocket. A chamber between the input and the output rotor is filled with MR fluid whose apparent viscosity depends directly on the magnetic flux density generated by a coil. Torque transmitted to the output rotor is modulated by controlling the amount of current flowing through the coil with an electrical drive (AZBDC20A8 by Advanced Motion Controls). The output rotor is directly coupled to a pulley used to transmit a linear force to the load. A particular feature of the designed clutch includes an expansion chamber which prevents overpressure of the MR fluid during its use and is therefore likely to increases its lifetime [28]. Cooling fins located on the clutch's outer shell which multiply its surface of convection by a factor of 3 limit the MR fluid's temperature during operation, another factor known to afflict the fluid's lifetime.

The clutch's magnetic circuit (Fig. 3.3-b) includes a 1.02 mm diameter (18 AWG) wire forming a 112-turn coil with a mean radius of 39.5 mm. Using a wire size of 18 AWG allows to keep the coil compact, but the resulting resistance of 0.57 $\omega$ dissipates about 130 W in Joule heating at 15 A.

The non-magnetic clutch's outer shell of the input rotor is made of aluminum as to minimize the clutch's inertia. All magnetic parts of the clutch, including the 7 drums used as shear surfaces to transmit torque from the input to the output rotor, are made of AISI 1010. The 3 input rotor drums are held in place with a AISI 304 part. AISI 304 is selected for this part as it is not ferromagnetic and has high electrical resistivity which limits the occurrence of eddy currents.

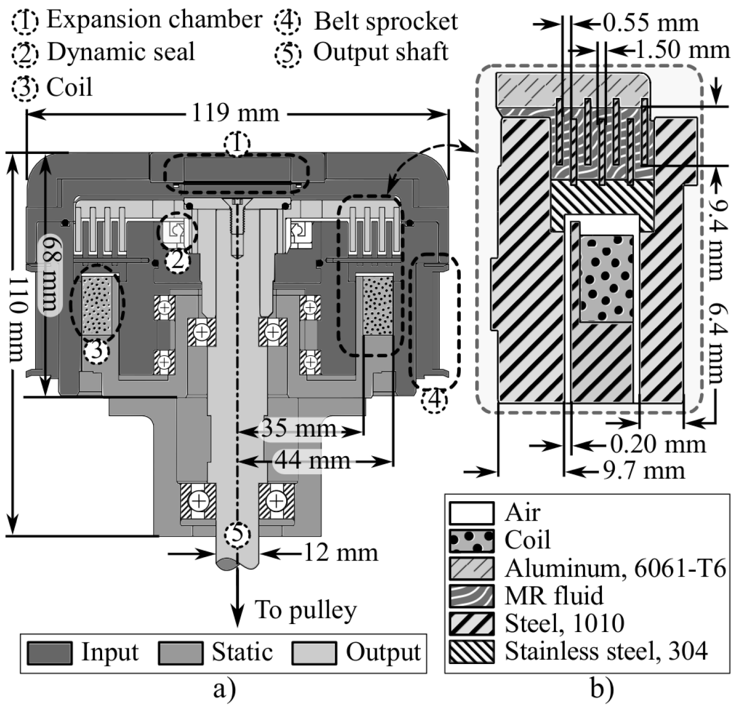


Figure 3.3 Schematic diagram of the clutch with (a) a simplified cutaway view and (b) a detailed view of the different components in the magnetic circuit of the clutch

The 0.55 mm gap between each of the three input rotors and four output rotor drums, filled with MRF-132DG MR fluid, was chosen as to offer a good tradeoff between weight and off-state viscous torque. Viscous torque is also kept to a minimum by using only one dynamic seal to keep the assembly oil tight (Fig. 3.3-a). Air gaps between the static stator and the input rotor, essential to the free rotation of the input rotor, are kept to a functional minimum of 0.2 mm. The minimal thickness of the air gap was chosen in accordance with the machining precision of standard manufacturing equipment and following a tolerance stack-up analysis of the assembly.

A static analysis using the Finite Element Method (FEM) was undertaken on the clutch magnetic circuit presented in Fig. 3.3-b to characterize the clutch. For this purpose, the clutch was simplified to a 2D axisymmetric model discretized into 62,189 triangular, 3-node elements. For excitation currents below 7 A, the static relationship between current and torque is linear (3.3±0.1 N·m/A, $R^2$ = 0.995). Over this level, the magnetic flux density reaches levels over 1 Tesla in some regions of the circuit (Fig. 3.4), which marks the end of the linear domain of the AISI 1010 steel B-H magnetization curve [2]. Above 12 A, changes in current result in marginal increases in torque (0.4±0.1 N·m/A) until a maximum of 30 N·m is reached at 15 A.

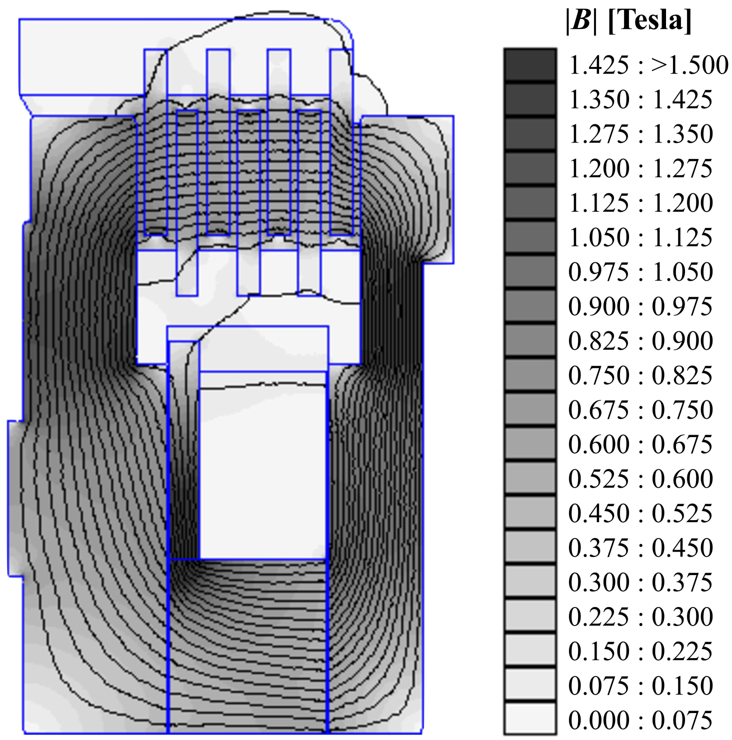


Figure 3.4 Magnetic flux density |B| inside the clutch magnetic circuit under a direct current (DC) of 7.2 A

Frequency also plays an important role in the clutch's dynamics for alternating currents (AC). A modal analysis using the same FEM model as for the static analysis predicts that the cutoff frequency of the clutch varies with the amplitude of the alternating current, going from 8.0 Hz at 1 A to 17.5 Hz at 12 A (Fig. 3.5). A linear model of the clutch is however approximated as a First Order (FO) low-pass filter with a cutoff frequency of 15 Hz. The decreasing value of torque for increasing frequencies is due to the formation of eddy currents within the magnetic housing which restricts the formation of the magnetic field. Larger bandwidth is achievable by selecting a magnetic housing material which has a higher electrical resistivity and minimizing its overall cross-section. Nonetheless, 15 Hz of bandwidth falls in line with the recorded road profile and is satisfactory for the application. Key characteristics of the clutch are summarized in Table 3.1.

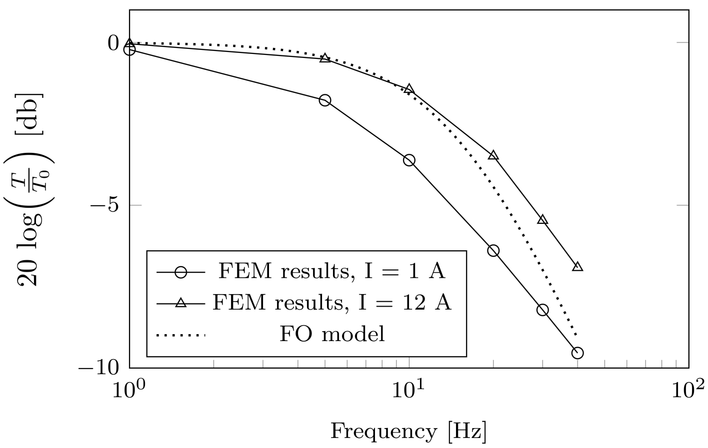


Figure 3.5 Normalized amplitude of a clutch's output torque (based on the ratio of the amplitude of the output torque over the static torque) at different frequencies simulated by FEM and first order model approximation

Table 3.1 Clutch key characteristics

| **Characteristic** | **Magnitude** |
|---|---|
| Torque max. | 30 N·m |
| Current max. | 15 A |
| Weight | 3.8 kg |
| Outer diameter | 119 mm |
| Width | 68 mm |
| Output inertia* | 3.99 kg·cm$^2$ |

*Includes the inertia of the pulleys and that of the clutches inner hubs.

## 3.6 Experimental Results

### 3.6.1 Size and Weight

The proof-of-concept actuator weighs 14 kg and can be contained in an enclosing box volume of 390 mm wide by 257 mm high by 210 mm deep which respects size and weight design requirements. The weight fraction of structural components such as sheet metal frames account for 22% of the actuator total weight and could be reduced by integrating components directly into the seat's frame. Although the actuator is over-designed and has yet to be optimized into a lighter and smaller embodiment, current dimensions and weight allow it to fit behind the seat of a typical highway truck.

### 3.6.2 Maximum Travel, Speed and Acceleration

Use of a cable and pulley system allows the actuator to act over the full range of the 14 cm seat travel with 100% of its maximum force. Moreover, tension can be maintained at all times in the actuator cables up to a seat relative speed of 0.54 m/s (largest daily value recorded in a dump truck on a quarry road) with respect to the cabin floor. To do so, the motor has to be driven at a constant speed faster than 1620 rpm (which represents about 25% of the motor-free speed and is equivalent to a clutch outer shell speed of 203 rpm).

The quasi-static force response of the actuator is evaluated using the test bench shown in Fig. 3.6. The MR cable driven actuator is mounted on a linear guide similar to the seat rigid frame. The force generated by the actuator was measured using a Futek (FSH02702) load cell which blocks the movement of the cable attachment frame.

The quasi-static force generated by the actuator is measured by slowly varying the amount of current supplied to each clutch from 0 A to 14 A and then back to 0 A while the electric motor maintains a constant slippage speed of 42 rpm. The actuator shows little hysteresis and demonstrates a linear behavior with $R^2 = 0.993$ and a standard error of 50 N representing about 5% of the maximum actuator force (Fig. 3.7). Based on the linear behavior of the actuator, it can be foreseen that closed-loop control of the actuator will not require compensation for non-linear effects.

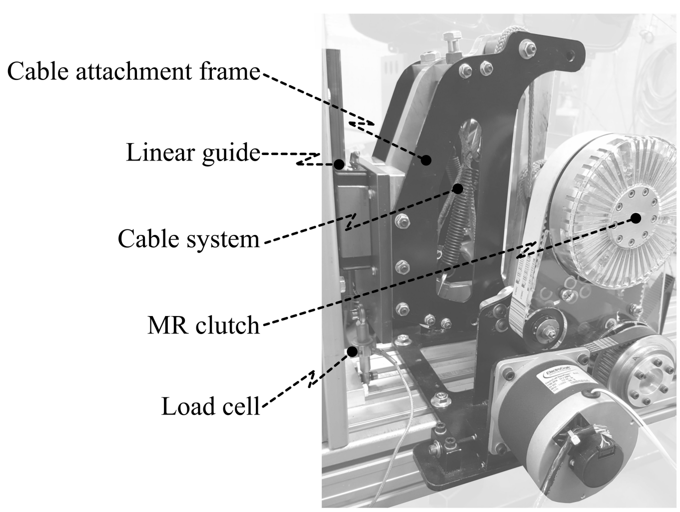


Figure 3.6 Picture of the test bench used to characterize the vertical force developed by the actuator

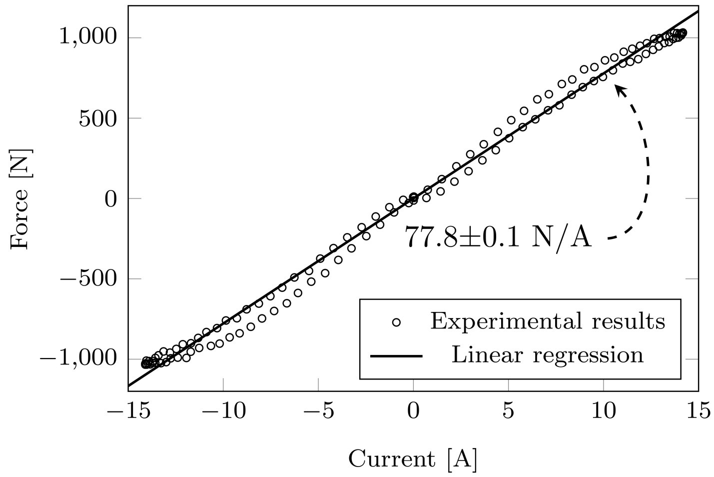


Figure 3.7 Static vertical force developed by the actuator as a function of applied current to the coil and linear regression. The motor side of the clutch spins at 42 rpm.

Negative current shows that only the left pulley was solicited while positive current shows that only the right one was solicited. The apparent symmetry in the force response of the actuator for a positsive current input compared to a negative current input underlines the symmetric behavior of both clutches.

In this work, the proof-of-concept actuator is chosen to be over-scaled such that the actuator has more than enough power output to perform the task. Taking the assumption of an 80 kg occupant in the seat and a seat mass of 20 kg, the actuator is scaled to output 1000 N, which represents a maximal vertical acceleration of 10 m/s$^2$. The actuator over-scaling factor is thus 1.3 with respect to the maximum acceleration and 15 with respect to the RMS acceleration recorded on a rough quarry road used to set the actuator requirements.

### 3.6.3 Open-Loop Force Bandwidth (Blocked Seat)

The open-loop response of the actuator was recorded by imposing a chirp current input ranging from 1 to 50 Hz to the clutches while the motor was driving the clutches at 42 rpm. The frequency response H of the actuator is calculated as :

$$H(f) = \frac{F(f)}{I(f)},$$

where $I$ is the current input to the clutch drives and $F$ is the measured force, both expressed as functions of frequency $f$. The gain $G$ and phase $\phi$ of the frequency response $H$ are respectively calculated as :

$$G(f) = 20\log\left(|H(f)|\right) - G_0 \tag{3.7}$$

$$\phi(f) = \angle H(f). \tag{3.8}$$

where the compensation for the DC gain $G_0$ is defined as :

$$G_0 = \lim_{f \to 0} 20\log\left(|H(f)|\right).$$

As plotted in Fig. 3.8, the dynamic response of the actuator on the test bench can be approximated by a third order linear model and a pure time delay of 2 ms, expressed as :

$$H(f) \approx \underbrace{e^{2\pi\tau f j}}_{\text{term \#1}} \cdot \underbrace{\frac{f_c}{fj + f_c}}_{\text{term \#2}} \cdot \underbrace{\frac{f_n^2}{2\xi f f_n j + f_n^2 - f^2}}_{\text{term \#3}} \tag{3.9}$$

where $\tau$ is the 2 ms pure time delay ; $f_c$ is the cutoff frequency of a low-pass first order filter ; $\xi$ is the damping ratio and $f_n$ the natural frequency of a second order transfer function.

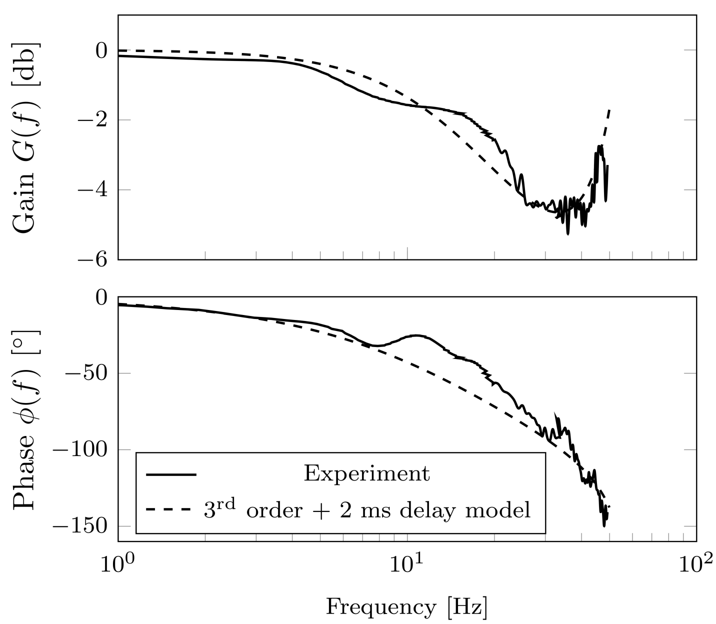


Figure 3.8 Bode plot of the DC compensated frequency response of the complete actuator relating the measured vertical force with the current input applied to the clutches. The clutch outer shell spins at 42 rpm.

The constants $\xi$ and $f_n$ are evaluated as :

$$f_n = \frac{1}{2\pi}\sqrt{\frac{k}{m}},\ \xi = \frac{b\pi}{mf_n}$$

where $b$, $k$ and $m$ are the damping, the spring rate and the mass of a second order mass-spring oscillator.

The 2 ms delay (term #1 of equation 4.1) is interpreted as the time required for the alignment of the ferromagnetic particles into chain-like structures that causes the sudden increase in yield stress of the MR fluid [40]. The first order component (term #2 of equation 4.1) of the system having a cutoff frequency $f_c$ of 15 Hz is interpreted as the time response of the MR clutches as impeded by eddy currents forming in the magnetic circuit. The second order model (term #3 of equation 4.1) was fitted using a natural frequency ($f_n = 60$ Hz) and damping ratio ($\xi = 0.1$). The fitted natural frequency $f_n$ is lower than the theoretical estimate from the cable stiffness and output inertia of the MR clutch which is in the range of 108-141 Hz. However, when accounting for the mass of the cable attachment frame (2.4 kg) and a low cable stiffness of 300 kN/m, the resulting natural frequency (56 Hz) is similar to $f_n$ (60 Hz). The damping ratio $\xi$ is due to the combined viscous effects of the two MR clutches as shown in 3.6.

### 3.6.4 Overall Dynamic Transparency

The clutches are designed to offer a small viscous torque such that the actuator is transparent to the driver-seat passive system. The resulting impedance is experimentally measured to about $55{\times}10^{-3}$ N·m·s. Although the actuator clutches demonstrated a breakaway torque (torque threshold to initiate movement) of 0.65 N·m, it has no significant impact on the dynamics of the actuator once the motor rotates, because the clutches are constantly slipping and negate each other's friction.

In order to measure the resulting transparency of the actuator with respect to the driver-seat passive system, the actuator was first mounted at the back of a CorsairTM seat (National SeatingTM) bolted to a vibrating platform (Fig. 9). The vibrating platform is made of a flat structure mounted on a scissor mechanism actuated by two Xcite hydraulic cylinders (see Table 2). A chirp excitation was then applied to the platform while data was acquired from two accelerometers (see Table 2) respectively fixed to the vibrating platform and to the seat rigid frame. A draw-wire encoder also recorded the position of the seat relative to the platform. The procedure was then repeated after removing the actuator from the back of the seat. In both cases, the actuator was kept inactive and the same 80 kg driver took place on the seat.

The frequency response Hseat of the seat-driver passive system relating the seat acceleration $A_{\text{seat}}$ to the floor acceleration $A_{\text{floor}}$ was then calculated as :

$$H_{\text{seat}}(f) = \frac{A_{\text{seat}}(f)}{A_{\text{floor}}(f)}.$$

The gain $G_{\text{seat}}$ and phase $\phi_{\text{seat}}$ of the frequency response $H_{\text{seat}}$ are calculated following Equations (8) and (9), except that no DC compensation is applied this time. For each tested actuator arrangement (coupled to the seat vs decoupled), the Bode plot of the Hseat transfer function is presented (Fig. 10). The similarity between the Bode plots of the Hseat frequency response with and without the actuator shows that the system is little affected by the presence of the actuator. The positive phase around 1.1 Hz for both the coupled and the uncoupled actuator shows that, in the neighborhood of this frequency, the vibrating platform is affected by the dynamics of the seat. This platform behavior is detrimental to the faithful reproduction of a cabin floor acceleration profile, but hard to avoid as an infinitely rigid platform is impossible to design.

Based on the transparent behavior of the actuator, it can be foreseen once again that its closed-loop control will not require compensation for its linear or non-linear dynamics.

## 3.7 On-Road Tests Results

On-road tests were conducted on a Peterbilt 379 highway truck rolling on a roadway in Eastern Canada with a setup similar to that introduced in Fig. 3.9. The weighted (ISO-2631-1) RMS vertical acceleration of the truck floor ranged between 0.43 and 0.63 m/s$^2$.

To isolate the seat occupant from harmful floor vibrations, the active suspension applies a vertical force F as determined by a fixed LQG controller. Based on the readings from the draw-wire encoder and the seat frame accelerometer, the LQG controller tries to minimize

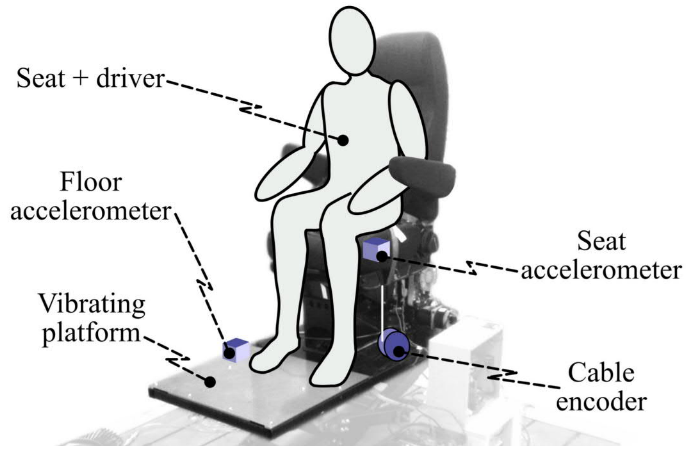


Figure 3.9 Experimental setup used to characterize the transparency of the actuator

Table 3.2 Equipment used for experiments

| Equipment type | Key features | Product number | Manufacturer |
|---|---|---|---|
| *Hydraulic system* | | | |
| Cylinder | 0-60 Hz<br>4450 N max.<br>51 mm stroke | 1107-4 | Xcite Systems |
| LVDT | 0-75 Hz | 0244-0000 | Trans-Tek |
| *Accelerometers* | | | |
| Seat pad | 0-200 Hz | 4030-006 | Measurement Specialties |
| Seat frame | 0-100 Hz | ADXL105EM | Analog Devices |
| Floor | 0-100 Hz | ADXL105EM | Analog Devices |
| *Encoder* | 2048 pulse/rot. | AMT102 | CUI INC |

the cost function

$$J(f) = \int_0^\infty \left[(\ddot{x}_w)^2 + (q_d \Delta x_w)^2 + (q_f f)^2\right] \tag{3.10}$$

where $\ddot{x}_w$ is the seat occupant's absolute vertical acceleration filtered according to the ISO-2631-1 standard, $\Delta x_w$ is the low-pass filtered (1st order, 0.3 Hz cutoff frequency) position of the seat relative to the cabin's floor, $q_d$ is the seat displacement weighting factor and $q_f$ is the actuator force weighting factor which accounts for limitations in the maximum actuator output force. The introduction of a seat displacement weighting factor allows to adjust tradeoffs between vibration attenuation levels and avoiding large seat travels that might cause the driver to lose contact with the pedals. Details on the design and implementation of the LQG controller are covered in [27].

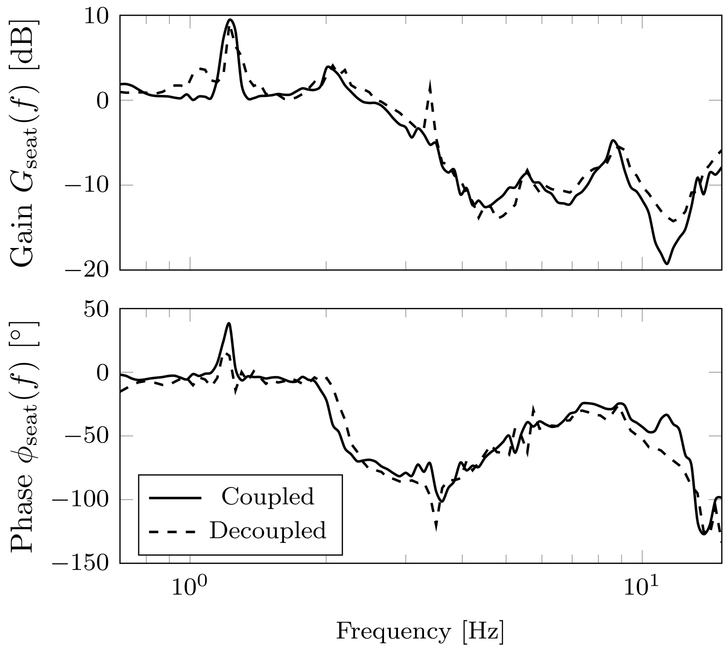


Figure 3.10 Approximated frequency response of the seat-driver passive system from the floor acceleration to the seat acceleration. Coupled : the actuator is not powered, but physically attached to the seat. Uncoupled : the actuator is removed from the back of the seat.

Results show that the active seat suspension can bring down the weighted (ISO-2631-1) RMS vertical acceleration of a seat pad placed right underneath the seat occupant from a range of 0.36-0.46 m/s$^2$ for the original damped passive suspension to a range of 0.19-0.32 m/s$^2$ which represents an improvement of about 46% in floor vibration attenuation. Corresponding transmissibility curves obtained as the ratio between the magnitude of the seat occupant's acceleration and the magnitude of the floor acceleration (in the frequency domain) are shown in Fig. 3.11.

These numbers fall in line with results reported under similar road conditions for the Bose Air Ride with a range between 40% [70] and 51% [30] improvement with respect to a damped passive suspension.

## 3.8 Conclusion

The design of a controlled slippage MR actuator was presented based on the requirements mostly derived from a baseline cabin floor acceleration profile recorded in a dump truck performing typical duties over a full day on a quarry road.

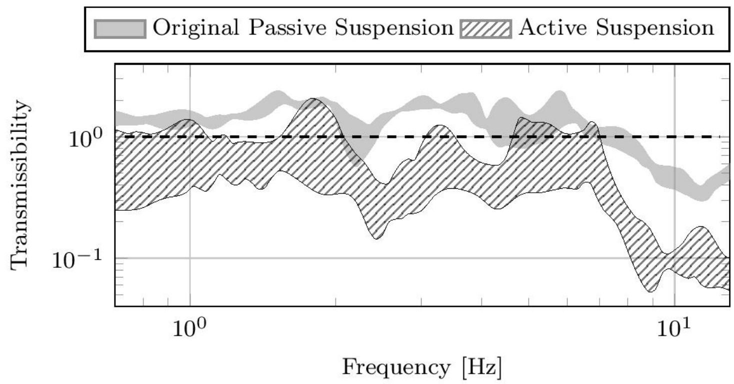


Figure 3.11 Transmissibility curves for the original passive and for the active seat suspensions. Each shaded area represents the envelope of 5 different spectra obtained from 5 consecutive 30 s runs.

The actuator weights 14 kg (including 10.9 kg of mobile components) and occupies a volume of 390 mm wide by 257 mm high by 210 mm deep which falls in line with commercially available active seat suspensions. Open-loop experiments showed that the actuator can provide a maximum force of 1000 N over the full-seat travel. Tension can be maintained in the actuator's cables up to a seat relative speed of 0.54 m/s (maximum value of the baseline cabin floor acceleration profile) given that the motor is driven at a sufficiently high speed. The actuator was also shown to have a cutoff frequency of 15 Hz which is higher than most of the floor vibrations. System identification of the seat with and without the inactive actuator showed that MR clutches effectively decouple dynamics of the mechanical power source from the load, thus making the actuator transparent to the seat. Finally, on-road validation on a long-haul truck demonstrates that the active seat suspension can match the performance of commercial alternatives under the tested road conditions.

Unlike an active seat suspension using a hydraulic actuator, the proposed active seat suspension is easy to retrofit in a heavy vehicle's cabin, because it does not need to accommodate for the hydraulic circuitry. The MR actuator also has a cutoff frequency three times higher than that of a typical hydraulic actuator thus enabling it to act over the whole road disturbance frequency band relevant to vibration discomfort. Moreover, unlike commercially available electric active seat suspensions which use a costly and bulky linear electric motor, the proposed system only uses a small and standard brushless direct current motor with a geared output.

Overall, characterization of the actuator presented in this paper allow to conclude that the actuator would meet all the requirements of an active seat suspension. The overall power consumption of the actuator and MR fluid lifespan however have yet to be characterized.

## 3.9 Acknowledgments

The authors would like to thank Exonetik for the technical assistance they have provided throughout the project. This research was funded by the NSERC Collaborative Research and Development grant CRDPJ 468488-14.

# CHAPITRE 4

# Validation Expérimentale d'un Actionneur MR utilisé comme Suspension Active de Siège de Véhicule Lourd

## 4.1 Avant-Propos

Suite à la conception d'un actionneur MR pour une suspension active de siège de camion, une étape fondamentale consistait à vérifier si l'actionneur permettait d'atteindre une performance similaire à d'autres suspensions actives de sièges disponibles sur le marché.

Dans les premiers mois de la maîtrise, un contrôleur a été développé, implanté et testé qui permet de minimiser les vibrations de la route transmises à l'occupant d'un siège de véhicule lourd. Les performances de la suspension active ont été obtenues expérimentalement en laboratoire sur une plateforme excitatrice et hors laboratoire à l'intérieur d'une cabine de camion semi-remorque. L'article suivant fait état des démarches entreprises pour y arriver.

**Titre :** Experimental Assessment of a Controlled Slippage Magnetorheological Actuator for Active Seat Suspensions

**Traduction française du titre :** Évaluation expérimentale d'un actionneur magnéto-rhéologique à glissement contrôlé pour suspensions de siège actif

**Revue :** ASME/IEEE Transactions on Mechatronics

**Auteurs :**

- Marc-André Bégin, étudiant à la maîtrise
- Patrick Chouinard, étudiant au postdoctorat
- Louis-Philippe Lebel, étudiant à la maîtrise
- Patrice Masson, Professeur
- Yann Pasco, Professionnel de Recherche
- Jean-Sébastien Plante, Professeur
- Alain Berry, Professeur

**Date de soumission :** 2 juin 2017

**État de l'acceptation :** Corrections mineures soumises

**Résumé de l'article :** Les ressorts pneumatiques passifs sont la norme de référence des suspensions de sièges de véhicules lourds, car ils constituent des moyens économiques d'isoler les conducteurs des vibrations de la route. Ils sont néanmoins susceptibles d'exposer les conducteurs à des niveaux de vibrations supérieurs à ceux recommandés par la norme ISO-2631-1 sur une période typique de 8 h. Bien que les suspensions actives commerciales de siège existantes aient prouvé leur supériorité sur les suspensions passives, des limitations pratiques telles que le coût ou le manque de performance dynamique globale ont ralenti leur adoption généralisée. Les actionneurs magnétorhéologiques à glissement contrôlé (MR) sont une alternative prometteuse, car ils offrent une performance dynamique similaire à celle des moteurs à entraînement direct pour un volume et un coût similaires à des motoréducteurs économiques. Cet article est le premier à évaluer expérimentalement les performances globales en boucle fermée d'une suspension de siège active actionnée par un actionneur MR à glissement contrôlé comprenant l'atténuation des vibrations, la consommation d'énergie et la course du siège. Contrairement aux actionneurs MR semi-actifs tels que les amortisseurs MR qui ont fait l'objet d'études approfondies, les actionneurs MR à glissement contrôlé sont totalement actifs et offrent une performance nettement meilleure pour les conditions routières difficiles. Le siège actif a été testé en laboratoire sur une plateforme vibrante recréant le profil d'accélération au sol d'un camion à benne roulant sur une route de carrière de pierre. Le siège a également été testé sur un

camion semi-remorque roulant sur une route principale. Les résultats montrent qu'avec un contrôleur linéaire quadratique gaussien (LQG), la suspension active proposée réduit efficacement les vibrations du plancher d'un facteur de 2 à 3 en utilisant une consommation d'énergie moyenne de 86 W RMS et une plage de déplacement relative moyenne de 1 à 10 mm RMS. Ces résultats correspondent aux suspensions de siège actives disponibles sur le marché.

## 4.2 Abstract

*Passive air-springs are the golden standard in heavy vehicle seat suspensions as they provide economical means to isolate drivers from road disturbances. They are nevertheless likely to expose drivers to vibration levels higher than recommended by the ISO-2631-1 standard over a typical 8 h shift. Although existing commercial active seat suspensions have proven their superiority over passive suspensions, practical limitations such as cost or lack of overall dynamic performance have slowed down their widespread adoption. Controlled slippage magnetorheological (MR) actuators are a promising alternative, because they offer a dynamic performance similar to direct-drive motors in a packaging and cost similar to economical geared motors. This article is the first to experimentally assess the overall closed-loop performance of an active seat suspension powered by a controlled slippage MR actuator including vibration attenuation, power consumption and seat travel. Unlike semi-active MR actuators such as MR dampers which have been extensively studied, controlled slippage MR actuators are fully active and offer a significantly better performance for rough road conditions. The active seat was tested in laboratory on a vibrating platform recreating the floor acceleration profile of a dump truck rolling on a quarry road. The seat was also tested on an actual highway truck rolling on a roadway. Results show that with a Linear-Quadratic-Gaussian (LQG) controller, the proposed active suspension effectively reduces floor vibrations by a factor of 2 to 3 while using an average power consumption of 86 W RMS and having an average relative travel range of 1 to 10 mm RMS. These results fall in line with commercially available active seat suspensions.*

## 4.3 Introduction

Work related exposure to whole body vibrations (WBV) has a negative health impact and is a prevailing issue in many types of vehicle using passive seat suspensions (Fig. 4.1). According to the ISO-2631-1 standard, helicopter and garbage truck drivers working on 8 h shifts are likely to experience health problems due to excessive exposure to WBV [63, 69]. Moreover, most heavy vehicles including excavators ; dumpers ; milk floats ; lift trucks ; mine dump trucks ; armored vehicles ; mobile cranes ; tractors ; grass rollers and highway trucks, expose drivers working on 8 h shifts to a weighted Root Mean Squared (RMS) acceleration higher than the caution threshold of 0.5 m/s$^2$ defined by ISO-2631-1 [11, 69, 85].

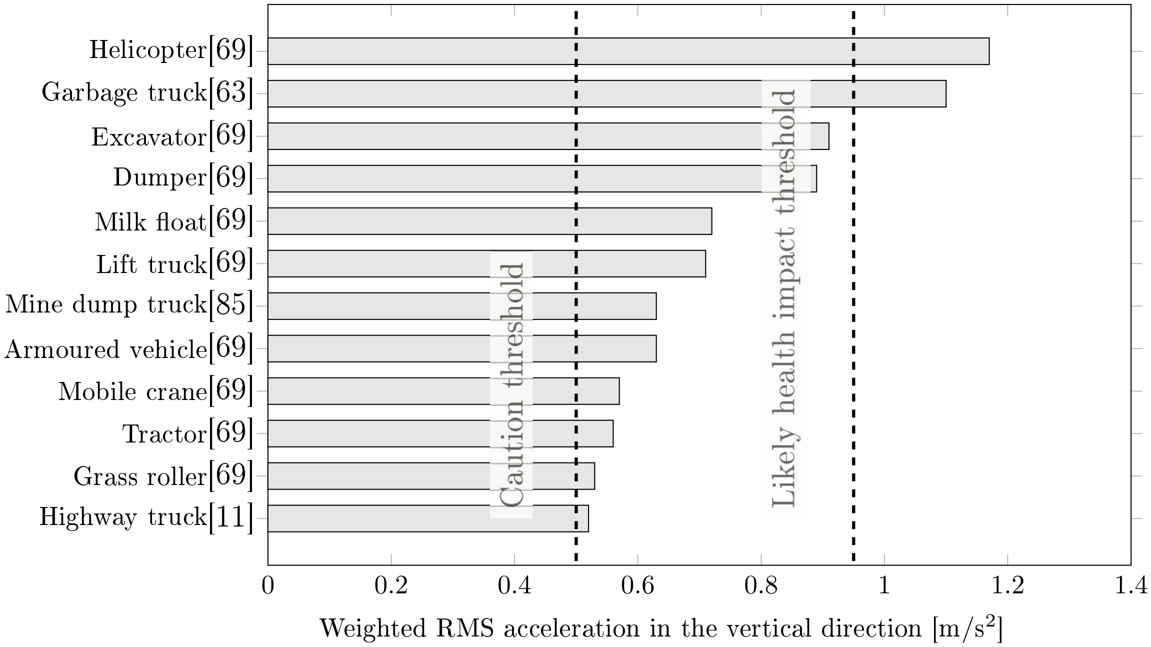


Figure 4.1 Typical frequency weighted RMS vertical acceleration for different vehicles performing normal operations compared to limit recommendations by ISO-2631-1 for a 8 h shift [11, 63, 69, 85]

.

Passive seat suspensions are generally made of a mechanical or pneumatic spring element in parallel with a damper. There have been numerous attempts in the past to improve passive seat suspensions performance including :

- switching from mechanical suspensions (assembly of steel leaf springs) to air suspensions [5] ;
- incorporating a manually adjustable damper to the suspension using, for example, a lever [88] ;
- improving the design of the end-stop buffers [77] ;
- selecting better foams for the seat cushion [16] ;
- redesigning the suspension into a non-linear mechanism as to obtain overall "negative stiffness" [58] ;
- optimizing the characteristics and structure of existing passive suspensions [100].

Regardless of the approach, performance of passive suspensions is fundamentally bounded to a restrictive design trade-off between vibration attenuation level and seat travel. In contrast, active systems are much less impeded by this trade-off, because they can add energy to the suspension, therefore achieving better attenuation levels than any passive suspension given similar seat travel and road conditions [94]. Other alternatives include semi-active suspensions based, for instance, on MR dampers [49, 59, 65], but they offer a mid-way solution since the seat dynamics are only affected by energy storage or dissipation. Multiple researches that compare the performance of semi-active and active solutions consistently demonstrate that active solutions offer greater performance for harsh road conditions with a suspension having a limited working space, most especially if the suspension is to operate over a variety of operating conditions [37, 50].

Even though various active suspensions have been successfully developed in the past, their widespread use is still limited mostly due to fundamental limitations in actuation technology. For example, solutions based on hydraulic actuators such as the Active Seat™ proposed by John Deere [96] have proven to effectively suppress vertical WBV in class 3 agricultural tractors for cab floor acceleration frequencies ranging from 1 to 4 Hz [31]. However, most hydraulic actuators have a cutoff frequency of about 4 Hz in order to limit their power consumption which restricts their use in other vehicles for which the vibration frequency content is broader, such as highway trucks. The complexity to retrofit a hydraulic active suspension to a vehicle once manufactured has also slowed down the spread of this technology.

Other active solutions use direct-drive electric actuators such as the Bose Ride® [70]. They feature a high bandwidth and a low impedance resulting in good overall dynamic performances. They can also achieve lower power consumption than hydraulic actuators due to a higher efficiency and an intrinsic ability to perform regenerative braking. Given the electrical power source readily available in the vehicle, it can also be easily retrofitted to existing trucks. Cost and weight of direct-drive solutions remain important and limit widespread adoption. Coupling electric actuators with high reduction ratio mechanisms improves drastically the compactness and cost of the technology. However, such mechanisms significantly decreases the apparent transparency of the actuator which is detrimental to the active suspension performance [67].

The current limited adoption of active seat suspensions, either due to their high cost, the low cutoff frequency and unhandiness of hydraulic actuators, or the limited performance of geared electric motors, underscore the need to introduce a new type of actuation technology into active suspensions.

With that respect, controlled slippage MR actuators offer a good alternative. In a controlled slippage MR actuator, one or several MR clutches are placed in series with a source of torque such as an electric motor and the motor spins in such the way that the clutches input port always spin faster than the clutches output port. The clutches are held in slippage to decouple the motor's inertia from the output leading to excellent system dynamics and transparency. Unlike conventional clutches, MR clutches input and output disks never come into contact as the gap between the two is filled with MR fluid. Instead, the transmitted torque is varied by adjusting the amount of current flowing through the clutch inner coil thus changing the rheology of the MR fluid which is dependent on the magnetic flux density going through it. Controlled slippage MR actuators are thus light weight and inexpensive electric actuators with the dynamic performance of a direct-drive equivalent [35, 91]. Such actuators have been successfully used in many generic haptic actuators [55, 83, 98, 105], but have never been implemented in an active vibration cancellation application before.

In this paper, the closed-loop performance of a controlled slippage MR actuator for a seat active suspension is experimentally assessed including vibration attenuation, power consumption and seat travel. To this end, a LQG controller is designed and tuned experimentally in a controlled vibratory environment. The active suspension is then tested on the passenger seat of a highway truck.

## 4.4 Hardware Description

The controlled slippage MR actuator studied in this paper is composed of an electric motor belted to two reduction stages making up a total reduction ratio of 8 (Fig. 4.2-a).

Through a transmission shaft, torque generated by a single motor is shared between two output shafts each attached to a pulley. Two custom-designed MR clutches, each sandwiched between an output shaft and its corresponding pulley, control the unidirectional torque transmitted to the pulleys (Fig. 4.2-b). This concept decouples the motor/reducer inertia and eliminates friction, mechanical backlashes and cogging [74] which avoids compensating for these hard-to-predict disturbances inside the actuator's controller as proposed by Ning for an active seat suspension using geared electric motors wi-

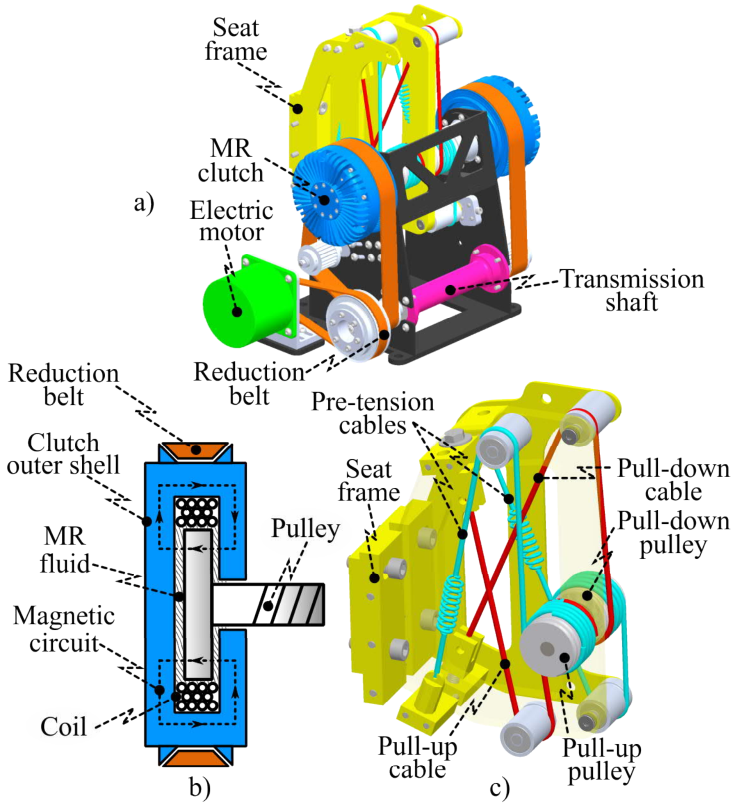


Figure 4.2 Computer assisted drawing of the proposed MR actuator with one electric motor belted to two reduction stages (a). The transmission shaft shares motor torque between two independent MR clutches (cutaway view in b). The MR clutches are linked to pulleys either pulling the seat up or down (c).

thout MR clutches [68]. Synthetic cables are wrapped around the pulleys and attached to the seat frame allowing the seat to be pulled up or down depending on the solicited clutch (Fig. 4.2-c).

The resulting prototype actuator can be contained within an enclosing box volume of 390 mm wide by 257 mm high by 210 mm deep. It is small enough to fit behind the seat of a Corsair™ (National Seating®) truck seat in parallel to the passive suspension composed of an air-spring and a damper (Fig. 4.3). The damper is manually taken off when the suspension is in active mode or when the undamped passive suspension is tested. The actuator maximum vertical force and other key features are summarized in Table 4.1.

The weight and size of the actuator exceeds that of most semi-active seat suspensions. For instance, the commercial MR damper RD-8040-1 by Lord™ has a mass of about 1 kg, an extended length of 20.8 cm and a body diameter of 4.21 cm according to the manufactu-

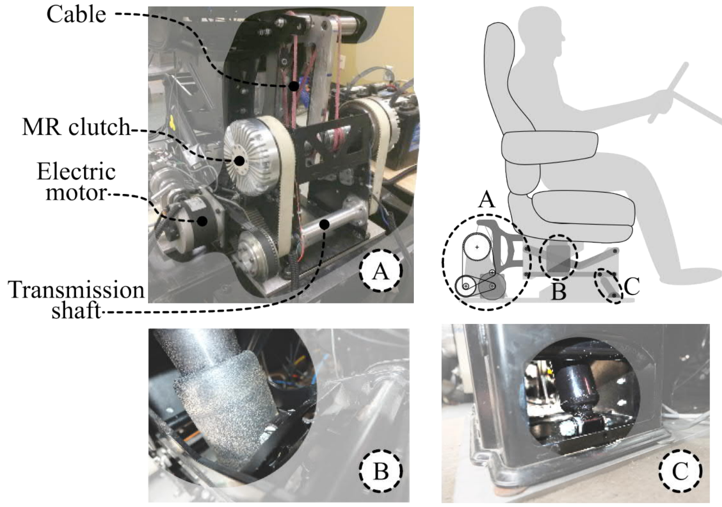


Figure 4.3 Photographs of the controlled slippage MR actuator (A), air-spring (B) and damper (C) and location of the different elements relative to the vehicle driver seat

rer's specifications. However, the Bose Ride® and the John Deere Active Seat™, which both have an enclosing box volume similar to that of the active seat suspension tested in this work, offer fairer comparisons given the superior performance of active seat suspensions over semi-active suspensions. Besides, these commercial active suspensions have shipping weights (including the seat itself) of about 73 kg and 86 kg respectively according to the manufacturers specifications. A typical completely passive truck seat such as the Corsair™ seat (National Seating™) weights 45 kg such that the weight of the actuators used by Bose™ and John Deere™ in their active seats are roughly approximated to 28 kg and 41 kg respectively. These are in the same order of magnitude as the weight of the proposed controlled slippage MR actuator (14 kg including 10.9 kg of mobile components). In other words, although the active suspension prototype has not yet been optimized for mass, it only adds an extra 14 kg to the vehicle's payload which is arguably a small fraction of the total weight of most heavy vehicles.

## 4.5 Controller Design

A common approach in controlling controlled slippage MR actuators is to separate the control of the electric motor from that of the MR clutches. The electric motor is typically [83, 98, 105] controlled as to maintain a constant rotational speed that allows the clutches input ports to always spin faster than their output port. The motor controller used in this work follows this structure, therefore it is not further detailed. Since the motor rotates

Table 4.1 Actuator Key Characteristics

| **Characteristic** | **Value** |
|---|---|
| Max. vertical force | 1000 N |
| Cutoff frequency | 15 Hz |
| Weight (total) | 14 kg |
| Mobile parts | 10.9 kg |
| Fixed parts | 3.1 kg |
| Output inertia* | 5.96 kg·cm$^2$ |
| Belts reduction ratio (tot.) | 8 |
| Cable type | 12 strands |
| Cable material | HMPES-HMPE mix |
| *Electric motor* | |
| Brand | ElectroCraft |
| Series | RP34-112V24 |
| Type | Brushless Direct Current (BLDC) |
| Power source | 24 VDC |
| Peak torque | 277 N·cm |
| *MR clutches* | |
| Viscous torque | $8 \cdot 10^{-3}$ N·m·s |
| Max. torque | 30 N·m |

*Output inertia comprises the pulleys and the MR clutches output shafts.

freely with respect to the seat, the force control of the actuator is accomplished by the MR clutches alone as long as they remain in slippage. Although the motor speed remains constant, the actuator as a whole is fully active as the antagonistic disposition of the MR clutches allows it to apply an upward or downward force to the seat no matter the state of the seat.

MR clutches are known to exhibit a non-linear hysteresis behavior due to their ferromagnetic clutch core [104]. To quantify the hysteresis behavior of the actuator, the actuator was mounted on a linear guide similar to the seat rigid frame. The force generated by the actuator was measured using a Futek (FSH02702) load cell which blocked the movement of the cable attachment frame. Raw data presented in Figure 4.4 relates directly the force output of the actuator to the current input oscillating at 2 (Fig. 4.4a) and 10 Hz (Fig. 4.4b). A simple model of the actuator relating the vertical force output with the current input can however be built from a pure time delay $\tau$ of 2 ms (term #1 of equation 4.1) in series with a first order low-pass filter with a cutoff frequency $f_c$ of 15 Hz (term #2) and a second order filter with a damping ratio $\xi$ of 0.1 and a natural frequency $f_n$ of 60 Hz (term #3). Each term in equation 4.1 models a different part of the actuator's dynamics. The first term is associated with the time required for the alignment of the ferromagnetic particles into chain-like structures that causes the sudden increase in yield stress of the MR fluid [40]. The second term represents the time response of the MR clutches as impeded by eddy currents forming in the magnetic circuit. Finally, the third term models the effects of cable stiffness, viscosity of the MR fluid in the two MR clutches and the mass of the cable attachment frame used to characterize the actuator.

$$H(f) \approx \underbrace{e^{2\pi\tau f j}}_{\text{term \#1}} \cdot \underbrace{\frac{f_c}{fj + f_c}}_{\text{term \#2}} \cdot \underbrace{\frac{f_n^2}{2\xi f f_n j + f_n^2 - f^2}}_{\text{term \#3}} \tag{4.1}$$

If the model were to perfectly represent the actuator, data acquired at a given frequency would in theory collapse onto a single line when subject to a phase compensation which cancels the lag predicted by the model. At 2 and 10 Hz, the RMS error between the collapsed data and the predicted lines represents 6-7 % of the maximum force recorded during test or below 2 % of the maximum force the actuator can output.

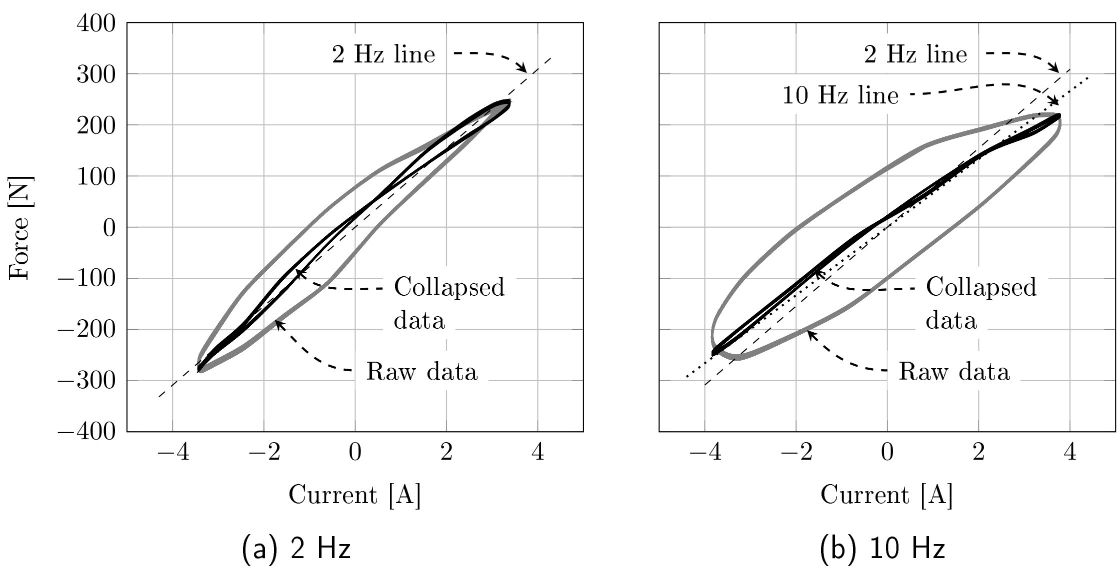


Figure 4.4 Force hysteresis loops of the MR actuator subject to an oscillating current

Other than some hysteresis, MR-cable systems thus have a relatively linear behavior without effects of backlash, cogging, and dry friction [98]. Given this property, a LQG controller is selected for its ease of implementation and for its ability to keep the system under optimal conditions at all times. LQG controllers also permit easier integration of frequency dependent control objectives [64]. The introduction of weighting factors in a pre-defined cost function also facilitates the management of the trade-offs between seat travel, vibration attenuation and power consumption objectives. Moreover, the Kalman filter embedded within the LQG controller allows to reduce the uncertainty on the state of the system by combining sensor readings with the output of a dynamic model of the seat.

For practical considerations however, the model formulated in equation 4.1 was not used to define the LQG controller. The actuator's dynamics were instead comprised within a reduced order model of the whole system (including the actuator, the seat and the driver) in order to limit the model size and because an LQG design approach does not support plant models with internal time delays. The controller thus uses a one degree of freedom (1DOF) model for the complete system comprising the actuator, the driver and the seat suspension, frame and cushion. Assuming that the force output of the actuator is directly proportional to the applied current (the clutch model being reduced to a simple static gain of 99.7 N/A of control current), the system equivalent stiffness $k$ = 7.55 kN/m, sprung mass $m$ = 62.45 kg, and damping constant $b$ = 412 N·s/m (Fig. 5.5) were all tuned to best fit experimental data based on a 68 kg driver given that about 1/3 of the driver mass is supported by the floor through his feet and that the seat moving mass is about 15 kg. Although more accurate models of the driver-seat system dynamics can be obtained by including the biomechanics of the driver in the model for instance [39], simple and robust 1 DOF models have repeatedly been used in literature to successfully implement active and semi-active control schemes [17, 43, 87].

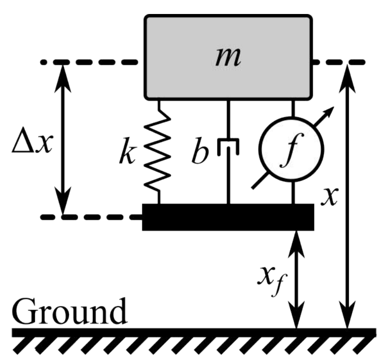


Figure 4.5 One degree of freedom model for the active seat suspension with mass $m$, stiffness $k$ and damping constant $b$ controlled with the actuator force $f$. Variations in the position $x_f$ of the cabin floor affects position $x$ of the rigid seat frame, also expressed as $\Delta x$ relative to the cabin floor.

As defined in the ISO-2631-1 standard, vibration frequencies between 1.5 and 12 Hz are more prone to harm vehicle drivers than others. For this reason, the norm applies a weighting factor to the driver vertical acceleration $\ddot{x}$ which depends on frequency (Fig. 4.6). Only the vertical acceleration is considered here since it is the dominant component for road going vehicles. A 2nd order filter can accurately approximate the frequency weighting on $\ddot{x}$

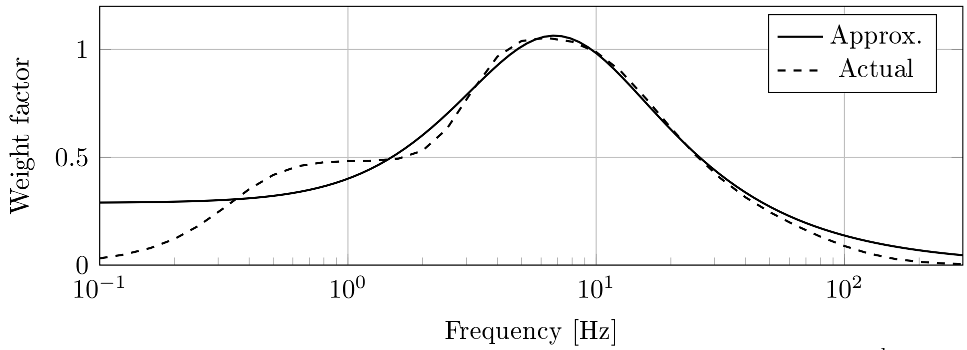


Figure 4.6 ISO-2631 actual frequency-weighting curve against 2nd order approximation used in this work

proposed by ISO-2631-1 for frequencies ranging from 1 to 100 Hz while limiting the total order of the system such that the weighted vertical acceleration of the driver $\ddot{x}_w$ is given by :

$$\ddot{x}_w = \mathbf{C}_{f_a} \begin{bmatrix} \alpha_1 & \alpha_2 \end{bmatrix}^T \tag{4.2}$$

and

$$\begin{bmatrix} \dot{\alpha}_1 & \dot{\alpha}_2 \end{bmatrix}^T = \mathbf{A}_{f_a} \begin{bmatrix} \alpha_1 & \alpha_2 \end{bmatrix}^T + \mathbf{B}_{f_a} \ddot{x} \tag{4.3}$$

where $\alpha_1$ and $\alpha_2$ are the filter state variables and

$$\mathbf{A}_{f_a} = \begin{bmatrix} -82.17 & -1892 \\ 1 & 0 \end{bmatrix}, \ \mathbf{B}_{f_a} = \begin{bmatrix} 1 \\ 0 \end{bmatrix},$$

$$\mathbf{C}_{f_a} = \begin{bmatrix} 86.51 & 546.1 \end{bmatrix}.$$

To avoid the driver losing contact with pedals, a 1st order low-pass filter with a cutoff frequency $f_c = 0.3$ Hz and a static gain of 4 is also introduced in the model on the relative displacement $\Delta x$ between the seat and the vehicle floor such that the weighted relative displacement $\Delta x_w$ is given by :

$$\Delta x_w = \mathbf{C}_{f_d} \beta \tag{4.4}$$

and

$$\dot{\beta} = \mathbf{A}_{f_d} \beta + \mathbf{B}_{f_d} \Delta x \tag{4.5}$$

where $\beta$ is the low-pass filter state variable and

$$\mathbf{A}_{f_d} = \begin{bmatrix}-2\end{bmatrix}, \ \mathbf{B}_{f_d} = \begin{bmatrix}2\end{bmatrix}, \ \mathbf{C}_{f_d} = \begin{bmatrix}4\end{bmatrix}.$$

A state-space model combining the 1DOF model of the system and the two filters with their three non-physical state variables introduced in (4.2) to (4.5) can thus be defined as :

$$\dot{\mathbf{x}} = \mathbf{A}\mathbf{x} + \mathbf{B}\mathbf{u} + \mathbf{G}w$$

where $w$ is the unknown white process noise. The system matrices $\mathbf{A}$, $\mathbf{B}$ and $\mathbf{G}$ can be written as :

$$\mathbf{A} = \begin{bmatrix} 0 & 1 & 0 & 0 & 0 \\ -k/m & -b/m & 0 & 0 & 0 \\ \multicolumn{2}{c}{\mathbf{B}_{f_a}\begin{bmatrix}-k/m & -b/m\end{bmatrix}} & \multicolumn{2}{c}{\mathbf{A}_{f_a}} & \begin{matrix}0\\0\end{matrix} \\ \mathbf{B}_{f_d} & 0 & 0 & 0 & \mathbf{A}_{f_d} \end{bmatrix},$$

$$\mathbf{B} = \begin{bmatrix} 0 & 1/m & \mathbf{B}_{f_a}^T/m & & 0 \\ 0 & -1 & 0 & 0 & 0 \end{bmatrix}^T,$$

$$\mathbf{G} = \begin{bmatrix} 0 & 1 & 0 & 0 & 0 \end{bmatrix}^T.$$

The state vector $\mathbf{x}$ and the known inputs vector $\mathbf{u}$ are defined as :

$$\mathbf{x} = \begin{bmatrix} \Delta x & \Delta\dot{x} & \alpha_1 & \alpha_2 & \beta \end{bmatrix}^T,$$

$$\mathbf{u} = \begin{bmatrix} f & \ddot{x}_f \end{bmatrix}^T,$$

where $\ddot{x}_f$ is the cabin floor acceleration which can be approximated using the measure $\ddot{x}_{f,\text{mes}}$ of an accelerometer corrupted with noise $v_f$.

The control variable is assumed to be a pure vertical force $f$ directly applied to the system because the dynamics of the electric motor (driven at constant speed) do not affect the system as long as clutches are used in continuous slippage. Moreover, as the 1DOF model of the system is identified experimentally using the actuator, no hysteresis compensation is applied to the clutches, because the effects of clutches dynamics are comprised within the

1DOF model. For a gain matrix $\mathbf{K}$ defined according to LQG theory, the state-feedback law :

$$f = -\mathbf{K}\mathbf{x}$$

minimizes the cost function formulated here by :

$$J(f) = \int_0^\infty \left[ (\ddot{x}_w)^2 + (q_d \Delta x_w)^2 + (q_f f)^2 \right] dt \tag{4.6}$$

which penalizes the driver acceleration $\ddot{x}_w$ weighted with ISO-2631-1, the low-pass filtered relative displacement $\Delta x_w$ and the actuator force $f$. The weighting gains $q_d = 10^0$ on the weighted relative displacement and $q_f = 10^{-4}$ on the actuator force were experimentally set to limit seat travel (as qualitatively perceived by the driver) and to limit the actuator force to a value that did not result in system instabilities. Equation 4.6 can alternatively be written as :

$$J(f) = \int_0^\infty \left[ \mathbf{x}^T \mathbf{Q} \mathbf{x} + \mathbf{R} f^2 \right] dt$$

where $\mathbf{Q}$ and $\mathbf{R}$ are determined from (4.6) such that :

$$\mathbf{Q} = \begin{bmatrix} 0 & 0 & 0 & 0 & 0 \\ 0 & 0 & 0 & 0 & 0 \\ 0 & 0 & (\mathbf{C}_{f_a})_1^2 & (\mathbf{C}_{f_a})_1 (\mathbf{C}_{f_a})_2 & 0 \\ 0 & 0 & (\mathbf{C}_{f_a})_1 (\mathbf{C}_{f_a})_2 & (\mathbf{C}_{f_a})_2^2 & 0 \\ 0 & 0 & 0 & 0 & \left(q_d (\mathbf{C}_{f_d})_1\right)^2 \end{bmatrix}$$

where subscripts indicate the index of a matrix element and

$$\mathbf{R} = \left[ q_f^2 \right].$$

The feedback matrix $\mathbf{K}$ is derived from the solution $\mathbf{S}$ to the Riccati equation [36] :

$$\mathbf{A}^T \mathbf{S} + \mathbf{S}\mathbf{A} - (\mathbf{S}\mathbf{B})\mathbf{R}^{-1}(\mathbf{B}^T \mathbf{S}) + \mathbf{Q} = \mathbf{0}$$

as given by :

$$\mathbf{K} = \mathbf{R}^{-1}(\mathbf{B}^T \mathbf{S}).$$

A Kalman filter uses the difference $\mathbf{y}_{\text{error}}$ between the output vector $\hat{\mathbf{y}}$ predicted by the 1DOF seat-driver model and the output vector $\mathbf{y}$ of the system to approximate the state vector $\mathbf{x}$ of the system as $\hat{\mathbf{x}}$ (Fig. 4.7). The output vector $\mathbf{y}$ is provided by measurements of a cable capacitive encoder and an accelerometer corrupted with a noise vector $\mathbf{v}$. The

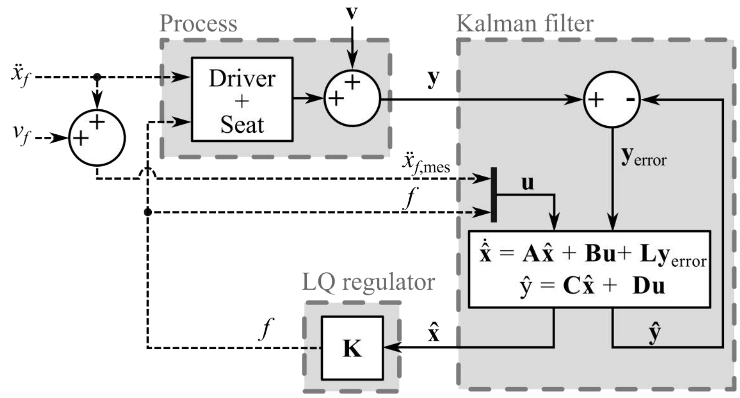


Figure 4.7 Control diagram of the active suspension. The measured process output $\mathbf{y}$ corrupted with noise $\mathbf{v}$ is processed with a Kalman filter which then passes on the estimated state $\hat{\mathbf{x}}$ to the LQ regulator. The LQ regulator imposes vertical force $f$ to the seat by applying the static controller gain matrix $\mathbf{K}$ to $\hat{\mathbf{x}}$.

cable encoder measures the relative displacement $\Delta x_{\text{mes}}$ between the seat and the vehicle floor. The accelerometer measures the seat's rigid frame acceleration $\ddot{x}_{\text{mes}}$. If the 1DOF model were to perfectly represent the system, then :

$$\underbrace{\begin{bmatrix} \Delta x_{\text{mes}} \\ \ddot{x}_{\text{mes}} \end{bmatrix}}_{\mathbf{y}} = \mathbf{C}\mathbf{x} + \mathbf{D}\mathbf{u} + \mathbf{v}$$

where $\mathbf{y}$ is the measured system outputs, $\mathbf{v}$ is the measurement noise vector (assumed to be white gaussian, non-correlated signals) and

$$\mathbf{C} = \begin{bmatrix} 1 & 0 & 0 & 0 & 0 \\ -k/m & -b/m & 0 & 0 & 0 \end{bmatrix}, \ \mathbf{D} = \begin{bmatrix} 0 & 0 \\ 1/m & 0 \end{bmatrix}.$$

The process noise covariance matrix $\mathbf{Q}_k$ and the measurement noise covariance matrix $\mathbf{R}_k$ are defined as :

$$\mathbf{Q}_k = E(w^2), \ \mathbf{R}_k = E(\mathbf{v}\mathbf{v}^T).$$

The matrix $\mathbf{R}_k$ was derived from the sensors data when the system sits motionless and no floor perturbations are present such that :

$$\mathbf{R}_k = \begin{bmatrix} 2.3\times10^{-7} & 0 \\ 0 & 3\times10^{-3} \end{bmatrix}.$$

However, the matrix $\mathbf{Q}_k$ was set experimentally to a single value of 0.1 which reflects the modeling errors associated with the 1DOF model. A state estimate $\hat{\mathbf{x}}$ can then be found as :

$$\dot{\hat{\mathbf{x}}} = \mathbf{A}\hat{\mathbf{x}} + \mathbf{B}\begin{bmatrix} f & \ddot{x}_{f,\text{mes}} \end{bmatrix}^T + \mathbf{L}\mathbf{y}_{\text{error}}$$

where $\mathbf{y}_{\text{error}}$ is the difference between measured outputs $\mathbf{y}$ and the 1DOF model outputs $\hat{\mathbf{y}}$ such that :

$$\hat{\mathbf{y}} = \mathbf{C}\hat{\mathbf{x}} + \mathbf{D}\begin{bmatrix} f & \ddot{x}_{f,\text{mes}} \end{bmatrix}^T.$$

Supposing no cross-correlation between process and measurement noise, the filter gain $\mathbf{L}$ is derived from the solution of an algebraic Ricatti equation incorporating $\mathbf{R}_k$ and $\mathbf{Q}_k$ [36].

## 4.6 Active Control

### 4.6.1 Laboratory Tests

#### Methodology

Tests were first undertaken in a laboratory environment with the use of a vibrating platform recreating the cabin floor profile of a dump truck (International®) performing off-road duty on a quarry road for a 30 s segment. The vibrating platform was actuated by two hydraulic actuators controlled in closed-loop with the feedback of two Linear Variable Differential Transformers (LVDT). The controlled slippage MR actuator was fitted to the back of a Corsair™ truck seat (National Seating™) equipped with a passive air-spring. When the active suspension was activated, the damper normally placed in parallel with the seat air-spring was removed. Passive test runs, on the other side, alternated use of the damper. Tests with an undamped passive suspension were used to show that gains in performance using the active suspension were not merely obtained by the removal of the seat damper.

A capacitive cable encoder measured the seat relative displacement and two accelerometers were respectively fixed to the platform and to the rigid frame of the seat (Fig. 4.8). All actuator components and sensors are powered by two 12 V batteries placed in series. A current probe (1146A - Keysight technologies) measured the output current of the batteries to assess actuator power intake. All tests were performed with the same 68 kg driver. In accordance with the ISO-10326-1 standard, a seat pad equipped with an accelerometer placed directly underneath the driver was used to measure the actual vibrations transmitted to the driver. A detailed list of equipment used in experiments is provided in Table 4.2. The LQG controller was implemented in a real-time Speedgoat target machine through a Matlab/Simulink interface.

### Results

As expected from acceleration profiles acquired on a dump truck, power spectral density (PSD) of the vibrating platform acceleration exhibits two dominant frequency components close to 1.5 and 10 Hz (Fig. 4.9).

Acceleration transmissibility curves (Fig. 4.10) are obtained by dividing the PSD of the seat pad acceleration by the PSD of the cabin floor acceleration. The result is then averaged by convolution with a 0.5 octave large Hanning window.

For frequencies up to 4-5 Hz, the driver experiences equal or higher vibrations when he sits on a passively suspended seat equipped with a damper than if the suspension were totally rigid. In comparison, the active suspension effectively attenuates vibrations in the same frequency range with a RMS force of 81 to 96 N. To generate this force, a RMS current between 0.81 and 0.96 A is applied to the clutches. Even if the damper is removed from the passive suspension, attenuation levels similar to those with the active suspension cannot be achieved, especially for frequencies ranging from 1 to 2 Hz. Acceleration transmissibility curves for the damped and undamped passive suspensions demonstrate that the use of a damper attenuates the seat resonance around the expected resonant frequency of 1.75 Hz, but causes increased vibrations over the rest of the frequency spectrum. Since the ISO-2631-1 frequency weighting filter peaks around 7 Hz (Fig. 4.6), a higher RMS weighted acceleration and SEAT ratio are therefore associated with the damped passive suspension compared to the undamped one (Table 4.3). The active suspension loosens this trade-off between seat travel associated with vibrations at low frequencies and transmissibility. To allow the driver to keep contact with the pedals, it can force the seat to follow the platform motion under 1 Hz, but still better attenuates vibrations than a passive suspension at any higher frequencies.

The SEAT ratio is defined as the RMS seat acceleration over the RMS acceleration of the vibrating platform both weighted with ISO-2631-1 [26]. For similar seat RMS travels, the

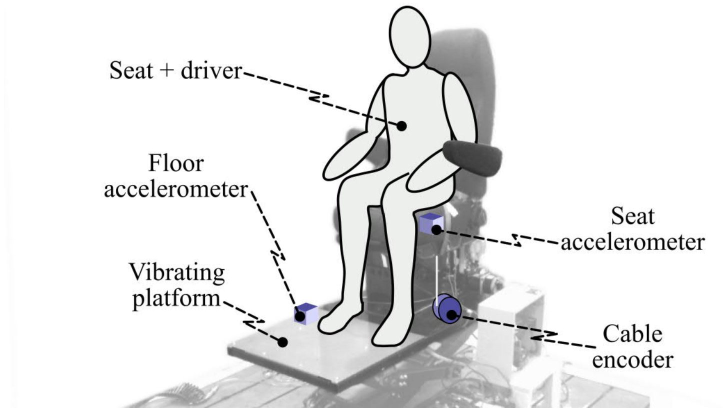


Figure 4.8 Laboratory experimental setup with a truck seat mounted on a vibrating platform. The whole system is equipped with a first accelerometer fixed to the platform, a second accelerometer fixed to the seat rigid frame and a cable encoder measuring the relative seat displacement.

Table 4.2 Equipment used for experiments

| **Equipment type** | **Key features** | **Product number** | **Manufacturer** |
|---|---|---|---|
| *Hydraulic system* | | | |
| Cylinder | 0-60 Hz<br>4450 N max.<br>51 mm stroke | 1107-4 | Xcite Systems |
| LVDT | 0-75 Hz | 0244-0000 | Trans-Tek |
| *Accelerometers* | | | |
| Seat pad | 0-200 Hz | 4030-006 | Measurement Specialties |
| Seat frame | 0-100 Hz | ADXL105EM | Analog Devices |
| Floor | 0-100 Hz | ADXL105EM | Analog Devices |
| *Encoder* | 2048 pulse/rot. | AMT102 | CUI INC |

active suspension can achieve SEAT levels 2 to 3 times smaller than the passive suspensions (Table 4.3).

### 4.6.2 Road Tests

#### Methodology

The goal of on-road tests was to assess the performance of the active suspension on a road and vehicle different than the laboratory platform used for tuning the gains of the LQG cost function. Any bias introduced by undesired dynamics of the platform, which has its own compliance and resonance, is also removed. Tests were conducted on a Peterbilt 379 highway truck rolling on a roadway in Eastern Canada. The same seat as in the labora-

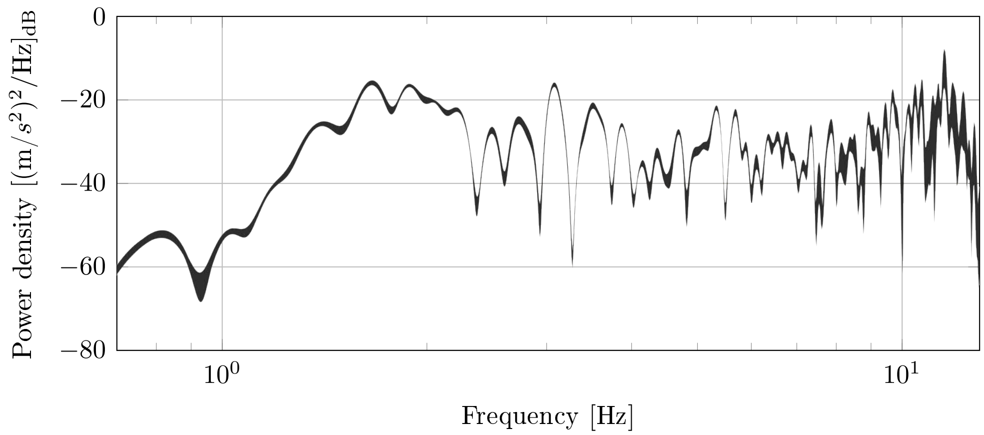


Figure 4.9 Power spectral density of truck floor acceleration reproduced by the vibrating platform. The shaded area represents the envelope of 15 different spectra obtained from 15 repetitions of the same 30 s segment.

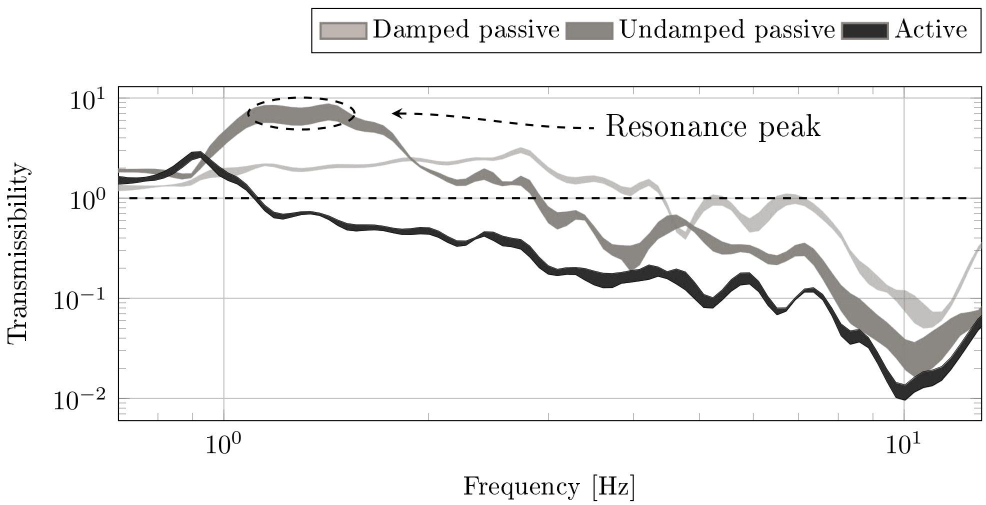


Figure 4.10 Transmissibility curves for the damped passive, undamped passive and active seat suspensions in a dump truck cabin vibratory environment recreated by a vibrating platform. Each shaded area represents the envelope of 5 different spectra obtained from 5 repetitions of the same 30 s segment.

Table 4.3 Range (min.-max.) of results obtained on a vibrating platform

| **Suspension type** | $a_{\mathbf{w},\ \mathbf{RMS}}[\mathbf{m/s^2}]$ | **SEAT** | $\mathbf{\Delta x}_{\mathrm{mes,RMS}}$[mm] |
|---|---|---|---|
| Rigid (floor accel.) | 0.94-1.07 | 1 (ref.) | N/A |
| Damped passive | 0.76-0.80 | 0.80-0.85 | 2.71-2.98 |
| Undamped passive | 0.58-0.59 | 0.54-0.56 | 9.15-10.12 |
| Active | 0.30-0.30 | 0.28-0.28 | 6.87-6.92 |

tory tests was bolted to the passenger side of the truck cabin with the same 68 kg human subject as in laboratory tests.

### Results

The truck cabin floor acceleration PSD features two dominant frequency components at about 2 and 8 Hz (Fig. 4.11). As results are based on 5 consecutive 30 s road segments rather than on one repeated segment, the PSD now displays up to 20 times larger variation than in laboratory.

Unlike the active suspension, the damped passive suspension does not attenuate vibrations over most of the frequency spectrum (Fig. 4.12). The undamped passive suspension however does not have a seat resonance like in laboratory tests. A possible explanation would be that the overall level of vibrations on the cabin floor is 30 % lower than in laboratory simulations and is too low to maintain seat resonance. This non-resonant response echoes in the acceleration transmissibility curves of the damped and undamped suspensions as they merge into one another. On average though, the active suspension still has an overall SEAT ratio about 2 times less than a passive suspension with a RMS force of 44 to 96 N (Table 4.4) which is consistent with results reported by laboratory tests. To generate this force, a RMS current between 0.44 and 0.96 A is applied to the clutches.

## 4.7 Discussion

As demonstrated in this article, the active suspension can improve driver comfort in a truck rolling on a quarry road by lowering the vertical weighted acceleration from 0.78 m/s$^2$ RMS down to 0.30 m/s$^2$ RMS (Table 4.3). According to the ISO-2631-1 standard standard, a driver using the MR cable active seat exposed to off-road floor vibrations could work for more than 22 h before entering the caution zone rather than 2-3 h for a passive suspension (Fig. 4.1). Based on the data recorded on roadway-like conditions, vibration levels are too weak to have a significant health impact on a driver working on a 8 h shift even though the active suspension attenuates vibrations better than a passive suspension by a factor of 2. To reduce on-road results variability, future tests should be undertaken over one reproducible segment of the road.

The weighting gains $q_d$ and $q_f$ defining the cost function (equation 4.6) used in this work were selected to associate a much larger cost to the weighted acceleration $\ddot{x}_w$ transmitted to the driver than to the seat weighted relative displacement $\Delta x_w$. Hence, for laboratory tests, the RMS relative displacement of the actively suspended seat is larger than that of

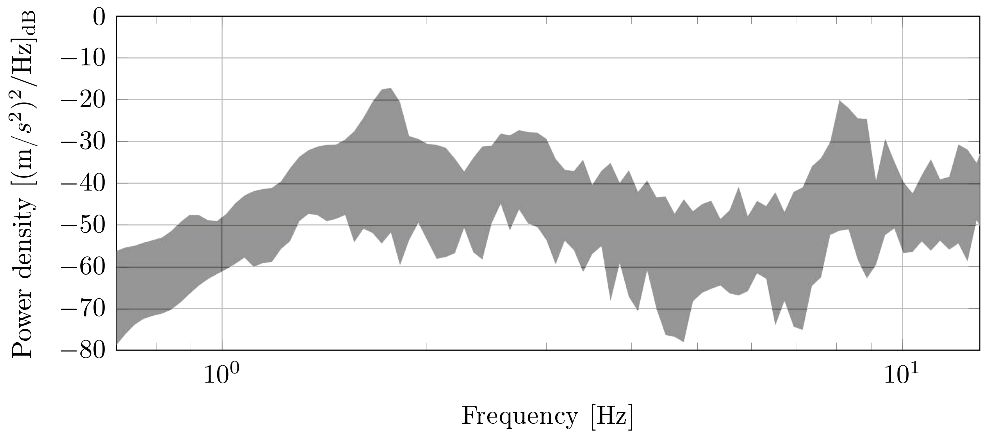


Figure 4.11 Power spectral density of highway truck floor acceleration. The shaded area represents the envelope of 15 different spectra obtained from 15 consecutive 30 s runs.

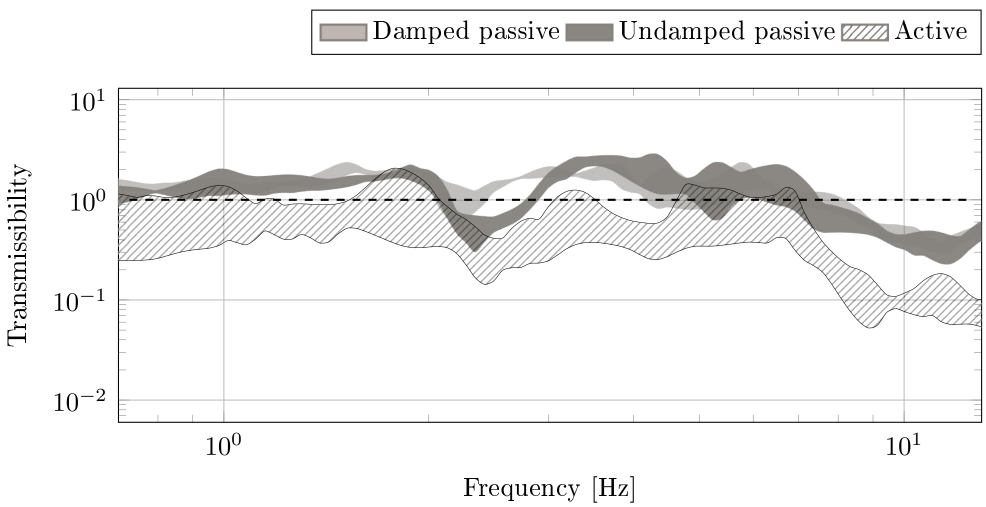


Figure 4.12 Transmissibility curves for the damped passive, undamped passive and active seat suspensions in a highway truck cabin vibratory environment. Each shaded area represents the envelope of 5 different spectra obtained from 5 consecutive 30 s runs.

Table 4.4 Range (min.-max.) of results obtained on a roadway

| **Suspension type** | $a_{\mathbf{w},\,\mathbf{RMS}}$**[m/s²]** | **SEAT** | $\mathbf{\Delta x}_{\text{mes,RMS}}$[mm] |
|---|---|---|---|
| Rigid (floor accel.) | 0.43-0.63 | 1 (ref.) | N/A |
| Damped passive | 0.36-0.46 | 0.84-0.87 | 0.24-0.57 |
| Undamped passive | 0.34-0.37 | 0.75-0.82 | 0.29-0.70 |
| Active | 0.19-0.32 | 0.40-0.53 | 0.74-1.47 |

the damped passive seat, yet smaller than that of the undamped passive seat (Table 4.3). For road tests, although the RMS relative displacement of the actively suspended seat is larger than that of both the damped and undamped passive seats, its magnitude is so small (less than 1.5 mm) that it is to be neglected (Table 4.4).

A rough benchmarking of the proposed active seat suspension with active and semi-active solutions reported in literature is offered in table 4.5. Because a detailed comparison (e.g. using transmissibility curves) cannot be made due to a lack of appropriate data in the literature, a global comparison based on SEAT ratios for various road conditions is proposed here instead.

Over both rough and smooth roads, the MR cable active suspension offers a performance similar to that of commercially available products which use electromagnetic (Bose Ride®) [6, 30, 52, 70] and hydraulic (John Deere Active Seat™) [31] actuators. The controlled slippage MR actuator can also be benchmarked with respect to an active suspension which uses only two geared electric motors [68]. In terms of cost, an active suspension using two electric motors is likely to be in the same price range as one using just one electric motor and two MR clutches as proposed in this article. In terms of controller complexity, using geared motors without MR clutches for an active suspension application requires to introduce a disturbance observer in the controller and to act upon the approximated disturbance state which can cause chattering [68]. Such friction compensation is not required for the controlled slippage MR actuator. Finally, in terms of performance, laboratory results presented in this work show that the active suspension reduces the SEAT ratio of a damped passive seat by 66 % on average compared to a reduction of 34 % reported for the active suspension based on two geared motors [68]. This difference might be explained by the fact that the suspension's controller cannot perfectly cancel disturbances due to the actuator's friction.

Since the fully active controlled slippage MR actuator tested in this work uses two MR clutches in its design, it can be relevant to benchmark its performance with respect to MR dampers even though these devices are only semi-active. Their performance seems however to vary widely in the literature as shown in table 4.5 [46, 59, 65]. With 66 % reduction, a fully active controlled slippage MR actuator, just like other commercially available active suspensions, attenuates vibrations better than suspensions using semi-active MR dampers.

In its current form, the proposed MR actuator has a maximal output force of 1000 N. Laboratory tests performed with a 68 kg occupant and considering rough-quarry road

Table 4.5 Mean experimental performance of different active and semi-active seat suspensions reported in literature for rough and smooth roads

| **Ref.** | **Suspension Type** | **Vehicle Type** | **Passive SEAT** | **A/S-A SEAT** | **Improv. %** |
|---|---|---|---|---|---|
| *Rough Roads (Bumpy / Vibrations close to seat resonance frequency)* | | | | | |
| [70] | A, linear EM (Bose) | A | 0.81 | 0.27 | 67% |
| **-Proposed MR Actuator-** | | **A** | **0.83** | **0.28** | **66%** |
| [6] | A, linear EM (Bose) | A | 0.75 | 0.26 | 65% |
| [31] | A, Hydraulic (John Deere) | B | 0.64 | 0.27 | 57% |
| [62] | A, Pneumatic | C | 0.95 | 0.48 | 50% |
| [68] | A, geared EM | C | 0.77 | 0.51 | 34% |
| [46] | S-A, MR damper | C | 1.73 | 1.22 | 29% |
| [59] | S-A, MR damper | D | 0.88 | 0.63 | 28% |
| [65] | S-A, MR damper | C | 1.10 | 1.05 | 5% |
| *Smooth Roads (Highway / Freeway like conditions)* | | | | | |
| [30] | A, linear EM (Bose) | A | 0.92 | 0.45 | 51% |
| **-Proposed MR Actuator-** | | **A** | **0.86** | **0.47** | **46%** |
| [52] | A, linear EM (Bose) | A | 1.05 | 0.62 | 42% |
| [70] | A, linear EM (Bose) | A | 0.59 | 0.36 | 40% |
| [1] | A, Hydraulic | C | 0.60 | 0.40 | 32% |

**Suspension types :** A- Long-haul truck, B- Tractor
C- Generic commercial heavy-duty vehicle, D- Bus
**Vehicle types :** A- Active, S-A- Semi-Active
EM- Electromechanical

conditions suggest that the force of the actuator could be limited to 277 N without any significant loss of suspension effectiveness. This indicates that the actuator could support heavier drivers and/or be downsized considerably. Further laboratory and on-road tests with drivers of various weight, sizes and postures will be undertaken to confirm the proper maximal force requirement for the actuator and further minimize the weight of the actuator.

The laboratory tests with the quarry road data show an average power requirement of 86 W RMS, which is higher than the reported 50 W RMS of the Bose Ride® (unknown road conditions) [70]. Because the MR clutches are used in continuous slippage, the fluid is constantly dissipating power equal to the product of transmitted torque by the differential speed of the clutch. Data show that 60 % of the total power consumption, or 52 W, is due to clutch slippage. Considering that the input motor speed was held constant in this study, there is a potential to drastically reduce power consumption by controlling the speed of the electric motor to minimize slippage depending on operating conditions.

On a completely different scale, semi-active suspensions using MR dampers do consume less power. Although exact power consumption figures of MR dampers are scarcely provided in literature, Hiemenz has reported a maximum applied current of 1.5 A and a maximum applied voltage of 10 V for an helicopter semi-active seat suspension [49] thus suggesting a peak current of 15 W. McManus also reported a maximum current of 1.5 A applied to the terminals of a Lord MR damper used in a heavy highway vehicle [65]. With a typical coil resistance ranging between 5 and 7 Ω according to the manufacturer, the peak current approximately lies between 11 and 16 W. In the context of heavy vehicles however, this difference in power consumption might be small when put in perspective with the power drawn by other accessory in the vehicle. According to the American National Renewable Energy Laboratory for instance, the air-conditioning of a small sedan is likely to require 1000 W in steady-state [34].

One challenge related to power consumption is the limited lifespan of MR fluids [12]. Interpolating on lifespan predictions based on the maximum allowable amount of energy dissipated by units of fluid volume (ranging between 6 and 10 MJ/mL), the MR fluid would be expected to last between 1850 and 3090 h if it was continuously solicited under the laboratory conditions [12, 103]. Since fluid lifespan is highly dependent on the clutches differential speed, important gains in fluid durability are expected from a variable-speed control of the motor.

In this study, robustness of the controller to parametric uncertainties was not investigated as the purpose was to demonstrate the active suspension capabilities. In future versions of the controller, an adaptive precompensator based on the inverse of the approximated cabin floor acceleration signal could be used to enhance the active suspension performance for any road conditions. The controller could also incorporate real-time identification of the seat-driver system as the seat response is dependent on driver physiology, posture and seat adjustments [7]. Other modern control algorithms which might be more robust to parametric uncertainties include $H_2$ [10], $H_\infty$ [108], fuzzy logic control [72] and neural networks [44]. Another promising avenue for improving the performance of the proposed active suspension would be to optimize the different physical parameters of the seat suspension in parallel with the parameters of the controller as proposed for instance by Digumarti & al. for a legged robot [29].

One more potential advantage of using a controlled slippage MR actuator is its ability to act on multiple degrees of freedom using a single mechanical power source [35]. This actuator could have an edge in vehicles such as garbage trucks for which horizontal vibration levels are of the same order of magnitude as vertical vibration levels [63].

## 4.8 Conclusion

This article presents the first experimental demonstration of a fully active MR actuator used for an active seat suspension as opposed to a typical semi-active MR damper. A fixed-gain LQG controller was designed to control a MR cable actuator used in a seat suspension. Experiments show that the proposed active suspension attenuates vibrations 2 to 3 times better than a damped or undamped passive suspension respectively for a dump truck rolling on a quarry road and for a highway truck rolling on a roadway.

Achieved vibration attenuation and power consumption levels fall in line with reported specifications of commercially available active suspensions. Unlike existing commercial active suspensions, use of a simple BLDC motor belted to two MR clutches allows the actuator to be made into a small and inexpensive embodiment without trading-off dynamic performance. Without MR clutches, the actuator would be unable to completely compensate the parasitic torque of the motor's gearbox which would directly affect the actuator's performance. On a different scale, even though the tested actuator is bigger and heavier, consumes more energy and is likely to be more expensive than MR dampers alone, these downsides are counterweighted by a better dynamic performance which can be significant under harsh road conditions. Besides, since the actuator presented in this work could fit underneath a standard truck seat and given the electric load of other auxiliary devices used in heavy vehicles, then the size, weight and energy consumption of the actuator are unlikely to be significant issues in a practical setting.

Future studies should include variable speed control of the actuator's motor to lengthen MR fluid lifespan and identification of the maximal required force to maintain performance in order to further minimize actuator weight. Robustness to parametric uncertainties could also be addressed through adaptive control to road conditions and real-time system identification. Subsequent tests should thus be conducted on several drivers with varied postures, heights and weights as well as for different road profiles or vehicles.

# CHAPITRE 5

# Évaluation d'une Stratégie de Contrôle minimisant la Consommation Énergétique et Augmentant la Durée de Vie d'un Actionneur MR

## 5.1 Avant-Propos

Le développement et les tests d'un contrôleur minimisant la consommation énergétique d'un actionneur MR et allongeant la durée de vie du fluide MR s'appuient grandement sur une étude de cas qui utilise la suspension active de siège présentée précédemment.

Cet article aborde le développement d'un modèle fidèle pour reproduire le comportement du système de suspension. Ce modèle permet de prédire la performance de l'actionneur MR pour différentes configurations du contrôleur. Ainsi, un simple asservissement du moteur qui vise à maintenir une vitesse de glissement constante peut, pour un même niveau d'atténuation des vibrations, réduire la quantité d'énergie dissipée dans les embrayages MR.

**Titre :** Controller Trade-Offs for Continuous Slippage Magnetorheological Actuators

**Traduction française du titre :** Compromis de Contrôle pour les Actionneurs Magnétorhéologiques à Glissement Continu

**Revue dans laquelle l'article a été soumis :** Journal of Low Frequency Noise, Vibration and Active Control

**Auteurs :**

- Marc-André Bégin, étudiant à la maîtrise

- Alain Berry, Professeur

- Patrick Chouinard, étudiant au postdoctorat

- Jean-Sébastien Plante, Professeur

**Date de soumission :** Non soumis

**État de l'acceptation :** L'article tel que présenté ci-dessous sera soumis au *Journal of Low Frequency Noise, Vibration and Active Control*.

**Résumé de l'article :** Les actionneurs magnétorhéologiques (MR) à glissement continu, avec leur faible inertie apparente et leur bande passante élevée en force, offrent des avantages uniques dans des domaines spécialisés de la robotique tels que les dispositifs haptiques. Leur nature de glissement implique cependant que de l'énergie est constamment dissipée dans le fluide, ce qui a des effets négatifs sur la consommation énergétique et la durée de vie du fluide. Alors que la plupart des ouvrages traitent ces problèmes en essayant d'améliorer la conception des fluides MR ou des actionneurs, cet article propose un système de contrôle visant à limiter la puissance dissipée en glissement dans les embrayages. Les modèles dynamiques et énergétiques développés dans le processus peuvent prédire les résultats expérimentaux. Ces résultats montrent qu'un contrôle limitant le glissement de l'actionneur peut entraîner une diminution de la consommation énergétique de 20% et augmenter la durée de vie du fluide de 40% sans une diminution significative des performances dynamiques de l'actionneur.

## 5.2 Abstract

Continuous slippage magnetorheological (MR) actuators, with their low apparent inertia and high force bandwidth, can provide unique advantages in specialized areas of robotics such as haptic devices. Their slippage nature however implies that power is constantly dissipated in the fluid which has negative effects on power consumption and fluid lifetime. Whereas most of the works in literature address these issues by trying to improve the MR fluids or the actuators design, this paper proposes a control scheme aimed at limiting the slipping power dissipated in the actuator clutches in a vibration control application consisting of an active seat suspension for heavy vehicles. Dynamic and energetic models developed in the process can accurately predict experimental results. These results show that a limited slip control of the actuator can lead to a decrease in power consumption of 20 % and increase the fluid lifetime by 40 % without a significant decrease in the actuator's dynamic performance, underscoring the need for future work on lifetime and efficiency oriented control of MR actuators.

## 5.3 Introduction

Direct drive electrical motors are today's gold standard for high bandwidth applications. However, they are limited to a torque/volume ratio of about 30 kN/m$^3$ due to intrinsic limitations of the technology such as the need for an external surface area sufficiently large to dissipate heat from Joule losses in the motor windings [51]. This restriction can be problematic for space limited or price sensitive applications as the price of a general purpose electric motor is directly proportional to its size. Although gearing the motor output would usually be a simple and inexpensive solution to this problem, gears used in sensitive robotic applications such as haptic devices lead to an unacceptable increase of the actuator's friction, backlash and flexibility which all hinder the controllability of the system.

Another solution to this problem is to decouple the dynamics of the geared electric motor from the load using magnetorheological (MR) clutches placed between the gearbox and the load. MR clutches transmit a variable amount of torque through changes in the apparent viscosity of MR fluid interfaces when a magnetic field is applied. In "controlled slip MR actuators", the clutches are maintained in slippage and used to transmit only the torque required by the application thus eliminating the parasitic torque generated by the gearbox. Unlike MR brakes or MR dampers which can only dissipate energy, controlled slip

MR actuators can be used to actively transfer power to the load and have been successfully implemented in applications such as haptic devices [61, 83, 97, 106], flight actuators [21, 55] and for an active seat suspension [22].

The boosted performance of MR actuators comes at the cost of fluid degradation over time. Although exact aging mechanisms remain unclear [28], the surest predictor for MR fluids lifetime proposed so far is based on the maximum amount of energy per unit volume that can be dissipated in the fluid with reported numbers ranging from $10^6$ to $10^7$ J/mL [12, 103]. Moreover, power losses due to MR clutches slippage and Joule's losses from the clutches inner coil inevitably makes MR actuators less energy efficient than geared motors alone.

Although many studies have focused their work on the improvement of MR fluids composition [54, 102] for extended life or hardware improvements [47], lifetime or efficiency oriented control of MR actuators have received no attention in literature so far. Yet, numerous efficiency oriented control approaches have been proposed for hydraulic actuators [18, 84] which are somewhat analogous to MR actuators.

Indeed, an analogy between MR and hydraulic actuators can be drawn using a bond graph framework [9]. The geared motor of an MR actuator controlled in closed-loop imposes an angular velocity $\omega_{\text{in}}$ at the clutch's input so that it can roughly be modeled as a pure source of flow $S_f$ (Fig. 5.1). This source of flow provides mechanical power to a clutch represented as a common effort junction with a resistive element $R_{\text{MR}}$, a function of the applied magnetic flux density. As long as the actuator is in positive continuous slippage, ($\omega_{\text{in}} > \omega_{\text{out}}$) $R_{\text{MR}}$ imposes a controlled torque $T_c$ both to the load and to the geared motor such that the whole MR actuator approaches a pure effort source $S_e$.

Likewise, the pump (and driving motor) of a hydraulic actuator provides a controlled upstream pressure $p_{\text{pump}}$ to a valve. This valve has a downstream pressure $p_{\text{load}}$ and is represented as a common flow junction with restriction $R_c$, a function of the valve opening. Is this case, the pump can be roughly seen as a source of effort whereas $R_c$ now imposes a flow $q$ to both the pump and the load such that the whole hydraulic actuator approaches a source of flow as long as the pump provides excess pressure ($p_{\text{pump}} > p_{\text{load}}$).

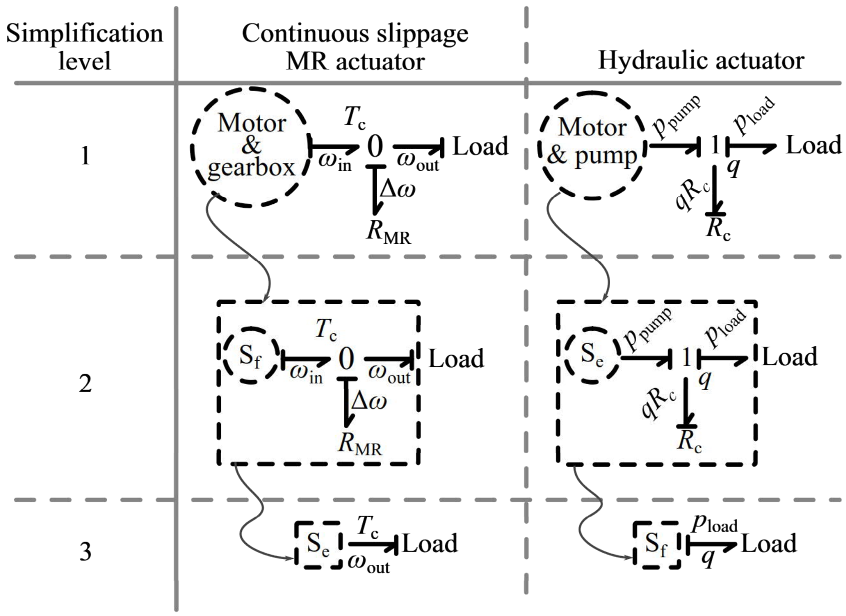


Figure 5.1 Bond graphs synthesis of a continuous slippage MR actuator and a hydraulic actuator with 3 levels of simplification.

In both instances, the presence of a fast responding resistance allows to increase the overall bandwidth of the actuator as long as $\omega_{\text{in}}$ or $p_{\text{pump}}$ are in excess. However, because power losses through an hydraulic actuator's valve or through an MR actuator's clutch increase alongside $p_{\text{pump}}$ and $\omega_{\text{in}}$, there exists a fundamental controller design trade-off between the overall performance of each actuator and its power consumption. An additional trade-off also exists between these actuators lifetime and performance as the energy dissipated in the clutch's fluid will eventually lead to fluid degradation.

The objective of this paper is to underscore the benefits of using an energy and/or lifetime conscious control strategy for an MR actuator. Through the case study of an MR actuator used in an active suspension, the widely used strategy of driving the motor at a constant speed is contrasted with a first attempt to minimize slipping power losses in the clutches using a limited slip control law.

System models are first introduced in Section 5.4 for both being able to correctly predict the actuator's dynamic performance, power consumption and lifetime and to serve as a basis for developing the actuator's controller presented in Section 5.5. A set of experiments is conducted on a bench test detailed in Section 5.6. Finally in Section 5.7, trade-offs predicted by simulation are discussed and validated.

## 5.4 Models

Selecting an MR actuator's control trade-off between its dynamic performance, power consumption and fluid longevity is highly application dependent. This paper focuses on an MR actuator used in an active seat suspension for heavy vehicles [4, 22] where the oscillating load (i.e. the driver and seat) is subject to frequent speed reversals. It is further assumed that the MR actuator is made of a geared electric motor sharing its output torque with two MR clutches (Fig. 5.2). Cable pulleys convert the clutches output torque into a vertical force applied on the seat which points upward or downward depending on which clutch is activated.

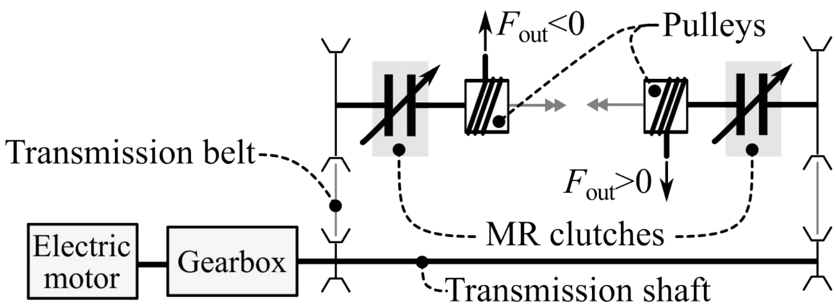


Figure 5.2 Schematics of an MR actuator with a geared motor sharing its output torque with two clutches

The two control commands of the MR actuator are the current command $u_1$ to the clutches drive and the current command $u_2$ to the electric motor drive (Fig. 5.3). Depending on the state of the cable pulleys, the input torque $T_{\text{in}}$ from the clutches may or may not be transmitted to $T_{\text{out}}$ which is seen as a load for the electric motor and the driving force $F_{\text{out}}$ of the driver-seat system. Measured states of the complete model are the seat relative position $x_{\text{rel}}|_{\text{mes}}$ and absolute acceleration $\ddot{x}_{\text{mes}}$ as well as the motor speed $\omega_m|_{\text{mes}}$.

Models developed in this section for the actuator and the driver-seat system use different levels of complexity depending on their intended purpose. A first set of nonlinear models are produced for the clutches, cable pulleys and driver-seat subsystem to accurately simulate the dynamics, power consumption and fluid lifetime of the actuator. A second set of linear models are produced for the design of the actuator's controller. A brief description and the value of all parameters used in the different models are included in Table 5.1. This model is to be valid only when the clutches are slipping ($\Delta\omega \neq 0$) such that the dynamics of the electric motor and that of the seat are decoupled from one another and only determined by the torque transmitted by the MR clutches (even though this model might seem non-causal at first sight).

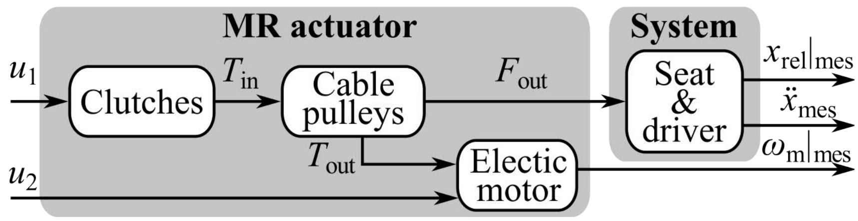


Figure 5.3 Schematics of the complete actuator and system models with underlying clutches, cables pulleys and electric motor submodels

### 5.4.1 MR Actuator Models

**MR Clutches** It is assumed that only one clutch is active when the cable pulley input torque $T_{\mathrm{in}}$ is positive and only the antagonistic one when $T_{\mathrm{in}}$ is negative. Then, for any given current command $u_1$ provided to the MR clutches electric drive, $T_{\mathrm{in}}(f)$ as a function of frequency $f$ was approximated in previous work [22] as

$$ {}_{1}T_{\mathrm{in}}\left(f\right) = k_{\mathrm{clutch}} \exp\left(2\pi\tau f j\right) \frac{f_c}{fj + f_c} u_1 \tag{5.1} $$

with a clutch current to torque ratio $k_{\mathrm{clutch}}$, pure time delay $\tau$ and first order cutoff frequency $f_c$. In developing the actuator's controller however, $T_{\mathrm{in}}$ is further simplified to the linear, $0^{\mathrm{th}}$ order approximation

$$ {}_{2}T_{\mathrm{in}} = k_{\mathrm{clutch}} u_1 \tag{5.2} $$

since the cutoff frequency $f_c$ (15 Hz) of the actuator is higher than the frequency of the oscillatory loads of this application (0-10 Hz).

**Cable Pulleys** Cables used in the cable-pulley transmissions to the seat can only transmit force while in tension. Supposing highly rigid cables and neglecting the effect of momentum transfer from the motor to the seat after a reestablished cable tension, then the force output $F_{out}$ of the cable-pulley transmission depends on the 2 discrete states of the activated clutch's cable such that

$$ {}_{1}F_{\mathrm{out}} = \begin{cases} k_{\mathrm{pulley}} T_{\mathrm{in}}, & \text{if the cable is stretched} \\ 0, & \text{if the cable is loose.} \end{cases} \tag{5.3} $$

Table 5.1 Model Parameters

| **Symbol** | **Value** | **Short description** |
|---|---|---|
| *Clutches* | | |
| $k_{\text{clutch}}$ | 2.48 N·m/A | Current to torque ratio |
| $\tau$ | 2 ms | Pure time delay |
| $f_c$ | 15 Hz | Cutoff frequency |
| $R_c$ | 0.1 Ω | Coil resistance |
| *Cable pulleys* | | |
| $k_{\text{pulley}}$ | 40.2 $\text{m}^{-1}$ | Clutch output torque to vertical force ratio |
| *Electric motor* | | |
| $J_{\text{tot}}$ | $1.84\times10^{-4}$ kg·$\text{m}^2$ | Total actuator input inertia* |
| $k_{\text{motor}}$ | $32.4\times10^{-3}$ N·m/A | Motor constant |
| $k_{\text{reduc}}$ | 15.8 | Gear ratio from motor to clutch input |
| $B_{\text{visc}}$ | $0.30\times10^{-4}$ N·m·s | Viscous coefficient |
| $T_{\text{dry}}$ | $89.4\times10^{-3}$ N·m | Dry friction torque |
| $R_m$ | 0.77 Ω | Motor coil resistance |
| *Nonlinear seat suspension* | | |
| $m$ | 100 kg | Suspended mass (human & seat) |
| $g$ | 9.81 N/kg | Earth's gravitational constant |
| $L_N$ | 10.0 cm | Distance from $A_o$ to $C_o$ |
| $L_A$ | 32.3 cm | Distance from $A_o$ to $C_o$ |
| $L_{As}$ | 15.5 cm | Distance from $A_o$ to $A_s$ |
| $L_B$ | 32.3 cm | Distance from $B_o$ to $B_n$ |
| $L_{C1}$ | 10.0 cm | Distance from $B_o$ to $C_o$ |
| $L_{C2x}$ | 13.0 cm | Horizontal distance from $C_o$ to $C_s$ |
| $L_{C2y}$ | 16.0 cm | Vertical distance from $C_o$ to $C_s$ |
| $x_{\text{rel}}\|_0$ | 27.5 cm | Initial relative position of the seat |
| $q_A\|_0$ | 11.6° | Initial value of angle $q_A$ |
| $q_B\|_0$ | 191.6° | Initial value of angle $q_B$ |
| $q_C\|_0$ | 90.0° | Initial value of angle $q_C$ |
| $A_s$ | $4.09\times10^{-3}\text{m}^2$ | Effective area of the spring |
| $p_0$ | 90 kpA | Pressure inside the spring at natural length |
| $L_s\|_0$ | 42.4 cm | Natural length of air spring |
| $b_{\text{nl}}$ | 4120 N·$\text{s}^4/\text{m}^2$ | Nonlinear air spring damping constant |
| $F_{\text{dry}}$ | 50 N | Nonlinear suspension dry friction force |
| *Linear seat suspension* | | |
| $k$ | 12 kN/m | Passive suspension stiffness |
| $b$ | 654 N·s/m | Passive suspension damping constant |

The cables are supposed to be initially stretched. Under a unidirectional control of the motor speed ($\omega_{\text{m}} > 0$), then the cable attached to the pulley of an active clutch becomes loose whenever

$$\omega_m < k_{\text{pulley}} k_{\text{reduc}} \left|\dot{x}_{\text{rel}}\right| \text{ and } T_{\text{in}} \dot{x}_{\text{rel}} > 0.$$

While the cable is still loose, the unwrapping angle $\theta_{\text{un}}$ is calculated as

$$\dot{\theta}_{\text{un}} = \theta_{\text{un}} + \text{sign}\left(T_{\text{in}}\right) \left( \frac{\omega_m}{k_{\text{reduc}}} - k_{\text{pulley}} \dot{x}_{\text{rel}} \right). \tag{5.4}$$

It then remains loose until the unwrapping angle is positive again or until the actuator no longer applies a force in the same direction as the velocity of the load ($T_{\text{in}}\omega_s < 0$). In developing the clutch controller however, it is assumed that the cables are always stretched such that

$$ {}_2F_{\text{out}} = k_{\text{pulley}} T_{\text{in}}. \tag{5.5} $$

**Electric Motor** Assuming that the clutches always remain in slippage and given the fast current response time (about 1 ms) of the motor, then the motor speed $\omega_m$ is prescribed by the dynamic equilibrium

$$ \dot{\omega}_m = \frac{\left(k_{\text{motor}} I - \frac{T_{\text{out}}}{k_{\text{reduc}}} - B_{\text{visc}}\omega_m - \frac{\omega_m T_{\text{dry}}}{|\omega_m| + 0.1\ \text{s}^{-1}}\right)}{J_{\text{tot}}}. \tag{5.6} $$

Phase commutation of the 4 poles, brushless, direct current motor used for experimentation is not included in the model, because it is irrelevant for predicting the motor's dynamics as demonstrated by comparing an open-loop response of the simulated motor against experimental data for the same arbitrary control signal $u_2$ sent to the motor (Fig. 5.4).

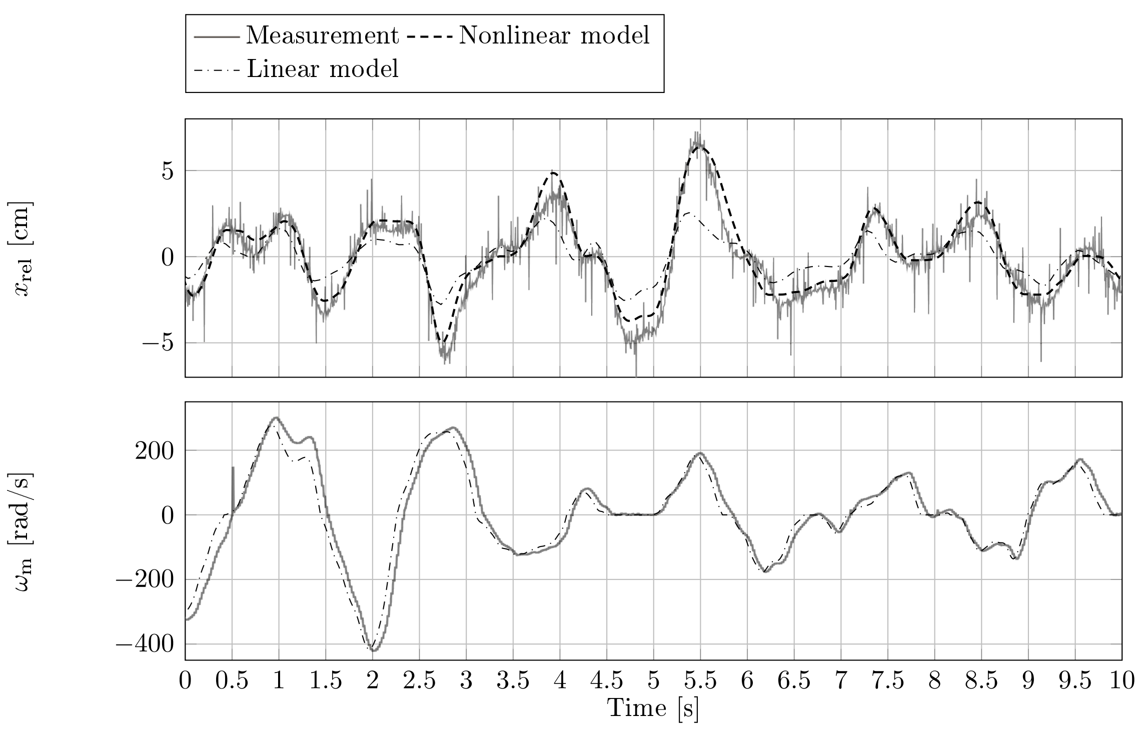


Figure 5.4 Open-loop time response of the centered seat relative position $x_{\text{rel}}$ and motor speed $\omega_m$ under arbitrary commands $u_1$ and $u_2$ without road disturbances

### 5.4.2 Driver-Seat System Models

Both the linear and the nonlinear models of the driver-seat system consider the driver and the seat to be one rigid body. The nonlinear model further uses a massless four-bar mechanism with pivot points $\mathrm{A}_o$, $\mathrm{C}_o$, $\mathrm{B}_o$ and $\mathrm{B}_n$ (Fig. 5.5-a) which approximates the design of a Corsair™ (National Seating®) truck seat suspension. An air spring is mounted on the four-bar mechanism between pivot points $\mathrm{A}_s$ and $\mathrm{C}_s$. The relationship relating the air pressure $p$ to volume $V$ inside the spring is roughly approximated by supposing air to be a perfect gas undergoing quasi-static isothermal compression-expansion such that

$$dpV = -pdV \text{ and } p_0 V_0 = pV, \tag{5.7}$$

where $p_0$ and $V_0$ are the volume and pressure of air inside the spring at its natural length $L_s|_0$. For a constant cross-section $A_s$, the net axial force $F_s$ developed by the spring is

$$F_s = pA_s. \tag{5.8}$$

Its length $L_s$ is also are expressed as

$$L_s = \frac{V}{A_s}. \tag{5.9}$$

Combining and simplifying equations 5.7 to 5.9 yields the nonlinear spring constant

$$k_{\mathrm{nl}} = -\frac{dF}{dL_s} = \frac{p_0 L_s|_0 A_s}{(L_s)^2}. \tag{5.10}$$

Supposing that the air spring has a viscous damping proportional to the 2nd power of its deformation speed, then the total force $F_{s,\mathrm{tot}}$ exerted by the air spring between $A_s$ and $C_s$ is

$$F_{s,\mathrm{tot}} = \frac{p_0 L_s|_0 A_s}{(L_s)^2} \left(L_s - L_s|_0\right) - b_{nl} \left(\dot{L}_s\right)^2. \tag{5.11}$$

The seat's suspension mechanism is also subject to friction which is modeled as a net vertical force $F_{\mathrm{fric}}$ applied on the seat. It is approximated using the numerically stable expression

$$F_{\mathrm{fric}} = -F_{\mathrm{dry}} \frac{\dot{x}_{\mathrm{rel}}}{|\dot{x}_{\mathrm{rel}}| + 0.001 \text{ m/s}}. \tag{5.12}$$

Based on the configuration parameters presented in Table 5.1 and using the generalized speed $\dot{x}_{\mathrm{rel}}$, the dynamics of the four bar suspension are solved using Kane's method [56]. Although Kane's method is generally known to produce a systematic and efficient com-

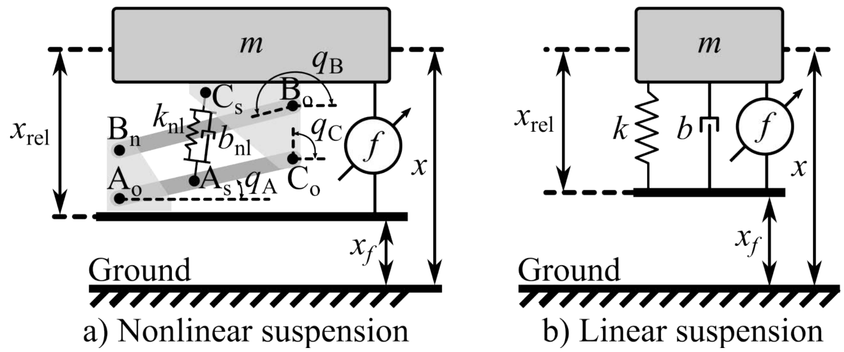


Figure 5.5 Nonlinear (a) and linear (b) model of the active seat suspension with mass $m$. Variations in the position $x_f$ of the cabin floor affect the position $x$ of the seat, also expressed as $x_{\text{rel}}$ relative to the cabin floor.

puter implementation, one might have also used Newton or Lagrange's method to obtain dynamic equations for this one-DOF problem with a similar efficiency.

Although the non-linear model of the suspension is used to more accurately predict the dynamic performance, power expenditures and fluid's expected lifetime of the MR actuator, a linear model is used as the basis for the design of the clutches' controller. The dynamics of the linear suspension schematized in Figure 5.5-b are determined from the dynamic equilibrium on the driver-seat rigid body with mass $m$ such that

$$\ddot{x} = \frac{1}{m}\left(-kx_{\text{rel}} - b\dot{x}_{\text{rel}} + k_{\text{pulley}}T_{\text{in}}\right) \tag{5.13}$$

where the pre-compression of the spring cancels earth's gravity pull acting on $m$. Moreover, for motion in one dimension,

$$\ddot{x} = \ddot{x}_f + \ddot{x}_{\text{rel}}, \tag{5.14}$$

where $\ddot{x}_f$ is the vehicle's cabin floor acceleration in a Newtonian reference frame. As shown in Figure 5.4 comparing the open-loop response of the seat under an arbitrary actuator command $u_1$ ($\ddot{x}_{\text{rel}} = 0$ m/s$^2$) with experimental data, the non-linear model of the suspension better approximates the driver-seat dynamics than the linear model. As it shall be later demonstrated, the linear model is however sufficient for developing an effective LQG controller.

As detailed in previous work, it is also convenient to introduce non-physical state variables in the model of the driver-seat system in order to create filtered versions of $x_{\text{rel}}$ and $\ddot{x}$ so that the actuator can target specific frequency ranges [4].

First, a $2^{\text{nd}}$ order filter applied on $\ddot{x}$ gives more weight to vibrations lying between 1.5 and 12 Hz which are more prone to harm vehicle drivers than others according to the ISO-2631-1 standard. The weighted vertical acceleration of the driver $\ddot{x}_w$ is thus given by

$$\ddot{x}_w = 86.51\alpha_1 + 546.1\alpha_2 \tag{5.15}$$

where $\alpha_1$ and $\alpha_2$ are the filter two state variables governed by equations

$$\dot{\alpha_1} = -82.17\alpha_1 - 1892\alpha_2 + \ddot{x} \tag{5.16}$$

$$\dot{\alpha_2} = \alpha_1. \tag{5.17}$$

Although an active suspension's main purpose is to limit $\ddot{x}_w$, the seat should not be allowed to move freely without restrictions on its maximum travel. A $1^{\text{st}}$ order low-pass filter with a cutoff frequency $f_c$ of 0.3 Hz and a static gain of 4 is thus applied on $x_{\text{rel}}$ such that the weighted relative displacement $x_{\text{rel,w}}$ is found as

$$x_{\text{rel,w}} = 4\beta \tag{5.18}$$

where $\beta$ is the low-pass filter state variable governed by

$$\dot{\beta} = -2\beta + 2x_{\text{rel}}. \tag{5.19}$$

All the non-physical state variables ($\alpha_1$,$\alpha_2$,$\beta$) can be approximated with a Kalman filter and can be used by the actuator's controller.

### 5.4.3 Global Energetic Model

This model is useful to evaluate, using simulations, the power consumption associated with different control strategies. Power balance at the actuator's boundaries imply that the power $P_{\text{supply}}$ provided by the power supply is found as

$$P_{\text{supply}} = P_0 + P_{\text{joule}} + P_{\text{fluid}} + P_{\text{friction}} + P_{\text{seat}} \tag{5.20}$$

where $P_0$ is the experimentally determined balance of plant, $P_{\text{joule}}$ are Joule losses in the motor windings, $P_{\text{fluid}}$ are the clutch slippage losses, $P_{\text{friction}}$ are friction losses and $P_{\text{seat}}$

is the power transfered to the seat. Irreversible power losses including $P_{\text{joule}}$, $P_{\text{fluid}}$ and $P_{\text{friction}}$ are calculated as

$$P_{\text{joule}} = R_m {I_m}^2 + R_c {I_c}^2, \tag{5.21}$$

$$P_{\text{fluid}} = \left| T_{\text{in}} \left( k_{\text{pulley}} \dot{x}_{\text{rel}} - \frac{\omega_m}{k_{\text{reduc}}} \right) \right|, \tag{5.22}$$

$$P_{\text{friction}} = B_{\text{visc}} \omega_m^2 + \left| T_{\text{dry}} \omega_m \right|. \tag{5.23}$$

The reversible power $P_{\text{seat}}$ transferred to the seat is expressed as

$$P_{\text{seat}} = F_{\text{out}} \dot{x}_{\text{rel}}. \tag{5.24}$$

## 5.5 Control Architectures

Given that the clutch decouples the dynamics of the gearbox from the load, the selected control approach is to create separate controllers for the clutches and the motor. The clutches controller supplies an input current to the clutch depending on measured acceleration and position. The motor controller objective is to maintain the clutches in slippage. In such controller, the clutch transmitted load are perceived as disturbances to the motor.

A unified LQG controller with three outputs (1 for the motor and 2 for the clutches) is not possible, because the required linearized model for the whole actuator is not obtainable given the hard nonlinearity that arises when the equivalent speed of the motor at the clutches input is smaller than the equivalent speed of the seat at the clutches output. Given the flexible cables, the actuator transmits no effort in such a case.

### 5.5.1 Clutches Controller

The control of MR clutches used in an active seat suspension can be synthesized using a Linear Quadratic Gaussian (LQG) approach [36] similar to the one used in previous work and briefly summarized here for completeness [4]. At any given time, the clutches control input $u_1$ is calculated as

$$u_1 = -\mathbf{K}\hat{\mathbf{x}} \tag{5.25}$$

where $\hat{\mathbf{x}}$ is an approximation of the state vector $\mathbf{x}$ of the linear driver-seat system expressed as

$$\mathbf{x} = \begin{bmatrix} x_{\text{rel}} & \dot{x}_{\text{rel}} & \alpha_1 & \alpha_2 & \beta \end{bmatrix}^{\text{T}}. \tag{5.26}$$

The control gain matrix $\mathbf{K}$ is found as to minimize, over an infinite time horizon, the cost function

$$J(u_1) = \int_0^{\infty} \left[ (\ddot{x}_w)^2 + (q_d x_{\text{rel,w}})^2 + (q_f u_1)^2 \right] dt \tag{5.27}$$

with $q_d$ and $q_f$ being user defined weighting factors set to 2.51 $\text{s}^{-2}$ and $1.00{\times}10^{-3}$ m·A/s$^2$ respectively. In order to build $\hat{\mathbf{x}}$, one only has access to the measured output vector

$$\mathbf{y} = \begin{bmatrix} x_{\text{rel}}|_{\text{mes}} \\ \ddot{x}_{\text{mes}} \end{bmatrix} = \mathbf{C}\mathbf{x} + \mathbf{D}u_1 + \mathbf{v} \tag{5.28}$$

combining the measure $x_{\text{rel}}|_{\text{mes}}$ of a cable encoder with the measure $\ddot{x}_{\text{mes}}$ of an accelerometer placed on the seat. The system output matrices $\mathbf{C}$ and $\mathbf{D}$ are directly found by rearranging equations 5.13 and 5.14. The measured output vector $\mathbf{y}$ is corrupted with the white measurement noise vector $\mathbf{v}$ with a covariance matrix approximated from experimental data as

$$\mathbf{R}_k = E(\mathbf{v}\mathbf{v}^T) = \begin{bmatrix} 1.15{\times}10^{-5} & 0 \\ 0 & 1.50{\times}10^{-2} \end{bmatrix}.$$

Moreover, the state equation

$$\dot{\mathbf{x}} = \mathbf{A}\mathbf{x} + \mathbf{B}u_1 + \mathbf{G}w \tag{5.29}$$

is supposed to be corrupted with the white process noise $w$ with a normalized variance

$$Q_k = E(w^2) = 1.$$

The system matrices $\mathbf{A}$ and $\mathbf{B}$ are directly found by rearranging equations 5.13 to 5.19 from Section 5.4.2. The process noise matrix $\mathbf{G}$ is set to :

$$\mathbf{G} = \begin{bmatrix} g_1 & g_2 & 0 & 0 & 0 \end{bmatrix}^{\text{T}}$$

with constants $g_1$ and $g_2$ experimentally tuned to values of 0.04 and -0.3 respectively to account for the unpredicted disturbances coming from road vibrations and modeling errors.

Finally, using a Kalman filter [36], the approximated state vector $\hat{\mathbf{x}}$ is found as

$$\frac{d\hat{\mathbf{x}}}{dt} = \mathbf{A}\hat{\mathbf{x}} + \mathbf{B}u_1 + \mathbf{L}\left(\mathbf{y} - \hat{\mathbf{y}}\right)$$

with

$$\hat{\mathbf{y}} = \mathbf{C}\hat{\mathbf{x}} + \mathbf{D}u_1.$$

Based on equations 5.28 and 5.29 and on the values of $Q_k$ and $\mathbf{R}_k$, the Kalman filter matrix $\mathbf{L}$ is found as to minimize the steady-state error covariance

$$P = \lim_{t\to\infty} E\left[\left(\mathbf{x} - \hat{\mathbf{x}}\right)\left(\mathbf{x} - \hat{\mathbf{x}}\right)^{\mathrm{T}}\right]. \tag{5.30}$$

### 5.5.2 Motor Controller

The electric motor of the MR actuator is controlled with a typical cascade scheme with a fast inner feedback loop on current and a slower outer loop on velocity as showed in Fig. 5.6.

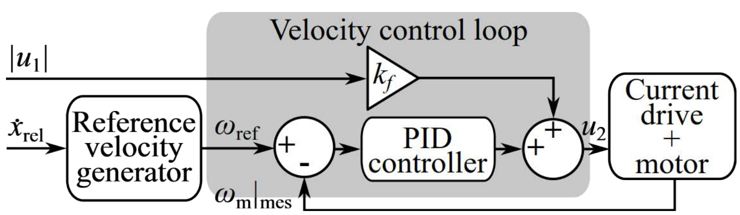


Figure 5.6 Control architecture of the BLDC electric motor used for the MR actuator

The velocity control loop of the motor uses a PID controller with an integral gain $k_{\omega i}$ of 1.05 A, a proportional gain $k_{\omega p}$ set to 0.136 A·s and a derivative gain $k_{\omega d}$ set to $5\times10^{-3}$ A·s$^2$. A first order low-pass filter with a 5.73 Hz cutoff frequency is applied to the derivative term of the controller and a saturation of ±5 A is applied to the integral term. The absolute value of the current command $u_1$ to the clutches is also fed forward to the motor current controller with a gain $k_f$ set to 1.5 such that the current command $u_2$ to the motor drive is

$$u_2 = k_{\omega i}\int_0^T \omega_{\mathrm{err}} dt + k_{\omega p}\omega_{\mathrm{err}} + k_{\omega d}\frac{d\omega_{\mathrm{err}}}{dt} + k_f\left|u_1\right| \tag{5.31}$$

with

$$\omega_{\mathrm{err}} = \omega_{\mathrm{ref}} - \omega_{\mathrm{m}}|_{\mathrm{mes}}. \tag{5.32}$$

At the core of this paper, two control strategies are contrasted for the generation of the reference motor velocity $\omega_{\mathrm{ref}}$. The simplest and most widely used strategy up to date is to impose

$$ {}_1\omega_{\mathrm{ref}} = \omega_{cs}, \tag{5.33} $$

where $\omega_{cs}$ is a constant. Another approach aimed at limiting the clutches slip speed is to impose

$$ {}_2\omega_{\mathrm{ref}} = \begin{cases} k_{\mathrm{reduc}} k_{\mathrm{pulley}} \left|\dot{x}_{\mathrm{rel}}\right| + \omega_{ls}, & \text{if } \dot{x}_{\mathrm{rel}} T_{\mathrm{in}} > 0 \\ 0, & \text{otherwise} \end{cases} \tag{5.34} $$

where $k_{\mathrm{reduc}} k_{\mathrm{pulley}} \left|\dot{x}_{\mathrm{rel}}\right|$ is the seat speed as seen from the clutch and $\omega_{ls}$ is again a constant, now representing a slippage margin. These strategies shall from now on be respectively referred as the "constant speed" and the "limited slip" control strategies.

## 5.6 Experimental Setup and Procedure

In order to test the actual benefits of using a limited slip motor control approach over a constant speed strategy, a continuous slippage MR actuator with a configuration similar to the schematics of Figure 5.2 was mounted on the back of a commercial truck driver's seat. The seat was bolted on top of a vibrating platform forced, using two Xcite 1107-4 hydraulic actuators and master controller, to recreate the floor vibrations of a dump truck rolling on a quarry road (Fig. 5.7). The cabin floor's acceleration dominant frequency components lie between 1 and 10 Hz with two dominant peaks around 1.5 and 10 Hz . The platform and seat accelerations are measured using accelerometers and the relative seat position, with a cable encoder. The total power drawn from the power supply is recorded using a current probe.

Depending on the type of motor control approach used, the value of $\omega_{cs}$ or $\omega_{ls}$ is varied between each tested road segments of 30 s. After a first set of experiments is completed with a first cabin floor acceleration profile (tagged as road A) with a Root Mean Square (RMS) acceleration of about 1.45 m/s$^2$, the platform's oscillation amplitude is increased and the procedure is now repeated with a floor RMS acceleration of about 2.15 m/s$^2$ (tagged as road B). These recorded accelerations profiles were the only experimental data inputed into the simulations afterward.

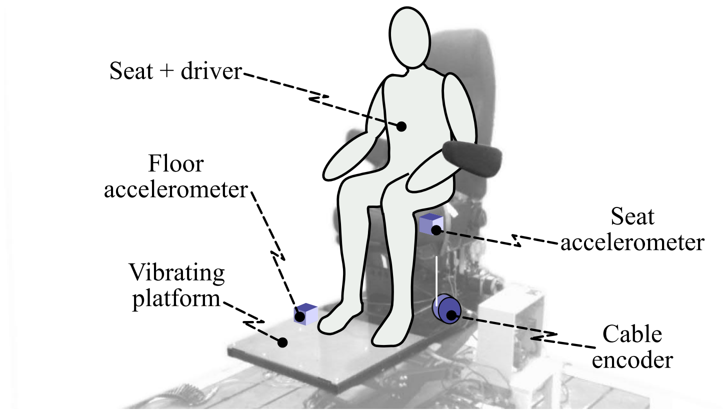

Figure 5.7 Experimental setup used to test the constant speed and limited slip motor control strategies on an MR actuator used in an active seat suspension

## 5.7 Results

In order to compare control strategies, three actuator quality metrics are introduced :

1- the dynamic cost

$$d_c = \sqrt{\frac{1}{T}\int_0^T \left[(\ddot{x}_w)^2 + (q_d x_{\text{rel,w}})^2\right] dt} \tag{5.35}$$

which uses $\ddot{x}_w$ from (5.15), $x_{\text{rel,w}}$ from (5.18), the weighting factor $q_d$ from (5.27), and quantifies the actuator's dynamic performance ;

2- the mean power losses

$$\bar{p}_{\text{loss}} = \frac{1}{T}\int_0^T P_{\text{supply}} dt \tag{5.36}$$

3- the MR fluid's expected lifetime

$$t_{\text{life}} = \frac{Q_{\max} V_{\text{fluid}}}{P_{\text{fluid}}} \tag{5.37}$$

where $Q_{\max}$ (6 MJ/mL) is the maximum volumetric energy density that can be dissipated in the MR fluid before failure [12], $V_{\text{fluid}}$ (60 mL) is the total volume of fluid in both clutches and $P_{\text{fluid}}$ is previously defined in (5.22). According to these quality metrics, a "good" MR actuator will have a low dynamic cost, low mean power losses and a high MR fluid's expected lifetime. For other applications, the dynamic cost should be redefined to reflect other intended control purposes.

The three quality metrics are plotted in Figure 5.8 against the constant motor speed command $\omega_{cs}$ and in Figure 5.9 against the constant slip speed command to access the fit between experimental and simulation results on road A and B. On road A and for constant

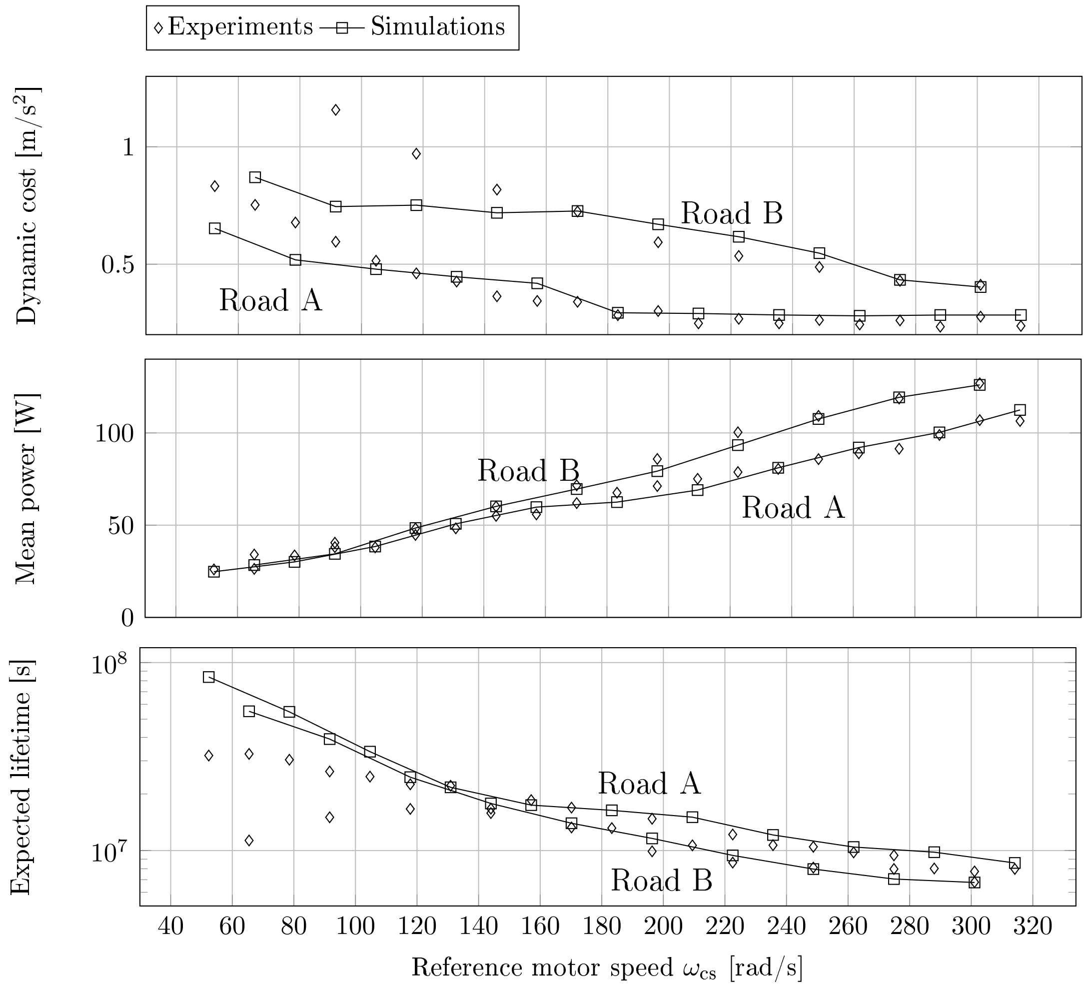


Figure 5.8 Comparison between simulated and experimental dynamic cost, mean power and expected lifetime using a constant speed motor control strategy over road A and B

speed commands above 105 rad/s, the mean absolute error between simulation and experiment quality metrics $d_c$, $\bar{p}_{\text{loss}}$ and $t_{\text{life}}$ are 0.04 m/s$^2$, 3.2 W and $2.5{\times}10^6$ s respectively. Similar figures are obtained on road B for constant speed commands above 144 rad/s with mean absolute errors of 0.05 m/s$^2$, 2.7 W and $9.0{\times}10^5$ s respectively. Similar agreements between simulations and experiments are reached with a limited slip control for limited slip constants $\omega_{ls}$ above 79 rad/s for both roads.

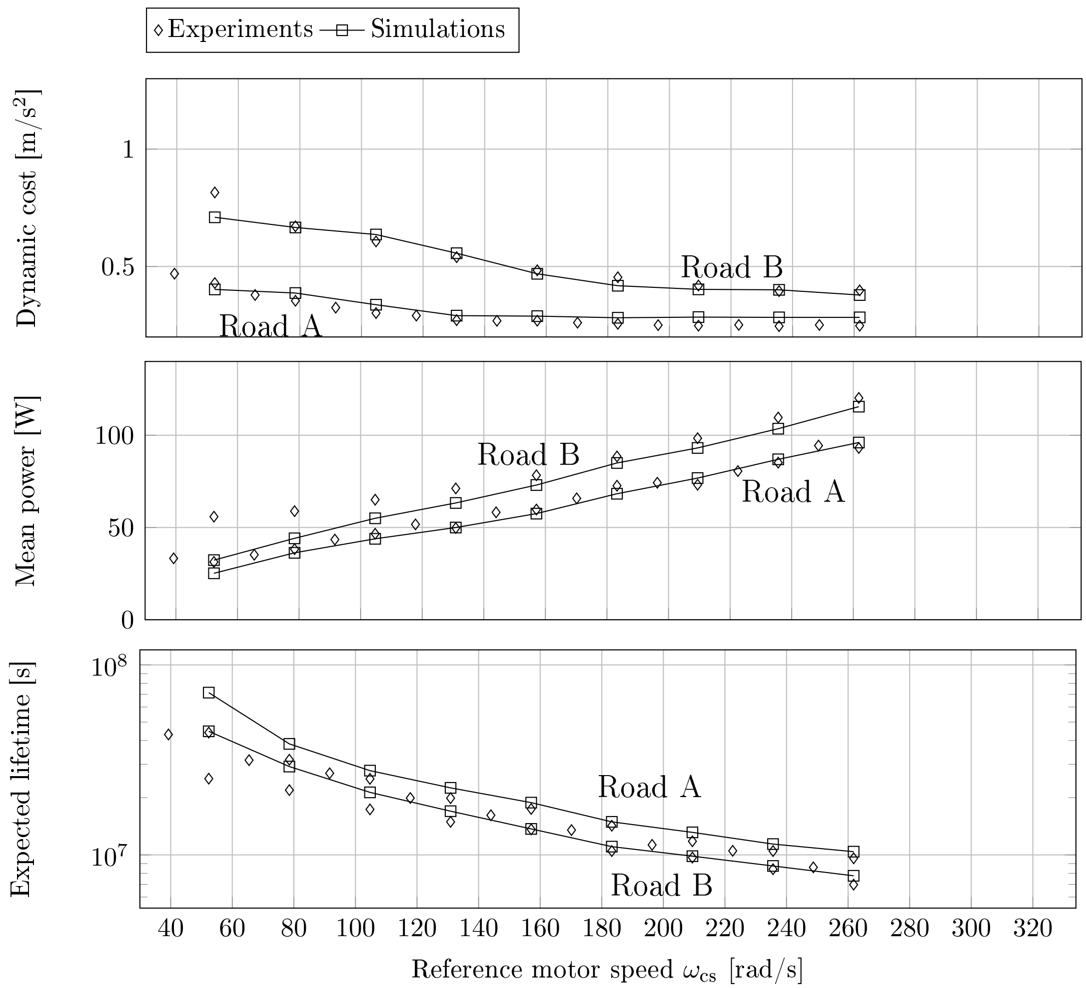


Figure 5.9 Comparison between simulated and experimental dynamic cost, mean power and expected lifetime using a constant slip speed control strategy over road A and B

To truly grasp the underlying controller trade-offs, it is convenient to plot the actuator's mean power and expected fluid life time as implicit functions of the dynamic cost (Fig. 5.10). At low motor reference speeds, the power consumed by the actuator is low and the MR fluid's expected lifetime is high although these improved quality metrics come with an unacceptable increase in the actuator's dynamic cost. On the opposite, at high motor reference speeds, any increase in reference speed no longer causes a decrease in dynamic cost, because the MR clutches are not hindered anymore by speed saturations. Before this limit, characterized by vertical asymptotes on the power and lifetime trade-off curves, both the simulation and experimental results show that any small change in the actuator's dynamic cost can lead to significant power reductions and lifetime increase. Even with a strong emphasis on minimizing the dynamic cost, a 20 % power reduction and 40 % lifetime increase is expected if one chooses a limited slip control approach over a constant motor speed.

## 5.8 Conclusions

In this paper, a model of an MR actuator used in an active seat suspension is first developed in order to predict the dynamic performance, power losses and lifetime of the actuator solely based on the knowledge of the input road disturbance. Two control approaches, one aiming to maintain a constant motor speed and the other aimed at limiting the MR clutches slip are then proposed and evaluated using both simulations and experiments.

Results show that a non-linear, yet simple model of the actuator and load system can correctly approximate the quality metrics of the actuator under a given disturbance profile. One could, based on a similar approach, use such a model as an effective tool in designing the hardware of an MR actuator system. For instance, there seems to be a non-trivial trade-off between, on one side, selecting a motor with a large inertia to have complete authority over the motor's angular velocity and, on the other side, selecting a small motor and drawing less current to follow a limited slip velocity trajectory.

Moreover, even as the actuator is subject to large disturbances and unpredicted changes in the load's velocity, a simple controller limiting the slip in the MR clutches rather than driving the motor at a constant speed can lead to a decrease of up to 20 % in power consumption and a lifetime increase of up to 40 % without any significant losses in dynamic performance. Higher improvements are possible, but at some performance cost. For applications such as an active seat suspension or haptic devices, human perception should be monitored to quantify indistinguishable levels of performance cost.

Such gains in power consumption and fluid lifetime are expected to be even higher if more advanced control techniques were implemented. For applications with varying disturbance profiles such as the transition from one road profile to another for an active seat suspension, an adaptive control scheme could be implemented to vary the clutches slip speed online. Because of its restricted order and simplicity, the MR actuator's model presented in this paper could also be integrated into a non-linear controller such as a model predictive controller constantly looking for the optimal commands to send to the motor and clutches in order to minimize a cost function expressed explicitly in terms of overall performance, power consumption and fluid predicted lifetime. Future work in the field should therefore investigate energy and lifetime conscious control techniques for MR actuators alongside other research avenues such as upgrades in the MR clutches design.

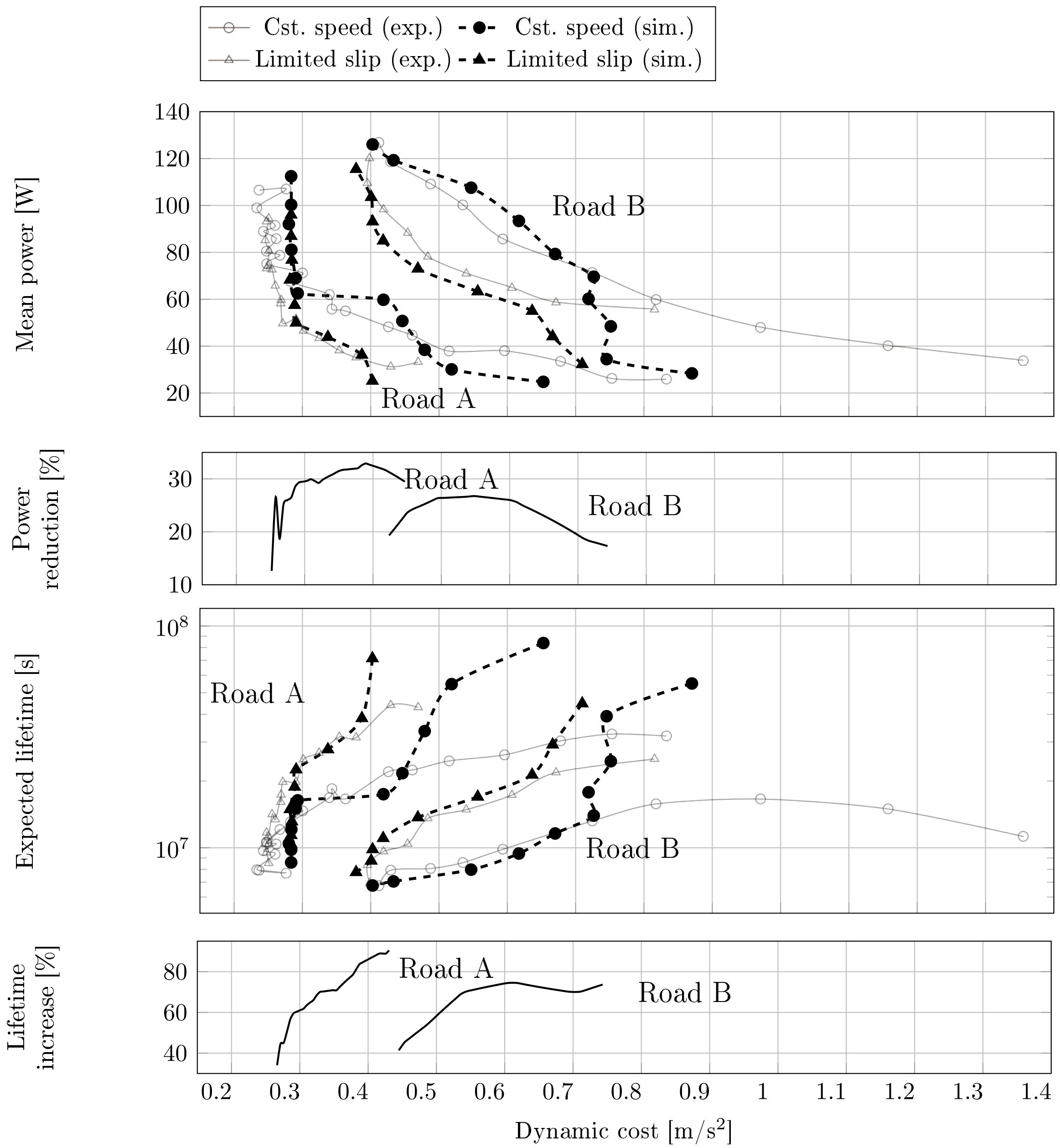


Figure 5.10 Trade-off curves obtained from experiments and simulation results along with experimental power reduction and lifetime increase curves. This figure is obtained as an implicit representation of figures 5.8 and 5.9.

# CHAPITRE 6

# Conclusion

## 6.1 Sommaire

En résumé, les travaux de recherche couverts dans le présent document ont abouti à la rédaction de trois articles scientifiques. Dans un premier temps, l'article «Preventing Lower Back Pain Among Truck Drivers : Design and Performance of a Controlled Slippage Magnetorheological Actuator for an Active Seat Suspension» soumis à la «42nd Mechanisms and Robotics Conference (MR)» de l'ASME a permis de caractériser un actionneur MR et de vérifier qu'il répond aux critères de conception requis pour une suspension active de véhicule lourd.

Dans un deuxième temps, l'article «Experimental Assessment of a Controlled Slippage Magnetorheological Actuator for Active Seat Suspensions» soumis au journal «Transactions on Mechatronics» expose l'élaboration d'un modèle linéaire de l'actionneur et du système de suspension en plus d'un premier contrôleur qui ne considère pas l'énergie dissipée dans les embrayages. Une évaluation expérimentale des différents indices de performance de cet actionneur démontre que la suspension active peut réduire de 66% les vibrations de la route transmises à l'occupant du siège par rapport à une suspension à air passive conventionnelle. De plus, ces niveaux d'atténuation atteints sont similaires aux suspensions actives commerciales exploitées dans des conditions similaires.

Enfin, une version modifiée de l'article «Controller Trade-Offs for Continuous Slippage Magnetorheological Actuators», initialement soumis au journal de «Robotics and Automation Letters», devrait être resoumise sous peu. Cet ouvrage aborde le développement d'un modèle non linéaire permettant de prédire les compromis existant entre les différents indices de performance pour un type donné de contrôleur. Une démonstration expérimentale y est offerte validant que ce modèle est fidèle à la réalité. Enfin, une stratégie de contrôle qui minimise l'énergie dissipée dans l'embrayage y est exposée. L'utilisation de cette stratégie de contrôle permet de réduire la consommation énergétique de l'actionneur d'environ 20% alors que la durée de vie prédite du fluide de l'actionneur est augmentée d'environ 40%.

## 6.2 Contributions

Les travaux présentés dans cet ouvrage ont d'abord contribué à l'avancement de la science en offrant une des premières démonstrations de l'utilisation d'un actionneur MR à glissement continu pour une application concrète alors que la plupart des dispositifs présentés jusqu'à maintenant dans la littérature ne visaient pas d'application particulière. Qui plus est, une comparaison des performances de la suspension active avec différentes alternatives commerciales permet de soutenir avec chiffres à l'appui un des points forts des actionneurs MR à glissement continu : à volume et coût réduits, ils peuvent égaler la performance d'un actionneur électrique à couplage direct.

Un modèle d'actionneur MR à glissement continu a également été développé permettant d'apprécier le compromis existant entre les différents indices de performance de l'actionneur : sa performance dynamique, sa consommation énergétique, et la durée de vie attendue du fluide MR. Bien que ce modèle ait été validé pour une application de suspension active, la méthodologie employée pourrait facilement être transposée à d'autres applications.

Enfin, il a été démontré que l'utilisation d'une méthode de contrôle simple visant à minimiser l'énergie dissipée dans les embrayages d'un actionneur MR peut contribuer de manière significative à réduire sa consommation énergétique et allonger la durée de vie du fluide pour une application de suspension active.

## 6.3 Travaux Futurs

Une extension prometteuse aux travaux résumés dans ce document consisterait à explorer l'interaction qui existe entre certains choix de conception, la stratégie de contrôle employée et différentes caractéristiques souhaitables de l'actionneur MR. Par exemple, une réduction de la taille du moteur utilisé pour entraîner un actionneur MR engendrerait d'une part une réduction de son coût, son volume et son poids. Cette réduction de taille pourrait cependant compromettre la possibilité d'utiliser une stratégie de contrôle qui vise à minimiser l'énergie dissipée dans les embrayages dû à une perte d'autorité sur l'asservissement de la vitesse du moteur.

Par ailleurs, certains aspects de l'analyse actuelle de la performance d'un actionneur MR pour une application de suspension active de siège de véhicule lourd n'ont pas été couverts dans les publications scientifiques et mériteraient de l'être. Il serait en effet pertinent de quantifier plus en détail la stabilité ainsi que la robustesse aux incertitudes paramétriques du contrôleur employé pour les tests. Les résultats d'une telle étude pourraient à eux seuls justifier l'emploi d'une technique de contrôle plus robuste qu'un contrôleur LQG. Il serait alors avisé de répéter l'analyse des nouveaux compromis entre les différents indice de performances obtenus avec cette nouvelle technique de contrôle.

# LISTE DES RÉFÉRENCES


[1] Alfadhli, A., Darling, J. et Hillis, A. J. (2017). The Control of an Active Seat with Vehicle Suspension Preview Information. *Journal of Vibration and Control*, p. 1–15.

[2] American Society for Metals (1966). *Metals Handbook*, *volume 1*, 8e édition.

[3] Avraam, M. T. (2009). *MR-Fluid Brake Design and Its Application to a Portable Muscular Rehabilitation Device*. Thèse de doctorat, Université Libre de Bruxelles.

[4] Bégin, M.-A., Chouinard, P., Lebel, L.-P., Masson, P., Berry, A., Plante, J.-S. et Pasco, Y. (2017). Experimental Assessment of a Controlled Slippage Magnetorheological Actuator for Active Seat Suspensions. *Transactions on Mechatronics*.

[5] Blood, R. P., Ploger, J. D. et Johnson, P. W. (2010). Whole Body Vibration Exposures in Forklift Operators : Comparison of a Mechanical and Air Suspension Seat. *Ergonomics*, volume 53, numéro 11, p. 1385–1394.

[6] Blood, R. P., Yost, M. G., Camp, J. E. et Ching, R. P. (2015). Whole-body Vibration Exposure Intervention among Professional Bus and Truck Drivers : A Laboratory Evaluation of Seat-suspension Designs. *Journal of Occupational and Environmental Hygiene*, volume 12, numéro 6, p. 351–362.

[7] Boileau, P.-É. et Rakheja, S. (1998). Whole-body Vertical Biodynamic Response Characteristics of the Seated Vehicle Driver : Measurement and Model Development. *International Journal of Industrial Ergonomics*, volume 22, numéro 6, p. 449–472.

[8] Bose (2013). Bose Ride Technical Data Sheet.

[9] Brown, F. T. (2006). *Engineering System Dynamics : A Unified Graph-Centered Approach*. CRC press.

[10] Camino, J. F., Zampieri, D., Takahashi, R. H. et Peres, P. L. (1997). H2 and LQR Active Suspension Control Schemes with Uncertain Parameters : A Comparison. Dans *Proceedings of the 7th International Conference on Dynamic Problems in Mechanics*. p. 226–228.

[11] Cann, A., Salmoni, A. et Eger, T. (2004). Predictors of Whole-body Vibration Exposure Experienced by Highway Transport Truck Operators. *Ergonomics*, volume 47, numéro 13, p. 1432–1453.

[12] Carlson, J. D. (2002). What Makes a Good MR Fluid ? *Journal of Intelligent Material Systems and Structures*, volume 13, numéro 7-8, p. 431–435.

[13] Carlson, J. D. et Catanzarite, D. M. (1998). Magnetorheological fluid devices and process of controlling force in exercise equipment utilizing same.

[14] Carlson, J. D., Catanzarite, D. M. et Clair, K. A. (1996). Commercial magneto-rheological fluid devices. *International Journal of Modern Physics B*, volume 10, numéro 23, p. 2857–2866.

[15] Carlson, J. D., LeRoy, D. F., Holzheimer, J. C., Prindle, D. R. et Marjoram, R. H. (1998). Controllable brake. Brevet US5842547.

[16] Casati, F. M., Herrington, R. M., Broos, R. et Miyazaki, Y. (1998). Tailoring the Performance of Molded Flexible Polyurethane Foams for Car Seats. *Journal of Cellular Plastics*, volume 34, numéro 5, p. 430–466.

[17] Cheok, K. C., Hu, H. X. et Loh, N. K. (1989). Discrete-Time Frequency-Shaping Parametric LQ Control with Application to Active Seat Suspension Control. *IEEE Transactions on Industrial Electronics*, volume 36, numéro 3, p. 383–390.

[18] Chiang, M. H., Lee, L. W. et Tsai, J. J. (2004). The concurrent implementation of high velocity control performance and high energy efficiency for hydraulic injection moulding machines. *The International Journal of Advanced Manufacturing Technology*, volume 23, numéro 3-4, p. 256–262.

[19] Cho, S. H. et Noskievič, P. (2012). Position tracking control with load-sensing for energy-saving valve-controlled cylinder system. *Journal of Mechanical Science and Technology*, volume 26, numéro 2, p. 617–625.

[20] Choi, S. B., Yook, J.-Y., Choi, M.-K. et Nguyen, Q. H. (2006). Speed control of a DC motor using magnetorheological clutch. Dans *Proceedings of the 10th International Conference on Electrorheological(ER) Fluids and Magnetorheological(MR) Suspensions*. p. 638–644.

[21] Chouinard, P. (2014). *Conception et validation expérimentale d'un système d'embrayages magnétorhéologiques à glissement continu pour les commandes de vol d'aéronef*. Thèse de doctorat, Universite de Sherbrooke, Sherbroole.

[22] Chouinard, P., Bégin, M.-A., Marchetta Fortin, J., Berry, A., Masson, P. et Plante, J.-S. (2017). Design and Open-Loop Performance of a Controlled Slippage Magnetorheological Actuator for Active Seat Suspensions. *Journal of Intelligent Material Systems and Structures*.

[23] Chouinard, P., Denninger, M. et Plante, J.-S. (2015). Reliable and lightweight primary flight control actuation using magneto-rheological clutches in slippage. Dans *2015 IEEE International Conference on Robotics and Automation (ICRA)*. IEEE, p. 213–219.

[24] Chouinard, P., Plante, J.-S. et Nfonguem, G. (2016). Aircraft flap and slat independent deployment using magneto-rheological (MR) fluid actuators. Dans *Proceedings of the seventh international conference on recent advances in aerospace actuation systems and components*.

[25] Claar, P. W. et Vogel, J. M. (1989). A Review of Active Suspension Control for On and Off-Highway Vehicles. Dans *SAE Technical Paper*. SAE International.

[26] Coyte, J. L., Stirling, D., Du, H. et Ros, M. (2016). Seated Whole-Body Vibration Analysis, Technologies, and Modeling : A Survey. *IEEE Transactions on Systems, Man, and Cybernetics : Systems*, volume 46, numéro 6, p. 725–739.

[27] de Vicente, J., Klingenberg, D. J. et Hidalgo-Alvarez, R. (2011). Magnetorheological fluids : A review. *Soft Matter*, volume 7, numéro 8, p. 3701.

[28] Desrosiers, J.-F., Bigué, J.-P. L., Denninger, M., Julió, G., Plante, J.-S. et Charron, F. (2013). Preliminary investigation of magneto-rheological fluid durability in continuous slippage clutch. *Journal of Physics : Conference Series*, volume 412.

[29] Digumarti, K. M., Gehring, C., Coros, S., Hwangbo, J. et Siegwart, R. (2014). Concurrent Optimization of Mechanical Design and Locomotion Control of a Legged Robot. Dans *Mobile Service Robotics*. World Scientific, p. 315–323.

[30] Du, B. (2016). *Effects of Seat Suspension Types on Truck Drivers' Vigilance*. Thèse de doctorat, University of Waterloo.

[31] Dufner, D. L. et Schick, T. E. (2002). John Deere Active Seat™ : A New Level of Seat Performance. Dans *Proceedings of the Agricultural Engineering*. volume 1716. p. 43–49.

[32] Einar Hreinsson (2011). *Durability of a Magnetorheological Fluid in a Prosthetic Knee Joint*. Thèse de doctorat, University of Iceland, Iceland.

[33] Ellis, R., Ismaeil, O. et Lipsett, M. (1996). Design and evaluation of a high-performance haptic interface. *Robotica*, volume 14, numéro 03, p. 321–327.

[34] Farrington, R. et Rugh, J. (2000). *Impact of Vehicle Air-conditioning on Fuel Economy, Tailpipe Emissions, and Electric Vehicle Range* (Rapport technique). National Renewable Energy Lab., Golden, CO (US).

[35] Fauteux, P., Lauria, M., Heintz, B. et Michaud, F. (2010). Dual-Differential Rheological Actuator for High-Performance Physical Robotic Interaction. *IEEE Transactions on Robotics*, volume 26, numéro 4, p. 607–618.

[36] Franklin, G. F., Powell, J. D. et Workman, M. L. (1998). *Digital Control of Dynamic Systems, volume 3*. Addison-wesley Menlo Park.

[37] Fuller, C. C., Elliott, S. et Nelson, P. A. (1996). *Active Control of Vibration*. Academic Press.

[38] Furusho, J., Sakaguchi, M., Takesue, N. et Koyanagi, K. (2002). Development of ER brake and its application to passive force display. *Journal of Intelligent Material Systems and Structures*, volume 13, numéro 7-8, p. 425–429.

[39] Gagorowski, A. (2012). Controlling the Magnetorheological Suspension of a Vehicle Seat Including the Biomechanics of the Driver. *Open Engineering*, volume 2, numéro 2, p. 264–278.

[40] Genc, S. et Derin, B. (2012). Field Responsive Fluids - A Review. *Key Engineering Materials*, volume 521, p. 87–99.

[41] Giovanini, L. (2007). Cooperative-feedback control. *ISA Transactions*, volume 46, numéro 3, p. 289–302.

[42] Gratzer, F., Steinwender, H. et Kušej, A. (2008). Magnetorheological AWD clutches. *ATZautotechnology*, volume 8, numéro 10, p. 32–37.

[43] Güçlü, R. (2003). Active Control of Seat Vibrations of a Vehicle Model Using Various Suspension Alternatives. *Turkish Journal of Engineering and Environmental Sciences*, volume 27, numéro 6, p. 361–373.

[44] Güçlü, R. et Gulez, K. (2008). Neural Network Control of Seat Vibrations of a Nonlinear Full Vehicle Model Using PMSM. *Mathematical and Computer Modelling*, volume 47, numéro 11, p. 1356–1371.

[45] Gudmundsson, K. H., Jonsdottir, F. et Thorsteinsson, F. (2010). A geometrical optimization of a magneto-rheological rotary brake in a prosthetic knee. *Smart Materials and Structures*, volume 19, numéro 3, p. 035023.

[46] Han, Shin, D. K., Shin, C. S. et Choi, S.-B. (2017). Robust Vibration Control of Vehicle Seat Suspension System Using MR Damper. *Transactions of the Korean Society for Noise and Vibration Engineering*, volume 27, numéro 3, p. 286–296.

[47] Hegger, C. et Maas, J. (2017). Weight and space saving design of energy-efficient MRF-based clutches for hybrid powertrains. Dans *SPIE Smart Structures and Materials+ Nondestructive Evaluation and Health Monitoring*. International Society for Optics and Photonics, p. 101642B–101642B.

[48] Herranen, M., Huhtala, K. et Vilenius, M. (2010). The Energy Balance of the Electro-Hydraulic Linear Actuation System. *Journal of Energy and Power Engineering*, volume 4, numéro 8, p. 57–63.

[49] Hiemenz, G. J., Hu, W. et Wereley, N. M. (2008). Semi-Active Magnetorheological Helicopter Crew Seat Suspension for Vibration Isolation. *Journal of Aircraft*, volume 45, numéro 3, p. 945–953.

[50] Hrovat, D., Margolis, D. L. et Hubbard, M. (1988). An Approach Toward the Optimal Semi-Active Suspension. *Journal of Dynamic Systems, Measurement, and Control*, volume 110, numéro 3, p. 288–296.

[51] Hunter, I. W., Hollerbach, J. M. et Ballantyne, J. (1991). A comparative analysis of actuator technologies for robotics. *Robotics Review*, volume 2, p. 299–342.

[52] Johnson, P. W., Dennerlein, J. T. et Kim, J. H. (2016). A Randomized Controlled Trial of New Truck Seats Intended to Reduce Whole Body Vibration Exposures and Low Back Pain. Dans *6th American Conference on Human Vibration*.

[53] Jolly, M. R., Bender, J. W. et Carlson, J. D. (1999). Properties and applications of commercial magnetorheological fluids. *Journal of intelligent material systems and structures*, volume 10, numéro 1, p. 5–13.

[54] Jones, W. (1953). Investigation of magnetic mixtures for clutch application. *Transactions of the American Institute of Electrical Engineers. Part III : Power Apparatus and Systems*, volume 72, numéro 2, p. 88–92.

[55] Julio, G., Plante, J.-S. et Latham, G. (2015). Development of a Magneto-Rheological fluid-based trim actuator with active tactile cueing capabilities. Dans *AHS 71st Annual forum*.

[56] Kane, T. R. et Wang, C. F. (1965). On the Derivation of Equations of Motion. *Journal of the Society for Industrial and Applied Mathematics*, volume 13, numéro 2, p. 487–492.

[57] Kavlicoglu, B., Gordaninejad, F., Evrensel, C., Fuchs, A. et Korol, G. (2006). A semi-active, high-torque, magnetorheological fluid limited slip differential clutch. *Journal of Vibration and Acoustics*, volume 128, numéro 5, p. 604.

[58] Lee, C. et Goverdovskiy, V. N. (2009). Type Synthesis of Function-Generating Mechanisms for Seat Suspensions. *International Journal of Automotive Technology*, volume 10, numéro 1, p. 37–48.

[59] Lee, Y. et Jeon, D. (2002). A Study on the Vibration Attenuation of a Driver Seat Using an MR Fluid Damper. *Journal of Intelligent Material Systems and Structures*, volume 13, numéro 7-8, p. 437–441.

[60] Li, W., Zhang, X. et Du, H. (2012). Development and simulation evaluation of a magnetorheological elastomer isolator for seat vibration control. *Journal of Intelligent Material Systems and Structures*, volume 23, numéro 9, p. 1041–1048.

[61] Liu, B., Li, W. H., Kosasih, P. B. et Zhang, X. Z. (2006). Development of an MR-brake-based haptic device. *Smart Materials and Structures*, volume 15, numéro 6, p. 1960–1966.

[62] Maciejewski, I. (2012). Control System Design of Active Seat Suspensions. *Journal of Sound and Vibration*, volume 331, numéro 6, p. 1291–1309.

[63] Maeda, S. et Morioka, M. (1998). Measurement of Whole-Body Vibration Exposure from Garbage Trucks. *Journal of Sound and Vibration*, volume 215, numéro 4, p. 959–964.

[64] Mazoyer, J. (2005). *Étude de la suspension active de siège*. Mémoire de maîtrise, Université de Sherbrooke.

[65] McManus, S., St. Clair, K., Boileau, P., Boutin, J. et Rakheja, S. (2002). Evaluation of Vibration and Shock Attenuation Performance of a Suspension Seat with a Semi-Active Magnetorheological Fluid Damper. *Journal of Sound and Vibration*, volume 253, numéro 1, p. 313–327.

[66] Nguyen, Q. H., Choi, S. B., Lee, Y. S. et Han, M. S. (2013). Optimal design of high damping force engine mount featuring MR valve structure with both annular and radial flow paths. *Smart Materials and Structures*, volume 22, numéro 11, p. 115024.

[67] Ning, D., Sun, S., Li, H., Du, H. et Li, W. (2016). Active Control of an Innovative Seat Suspension System with Acceleration Measurement based Friction Estimation. *Journal of Sound and Vibration*, volume 384, p. 28–44.

[68] Ning, D., Sun, S., Wei, L., Zhang, B., Du, H. et Li, W. (2017). Vibration Reduction of Seat Suspension using Observer Based Terminal Sliding Mode Control with Acceleration Data Fusion. *Mechatronics*, volume 44, p. 71–83.

[69] Paddan, G. et Griffin, M. (2002). Evaluation of Whole-Body Vibration in Vehicles. *Journal of Sound and Vibration*, volume 253, numéro 1, p. 195–213.

[70] Parison, J. (2010). The Bose Ride$^{TM}$ System.

[71] Park, E. J., da Luz, L. F. et Suleman, A. (2008). Multidisciplinary design optimization of an automotive magnetorheological brake design. *Computers & Structures*, volume 86, numéro 3-5, p. 207–216.

[72] Phu, D. X., Choi, S.-B., Lee, Y.-S. et Han, M.-S. (2016). Vibration Control of a Vehicle's Seat Suspension Featuring a Magnetorheological Damper Based on a New Adaptive Fuzzy Sliding-Mode Controller. *Proceedings of the Institution of Mechanical Engineers, Part D : Journal of Automobile Engineering*, volume 230, numéro 4, p. 437–458.

[73] Plante, J., Denninger, M., Chouinad, P., Julio, G., Lucking, B., Huppe, N. et Desrosiers, J. (2015). Magnetorheological fluid clutch apparatus and control systems. Brevet CA2934582.

[74] Plante, J.-S., Denninger, M., Chouinard, P., Julio, G., Lucking-Bigué, J.-P., Huppe, N. et Desrosiers, J.-F. (2016). Magnetorheological Fluid Clutch Apparatus and Control Systems.

[75] Rabinow, J. (1948). The magnetic fluid clutch. *Electrical Engineering*, volume 67, numéro 12, p. 1167–1167.

[76] Rabinow, J. (1951). Magnetic Fluid Torque and Force Transmitting Device.

[77] Rebelle, J. (2004). Methodology to Improve the Performance of the End-stop Buffers of Suspension Seats. *Vehicle System Dynamics*, volume 42, numéro 4, p. 211–233.

[78] Roos, F., Johansson, H. et Wikander, J. (2006). Optimal selection of motor and gearhead in mechatronic applications. *Mechatronics*, volume 16, numéro 1, p. 63–72.

[79] Samson Rope Technologies Inc (2009). Stena performance mooring lines case study.

[80] Sarkar, C. et Hirani, H. (2013). Design of a squeeze film magnetorheological brake considering compression enhanced shear yield stress of magnetorheological fluid. *Journal of Physics : Conference Series*, volume 412, p. 012045.

[81] Schempf, H. et Yoerger, D. R. (1993). Study of dominant performance characteristics in robot transmissions. *ASME Journal of Mechanical Design*, volume 115, p. 472–472.

[82] Schwarze, S., Notbohm, G., Dupuis, H. et Hartung, E. (1998). Dose-response relationships between whole-body vibration and lumbar disk disease-a field study on 388 drivers of different vehicles. *Journal of Sound and Vibration*, volume 215, numéro 4, p. 613–628.

[83] Shafer, A. et Kermani, M. (2011). On the Feasibility and Suitability of MR Fluid Clutches in Human-Friendly Manipulators. *IEEE/ASME Transactions on Mechatronics*, volume 16, numéro 6, p. 1073–1082.

[84] Shang, T. (2004). *Improving Performance of an Energy Efficient Hydraulic Circuit*. Thèse de doctorat, University of Saskatchewan, Canada.

[85] Smets, M. P., Eger, T. R. et Grenier, S. G. (2010). Whole-Body Vibration Experienced by Haulage Truck Operators in Surface Mining Operations : A Comparison of Various Analysis Methods Utilized in the Prediction of Health Risks. *Applied Ergonomics*, volume 41, numéro 6, p. 763–770.

[86] Smith, A. L. et Usoro, P. B. (2003). Method for slip power management of a controllable viscous fan drive. Brevet US20030079952.

[87] Stein, G. J. (1997). Vibration Control System with a Proportionally Controlled Pneumatic Actuator. Dans *Control Conference (ECC), 1997 European*. IEEE, p. 1814–1818.

[88] Stein, G. J., Múčka, P. et Gunston, T. P. (2009). A Study of Locomotive Driver's Seat Vertical Suspension System with Adjustable Damper. *Vehicle System Dynamics*, volume 47, numéro 3, p. 363–386.

[89] Sulakhe, V. N., Thakare, C. Y. et Aute, P. V. (2013). Review - MR fluid and its application. *International Journal of Research in Aeronautical and Mechanical Engineering*, volume 1, numéro 7, p. 125–133.

[90] Sun, N. N. (2012). *Development of a New High Speed Cable-Based Planar Parallel Manipulator*. Mémoire de maîtrise, University of Waterloo, Canada.

[91] Takesue, N., Asaoka, H., Lin, J., Sakaguchi, M., Zhang, G. et Furusho, J. (2000). Development and experiments of actuator using MR fluid. volume 3. p. 1838–1843 vol.3.

[92] Tiemessen, I. J., Hulshof, C. T. et Frings-Dresen, M. H. W. (2008). Low back pain in drivers exposed to whole body vibration : analysis of a dose–response pattern. *Occupational and environmental medicine*, volume 65, numéro 10, p. 667–675.

[93] Tivay, A., Rezaei, S. M., Baghestan, K. et Zareinejad, M. (2013). Energy-saving cooperative position tracking control of electro-hydraulic servo systems. Dans *RSI/ISM International Conference on Robotics and Mechatronics (ICRoM)*. IEEE, p. 511–516.

[94] Tseng, H. E. et Hrovat, D. (2015). State of the Art Survey : Active and Semi-Active Suspension Control. *Vehicle System Dynamics*, volume 53, numéro 7, p. 1034–1062.

[95] Ulicny, J. C., Hayden, C. A., Hanley, P. M. et Eckel, D. F. (2007). Magnetorheological fluid durability test—Organics analysis. *Materials Science and Engineering : A*, volume 464, numéro 1-2, p. 269–273.

[96] Van Gerpen, H. W. (1982). Active Seat Suspension Control System.

[97] Viau, J. (2015). *Développement et Validation Expérimentale d'un Système d'embrayages Magnétorhéologiques Pour Le Contrôle de Robots à Tendons*. Thèse de doctorat, Sherbrooke.

[98] Viau, J., Chouinard, P., Bigué, J. P. L., Julió, G., Michaud, F. et Plante, J. S. (2017). Tendon-Driven Manipulator Actuated by Magnetorheological Clutches Exhibiting Both High-Power and Soft Motion Capabilities. *IEEE/ASME Transactions on Mechatronics*, volume 22, numéro 1, p. 561–571.

[99] Viau, J., Chouinard, P., Bigué, J. P. L., Julió, G., Michaud, F., Shimoda, S. et Plante, J. S. (2015). Projected PID controller for Tendon-Driven Manipulators actuated by magneto-rheological clutches. Dans *2015 IEEE/RSJ International Conference on Intelligent Robots and Systems (IROS)*. p. 5954–5959.

[100] Wang, C., Zhang, X., Guo, K., Lv, J. et Yang, Y. (2016). Hierarchical Optimisation on Scissor Seat Suspension Characteristic and Structure. *Vehicle System Dynamics*, volume 54, numéro 11, p. 1538–1553.

[101] Wensing, P. M., Wang, A., Seok, S., Otten, D., Lang, J. et Kim, S. (2017). Proprioceptive Actuator Design in the MIT Cheetah : Impact Mitigation and High-Bandwidth Physical Interaction for Dynamic Legged Robots. *IEEE Transactions on Robotics*, volume 33, numéro 3, p. 509–522.

[102] Wereley, N. M. (2006). Bidisperse magnetorheological fluids using Fe particles at nanometer and micron scale. *Journal of Intelligent Material Systems and Structures*, volume 17, numéro 5, p. 393–401.

[103] Wiehe, A. et Maas, J. (2013). Large-Scale Test Bench for the Durability Analysis of Magnetorheological Fluids. *Journal of Intelligent Material Systems and Structures*, volume 24, numéro 12, p. 1433–1444.

[104] Yadmellat, P. et Kermani, M. R. (2016). Adaptive Control of a Hysteretic Magnetorheological Robot Actuator. *IEEE/ASME Transactions on Mechatronics*, volume 21, numéro 3, p. 1336–1344.

[105] Yadmellat, P., Shafer, A. S. et Kermani, M. R. (2014). Design and Development of a Single-Motor, Two-DOF, Safe Manipulator. *IEEE/ASME Transactions on Mechatronics*, volume 19, numéro 4, p. 1384–1391.

[106] Yamaguchi, Y., Furusho, J., Kimura, S. et Koyanagi, K. (2004). High-performance 2-D force display system using MR actuators. Dans *IEEE/RSJ International Conference on Intelligent Robots and Systems*. volume 3. IEEE, p. 2911–2917.

[107] Yin, X., Guo, S., Xiao, N., Tamiya, T., Hirata, H. et Ishihara, H. (2016). Safety Operation Consciousness Realization of a MR Fluids-Based Novel Haptic Interface for Teleoperated Catheter Minimally Invasive Neurosurgery. *IEEE/ASME Transactions on Mechatronics*, volume 21, numéro 2, p. 1043–1054.

[108] Zhang, H., Zheng, X., Yan, H., Peng, C., Wang, Z. et Chen, Q. (2017). Co-Design of Event-Triggered and Distributed H-Infinity Filtering for Active Semi-Vehicle Suspension Systems. *IEEE/ASME Transactions on Mechatronics*, volume 22, numéro 2, p. 1047–1058.